Final Report on the Cooperative VAS Program

with the Marshall Space Flight Center

Contract No. NAS8-34732

for the period of

July 1982 to December 1987

submitted by

George R. Diak
W. Paul Menzel

Cooperative Institute for Meteorological Satellite Studies (CIMSS)
University of Wisconsin-Madison
1225 West Dayton Street
Madison, Wisconsin 53706

July 1988

Table of Contents

1. INTRODUCTION

Over the life span of this NASA-VAS cooperative program, work has been divided between analysis/forecast model development and evaluation of the impact of satellite data in mesoscale numerical weather prediction (NWP) and also development of the Multispectral Atmospheric Mapping Sensor (MAMS) and related research.

The modelling effort has seen the CIMSS Synoptic Scale Model (SSM) progress from a relatively basic analysis/forecast system at the inception of the program to a package which now includes such features as nonlinear vertical mode initialization, comprehensive Planetary Boundary Layer (PBL) physics and the core of a fully four-dimensional data assimilation package which will be expanded on for subsequent NASA sponsored research. Investigations on the use of satellite information have been rewarding in an educational sense, but sometimes frustrating in practical application, in that the data have not had the impact on mesoscale prediction which the research community had hoped for. In retrospect, the analysis and forecast problems associated with characteristics of the data could have been understood earlier by an amalgamation of expertise from the data producers and analysis-forecasting groups. It has been this NASA program and similar efforts which have inspired the community to consolidate the experience of these groups into a common ground of expertise which will enable more timely and beneficial use of the information from future remote sensing data sources.

The MAMS effort has produced a calibrated visible and infrared sensor that produces imagery at high spatial resolution. The MAMS has been developed in order to study small scale atmospheric moisture variability, to monitor and classify clouds, and to investigate the role of surface characteristics in the production of clouds, precipitation, and severe storms. The NASA-VAS

cooperative program has been the starting point for the testing of this aircraft instrument; the design of a future space borne sensor in low earth or geostationary orbit with similar monitoring capabilities in planned with EOS and beyond. The effort funded here has demonstrated good quality data from the MAMS from intercomparison with other instruments.

2. SATELLITE DATA ASSIMILATION RESEARCH

With the satellite era has come the first mesoscale data base available to the meteorological community on a routine basis. While these satellite systems have made sizable contributions to the understanding of global-scale processes, contributions to mesoscale meteorology have been slower to evolve. Both case study work and observing system simulation experiments (OSSES) echo the same theme. On the mesoscale, traditional methods of looking at his data base must be modified and not only the data errors and sampling characteristics, but also the physical meaning of the measurements must be well-understood. Though research approaches vary between investigators, there is a common underlying theme to satellite data assimilation. It is evident that, almost without exception, the techniques have been designed to access the information content of the data while circumventing one or more of the problematic aspects of the observing system.

Table 1 contains a brief summary of qualitative characteristics of the TOVS, VAS and cloud and water vapor drift wind (CDWVW) measurements which have somewhat subjectively divided into "advantages" and "disadvantages". Most of these are well-known, but will provide a convenient context in which to discuss some of the methods used to analyze and assimilate the data.

Table 1. Characteristics of Satellite Data

TOVS	VAS	CDWVW
Advantages:		
moderate/high horizontal resolution	high horizontal resolution	high horizontal resolution where tracers exist
regular coverage at set times depending on orbits	user-selected frequent coverage in clear areas	frequent coverage if rapid-scan mode used
spatially correlated errors-good gradient information	spatially correlated errors-good gradient information	
Disadvantages:		
low vertical resolution	low vertical resolution	level assignment uncertainties
different error characteristics for clear, partly and cloudy retrievals	gaps in coverage in cloudy areas	single level only
spatially correlated errors (biases)	spatially correlated errors (biases)	

A. TEMPERATURE AND MOISTURE RETRIEVALS

On the global scale, TOVS and VAS temperature and moisture retrievals may be treated similar to their radiosonde counterparts and show generally positive impact on global forecasts, especially in areas of low conventional data density such as the southern hemisphere. In these data-poor regions, the satellite data represent an improvement in the designation of atmospheric state over that achieved by conventional synoptic information and lower resolution forecast models alone. However, most of the operational global scale assimilation schemes use statistical interpolation methodologies in

which satellite data are allocated greater observational error and differing covariance functions than radiosonde data and also utilize data quality algorithms so that a high quality observation cannot be overwhelmed or rejected by a larger number of satellite observations of lesser quality.

On the mesoscale, however, and especially in regions of relatively high density synoptic data and high resolution forecasts such as the continental United States or Europe, the characteristics of satellite soundings can lead to a degradation of forecast quality when they are assimilated in a standard scalar fashion. Our research efforts on the mesoscale have concentrated on methods to access the information content of the soundings or radiances while circumventing their problematic features.

Probably the most detrimental feature of VAS and TOVS soundings to mesoscale assimilation work is their biases, which can be large and situation dependent. The biases arise from a number of sources. The limited vertical resolution of these satellite instruments (optimistically five levels of vertical information) immediately dictates that atmospheric features with small vertical scales may be missed or only accounted for in a vertically integrated manner. A second source of bias error comes from the retrieval algorithms themselves. Implicit or explicit in these algorithms, whether they be statistical or physical, is a comparison of measured radiances to "forward" radiances calculated from the background atmosphere for the retrieval. Errors in the knowledge of atmospheric transmission, instrument calibration error, errors in the assignment of surface emissivity, undetected sub-field-of-view clouds for infrared instruments and other errors may all enter and degrade the retrieval process. Even when the background field for retrieval is essentially "perfect" (a high resolution analysis from raob data), we have shown that errors associated with the retrieval process may significantly

alter the satellite soundings to the point where they cannot be used for mesoscale NWP.

Our research to mitigate this problematic aspect of satellite soundings has two facets. At the assimilation end, we have concentrated on developing methods for the assimilation of the horizontal gradients of temperature and moisture from VAS atmospheric soundings using variational techniques.

Diak (1987) investigated the assimilation of VAS information by both scalar and gradient methods for the AVE/VAS case study day of 6 March 1982. On this day, there was a mesoscale network of raob observations in the Texas region for verification of analyses and forecasts. It was a day of large temporal changes in the region from a fast-moving cold frontal system and also a day in which large VAS data biased existed. Figure 1 shows 1500 UTC analyses of 500mb height errors for VAS data versus special network raobs using the VAS information as scalar (1A) and gradient (1B) information, respectively. As shown, the gradient approach significantly reduced error over the region compared to the scalar analysis.

A forecast made from the gradient (1500-0000 UTC) was superior to the corresponding scalar forecast and similar in quality of primary variables to a forecast (1200-0000 UTC) initialized with only synoptic data. Improvements were noted in vertical motion and precipitation patterns in the gradient versus the synoptic forecast. More details on this experiment can be found in the enclosed reprint.

While gradient methods mitigate some of the problems of biased data, it can be seen in principle that they are not a panacea. Gradient methodologies essentially solve a boundary value problem; that is, while gradients within a data region may be well-depicted, the absolute values of an observable in the region will depend on the invariant values of the background field on the data

boundaries. Our research has indicated that the gradient methodology performs best when satellite gradients are combined with measurements from raobs to "lock in" the absolute values of an observable at the synoptic locations

Figure 2 shows an example of where this technique may be useful in the western Atlantic Ocean region. Figure 2a illustrates the problem of trying to produce a realistic analysis of moisture with the limited conventional data available in the western Atlantic. As shown, the result of limited data in our analysis system and others such as the LFM and RAFTS is often the "Bermuda Bulls Eye" where the Bermuda raob and the background field for analysis (in this case, the NMC Global forecast) are at odds. Figure 2b is an analysis made from a combination of satellite gradient and raob absolute value information. The satellite gradients have filled in the data voids between synoptic locations and improved the coherence of the moisture analysis in this case.

In addition to gradient analysis methods, some research progress had been made in mitigating data biases through retrieval techniques which rely on measurements of the time change of radiances. The method acknowledges that in areas of dense synoptic station coverage the best depiction of the atmosphere is at synoptic times. The retrieval problem can then be formulated as the time change of atmosphere (radiances) from this well-known initial state, that is:

$$B_R = B_F + \Delta B_M$$

B_R = radiance for atmospheric retrieval

B_F = "forward" calculation of radiance at synoptic time

ΔB_M = measured change in radiance (data time-synoptic time)

Very important in this retrieval methodology is that bias errors from instrument sources, atmospheric transmissivity errors, surface emissivity

errors and other sources, drop out of the retrieval process in a first order fashion.

At this writing, a retrieval algorithm using the time change of radiances has been written and required only minor modifications to the standard CIMSS physical retrieval method to develop. It is planned that investigation of this technique will proceed under other existing NASA/CIMSS programs.

Some positive preliminary results have been drawn from a conceptually very similar experiment (synthetic radiances and soundings) using the time change of the VAS retrievals themselves. Figure 3a shows an initial 500mb temperature state analyzed from raob special network observations at 1500 UTC 6 March 1982. Figures 3b and 3c are two satellite analyses of VAS retrievals of 500mb temperature at 1800 UTC on the same day. The first is an analysis of VAS retrievals made in the standard manner, while the second analysis was made using the 1500 UTC initial state (2a) augmented by the time change of the VAS retrievals 1800 minus 1500 UTC. All retrievals were made using an LFM first guess. Comparing these two analyses to the 1800 UTC verification (3d), another special network raob analysis, it can be seen that the temporal scheme was superior in maintaining small-scale features and the strengths of the temperature gradients in the region. The time-changes (4b) show reasonable correspondence to those from the special network analyses (3a) and importantly add information to the time changes depicted in the LFM guess fields which were used to make these soundings (4c).

It can be seen that the time change of atmospheric radiances can be a useful tool, not only in dealing with satellite data biases, but in the more general framework of understanding the coupling of thermodynamic and radiative processes in the atmosphere.

Perhaps the poorest understood element of satellite soundings in an assimilation context is the effects of their spatial and temporal sampling characteristics. Polar orbiting instruments sample atmosphere radiances at a given location only once or twice per day, while geostationary infrared instruments are subject to large data voids caused by clouds. On the global scale it is standard procedure to bin their observations into a designated time window of about six hours for assimilation. One mesoscale experiment at the CIMSS has shown that as little as a two hour difference in time between data from raob and TOVS sources noticeably degraded the quality of an analysis of a fast moving cyclone made from the combination of the two data types.

We have achieved some success using complementary data sources to fill in the data voids of infrared sounder. LeMarshall et al. (1985) and Diak et al. (1986) both describe the complementary nature of the spatial distribution of VAS soundings and cloud and water vapor drift winds. In these studies, the CDWVW were used as indicators of geopotential gradient and helped describe the mass field in sounding data voids. Unfortunately (as will be described in the next section), the single-level nature of these winds limits their routinely demonstrating positive impact on numerical analyses and forecasts.

B. CLOUD DRIFT AND WATER VAPOR WIND DATA

There are two problems which can be immediately identified with the use of CDWVW data in analyses and forecasting. The first is one of height assignment. Given that the cloud or water vapor tracer has some depth, to what level should the wind vector associated with the tracer be assigned. Multispectral techniques, more sophisticated that simply assigning low middle and high levels, are in common use, but for the time being at least many assimilation schemes make some allowance for the uncertainty in level

assignment by allocating a greater observational error to the data in statistical interpolation and by using appropriate data rejection algorithms, particularly if the observation is near a jet stream.

The second problem is that these data are at single levels and cannot by themselves provide a three-dimensional wind analysis, foreshadowing the possibility that they will not be well accepted by a forecast model. The variational analysis scheme which we employ does spread the influence of these winds in the vertical, however, not as effectively as an explicitly three-dimensional optimal interpolation procedure.

A feature of the CDWVW data, as pointed out by LeMarshall et al. (1985) and Diak et al. (1986), and mentioned in the previous section is that they frequently complement the coverage of infrared satellite soundings. Figures 5a and 5b show, respectively, the VAS and cloud and water vapor drift wind distribution at 1600 UTC on the AVE/VAS case study day of 26 April 1982. On this day, a small closed low developed at 500 mb in the southern Illinois region between synoptic stations and synoptic times (evidenced in the cloud circulations). The feature did not develop in a 12-hour mesoscale model run from a synoptic analysis made at 1200 UTC 26 April. Figures 5c and 5d are two 500mb analyses made at 1600 UTC using this forecast as a guess. The first (5c) is an analysis which used only the VAS soundings (as gradient information, see prior section) as input, while the second (5d) contains both VAS and WVCDW data. As shown, the CDWVW information was instrumental in the analysis of this feature. Three similar pairs of analyses for later times (with and without CDWVW data) yielded the same character of results. While the quality of results for this case is somewhat fortuitous owing to the good horizontal and vertical distribution of satellite wind data on April 26, it suggests that these data may be of at least periodic benefit when assimilated

in a consistent manner with other observations. LeMarshall et al. (1985) similarly found improvements in the forecast position of a tropical cyclone when both VAS and CDWVW data bases were used in the analysis.

We expect that the forthcoming upgrade of our analysis system to a combination of optimal interpolation-variational blending will increase the frequency with which CDWVW data display positive analysis and forecast results.

3. MULTISPECTRAL ATMOSPHERIC MAPPING SENSOR (MAMS)

This final report will describe the characteristics of the instrument design that evolved from this study, present the results of some of the VAS and MAMS intercomparisons, and summarize the science data that has been gathered. This work is continuing in a follow on contract with NASA, so that a more complete final report will be forthcoming at the end of that contracted effort.

A. MAMS INSTRUMENT CHARACTERISTICS

The MAMS is a modification of NASA's Airborne Thematic Mapping (Daedalus, 1982) that was suggested by UW. The MAMS has two major components, the scan head and the spectrometer. The scan head consists of the primary collecting telescope, a rotating scan mirror, a motor encoder assembly, and two controlled thermal sources. The field of view is defined by the aperture which is available in two different sizes: 2.5 mrad and 5.0 mrad. The spectrometer consists of optical elements which spectrally separate the polychromatic input energy, lenses which focus the separated energy onto sensors, detectors which convert optical energy to an electrical signal, and pre-amplifiers which condition the signal. The energy collected by the

spectrometer is separated into four distinct optical paths using dichroic filters; three paths for the infrared data (one for each spectral band) and one for the visible and near infrared data. The spectrometer detectors are silicon for the visible radiation and mercury cadmium telluride for the thermal infrared radiation. The visible detector is an eight element array which converts optical energy to electrical energy. The spectral response of each band is determined by the dispersion characteristics of the prism placed in the optical path and the location of the array in the dispersed beam. The thermal infrared detectors are each housed in a vacuum dewar which contains a cooled longwave filter which defines the particular spectral band. Each infrared detector has an associated pre-amplifier to process the electrical signal. The spectral bands are summarized in Table 2. The spectral response functions for the three infrared channels of the MAMS were specified to be similar to the 6.7, 11.2, and 12.7 micron channels on VAS.

Table 2

Range of MAMS Spectral Bands

8 visible (microns)	3 infrared (microns)
.42- .45	6.20-6.85 (upper level water vapor)
.45- .52	10.32-12.02 (window)
.52- .60	12.20-12.56 (lower level water vapor)
.60- .62	
.63- .69	
.69- .75	
.75- .90	
.90-1.05	

The MAMS produces high resolution imagery in these visible and infrared spectral bands from a high altitude aircraft at 20 km. The horizontal ground resolution of each individual field of view is 100 meters (50 if the smaller 2.5 mrad optics are used). The total field of view for one scan is 86° which covers the width of the entire cross path of roughly 40 km. The scan rate is 6.25 revolutions per second (12.50 when the 2.5 mrad optics are used) and

produces 67% overlap, 1-P, of each scan line with the previous one for nominal aircraft speed (740 km/hr). On each scan line, 716 samples are taken so that there is 52% overlap of neighboring pixels along a scan line (4% when the 2.5 mrad optics are used). These overlaps can be used to reduce the noise in the scene by spatial averaging.

Radiometric calibration of the infrared data is accomplished by viewing two blackbody sources and by assuming the detector response is linear with respect to radiance (a fractional nonlinearity of less than $5x10^{-4}$ is observed). Calibration occurs every scan line by viewing a warm and than a cold blackbody of known temperature. For a given spectral band, the radiance is determined from the temperature through the convolution of the normalized spectral response and the Planck function. The calibrated radiances are transformed back into temperatures using the inverse Planck relation with the nominal spectral band center wavelength.

Prior to flight, the gain and offset for each spectral band are adjusted electronically in order to minimize the likelihood of saturation over hot scenes and to maximize the effective operating range. The 6.5 micron band is adjusted to cover 210 to 280°K, while the 11.2 and 12.3 micron bands operate from 220 to 340°K. An eight bit digitizer is used so that for the 6.5 micron band, the gain is approximately .3°K per count, and for the remaining surface viewing bands it is approximately .5°K per count Truncation errors are assumed to be roughly half these values.

The infrared detectors on MAMS exhibit some low frequency noise so that samples taken at 52 microsecond intervals for the spin rate of 6.25 revolutions per second (26 microsecond sampling occurs at 12.5 rps) experience noise contributions with significant correlation. An analysis of covariance of the noise with the 5 mrad aperture reveals that after averaging ten

consecutive samples, noise is reduced by a factor of .54, .52, and .37, respectively, in the three infrared spectral bands in order of increasing wavelength (uncorrelated noise would have a factor of $1/\sqrt{10}$ or .32).

Inflight single sample noise values were determined from multiple samples over a uniform portion of the ocean. For a sample size of 100, the single sample noise values with the 5 mrad aperture were found to be .2, .1, and .4°K, respectively, for the spectral bands in order of increasing wavelength (for the 2.5 mrad aperture the values were .5, .2, and .9°K).

B. DATA INTERCOMPARISON

Radiances from the MAMS and VAS spectral responses were simulated for each band and sensor in a radiative transfer calculation. A representative atmospheric transmittance was computed using a band model and radiosonde temperature and moisture profiles. Table 3 shows that the MAMS detects radiances within one to two mW/ster/m^2/cm^{-1} of the VAS detected radiances. The MAMS spectral responses are shifted to shorter wavelengths, hence less radiance is detected. This converts into brightness temperature differences of less than a degree Kelvin.

Table 3

Intercomparison of Simulated Data

	6 micron	11 micron	12 micron
R(MAMS)	7.86	96.5	109.5
T(MAMS)	254.8	287.3	286.0
R(VAS)	8.73	97.5	111.6
T(VAS)	253.9	287.3	285.4
$\Delta T_{MAMS-VAS}$	0.9°K	0.0	0.6

radiances in mW/ster/m^2/cm^{-1}, temperatures in °K

Radiances from the MAMS and VAS were collected simultaneously over a relatively isothermal area of ocean off the California coast on 18 May 1985. Table 4 presents the comparison. After compensating for the inherent spectral differences of the two instruments, the MAMS data is within .5, 2.5, and 1.5°K of the VAS data, respectively, for the spectral bands in order of increasing wavelength. The observed split window channel differences (11 micron less 12 micron) are comparable, 2.5°K for MAMS and 2.1°K for VAS and thus showing similar low level moisture concentrations. The observed water vapor channel data (6 micron) show MAMS detecting upper level moisture concentrations very much like VAS. with MAMS showing somewhat less attenuation than VAS. The comparisons are quite reasonable, since the spatial resolution of each sensor is very different (VAS at 7 km and MAMS at .05 km at nadir), the navigation of the MAMS data is from visual siting of landmarks only, and non-nadir viewing of the MAMS has not yet been taken into account.

Table 4

Intercomparison of Observed Data

	6 micron	11 micron	12 micron
R(MAMS)	6.01	99.9	111.1
T(MAMS)	247.1	289.5	287.0
R(VAS)	6.80	97.0	111.1
T(VAS)	246.5	287.1	285.0
$\Delta T_{MAMS-VAS}$	0.6°K	2.4	2.0

radiances in $mW/ster/m^2/cm^{-1}$, temperatures in °K

Imagery from the MAMS and VAS were compared from flights over Oklahoma and Kansas on 12 May 1985. The goal of the intercomparison is to verify small scale features observed in the VAS water vapor images with the high resolution MAMS data. These water vapor inhomogeneities in the VAS data have been used to obtain motion vectors when several images are considered in sequence.

While the imagery is often too amorphous to track winds reliably with a correlation technique, it has produced good wind fields by single pixel tracking. The MAMS data tends to verify that small scale gradients (down to several single pixels) in the VAS data are real.

C. MAMS DATA ARCHIVE

The MAMS has been flown on a NASA U2/ER2 high altitude aircraft for both engineering checkout flights and scientific missions. Flight dates and general information are listed in Table 5. While the January 1985 flights served primarily as engineering checkout of instrument and/or hardware problems, many interesting atmospheric and land features were observed with the instrument. In particular, mountain wave features in the lee of the Sierra Nevadas were observed in the water vapor imagery from 22 January (see Jedlovec paper on this subject).

The MAMS flights during May and June 1985 were conducted to sample a variety of weather conditions and also corresponded to a period of special ground-based observations of the Pre-STORM field experiment.

Several days are of particular interest. The first part of the 18 May flight contained ocean data, which provided an ideal situation to study the noise characteristics of the MAMS over a relatively stable background scene. Corresponding data from the VAS and AVHRR were available over this region at approximately the same time. Also, 20 and 24 May and 26 June are interesting because they sampled a humid summertime environment preceding thunderstorm activity. Flights on the 22 and 23 June were constructed such that four passes over the same area region occurred at one hour intervals, thereby providing high horizontal resolution with increased temporal frequency to monitor environmental changes.

The MAMS flights in January 1986 tested several new configurations for improving the signal-to-noise ratios. The speed of the scan head was halved (as well as the digitizing rate) and the 5.0 mrad aperture was thoroughly tested. From the data of these four flights, it was apparent that the signal-to-noise was substantially improved.

5. LIST OF PUBLICATIONS ACKNOWLEDGING SUPPORT FROM NAS8-34732

[1] indicates modelling publication, [2] signifies MAMS publication

[1]Diak, G. R., 1987: Assimilation of scalar versus horizontal gradient information from the VAS into a mesoscale model. J. Clim. Appl. Meteor., 26, 738-748.

[1]Diak, G. R., G. A. Mills, and G. M. Callan, 1986: The assimilation of satellite data and products into the McIDAS analysis/prognosis/display system. Preprints, Second International Conference on Interactive Information and Processing Systems for Meteorology, Oceanography and Hydrology, Miami, FL, January 14-17, 337-341.

[1]Earl, P. L., 1985: Impact of the initial specification of moisture and vertical motion on precipitation forecasts with a mesoscale model. Masters thesis, University of Wisconsin-Madison, 87 pp.

[1]Fields, G., 1988: A case study evaluation of satellite-derived rainfall estimates and their application to numerical model precipitation forecast verification. Masters thesis, University of Wisconsin-Madison, 96 pp.

[1]Goodman, B. M., G. R. Diak, and G. A. Mills, 1986: Analysis and forecast experiments incorporating satellite soundings and cloud and water vapor drift wind information. Reprint volume, Second Conference on Satellite

Meteorology/Remote Sensing and Applications, Williamsburg, VA, May 13-16, 142-145.

[2]Jedlovec, G. J., W. P. Menzel, G. S. Wilson, R. J. Atkinson, 1986: Detection of mountain-induced mesoscale wave structures with high-resolution moisture imagery. Reprint volume, Second Conference on Satellite Meteorology/Remote Sensing and Applications, Williamsburg, VA, May 13-16, 365-369.

[2]Jedlovec, G. J., W. P. Menzel, R. Atkinson, G. S. Wilson, and J. Arvesen, 1986: The Multispectral Atmospheric Mapping Sensor (MAMS): instrument description, calibration and data quality. NASA Technical Memorandum NASA TM-86565, 37 pp.

[1]LeMarshall, J.F., W. L. Smith, and G. M. Callan, 1985: Hurricane Debby - an illustration of the complementary nature of VAS soundings and cloud and water vapor drift winds. Bull. Am. Meteor. Soc., 33, 258-263.

[2]Menzel, W. P., G. Jedlovec, and G. Wilson, 1986: Verification of small-scale water vapor features in VAS imagery using high resolution MAMS imagery. Reprint volume, Second Conference on Satellite Meteorology/Remote Sensing and Applications, Williamsburg, VA, May 13-16, 108-111.

[1]Mlynczak, P. E., G. R. Diak, and D. D. Houghton, 1986: Impact of the initial specification of moisture and vertical motion on precipitation forecasts with a mesoscale model - implications for a satellite data base. Reprint volume, Second Conference on Satellite Meteorology/Remote Sensing and Applications, Williamsburg, VA, May 13-16, 136-141.

[1]Raymond, W. H., 1988: High-order low-pass tangent filters for use in finite area calculations. Accepted for publication, Mon. Wea. Rev.

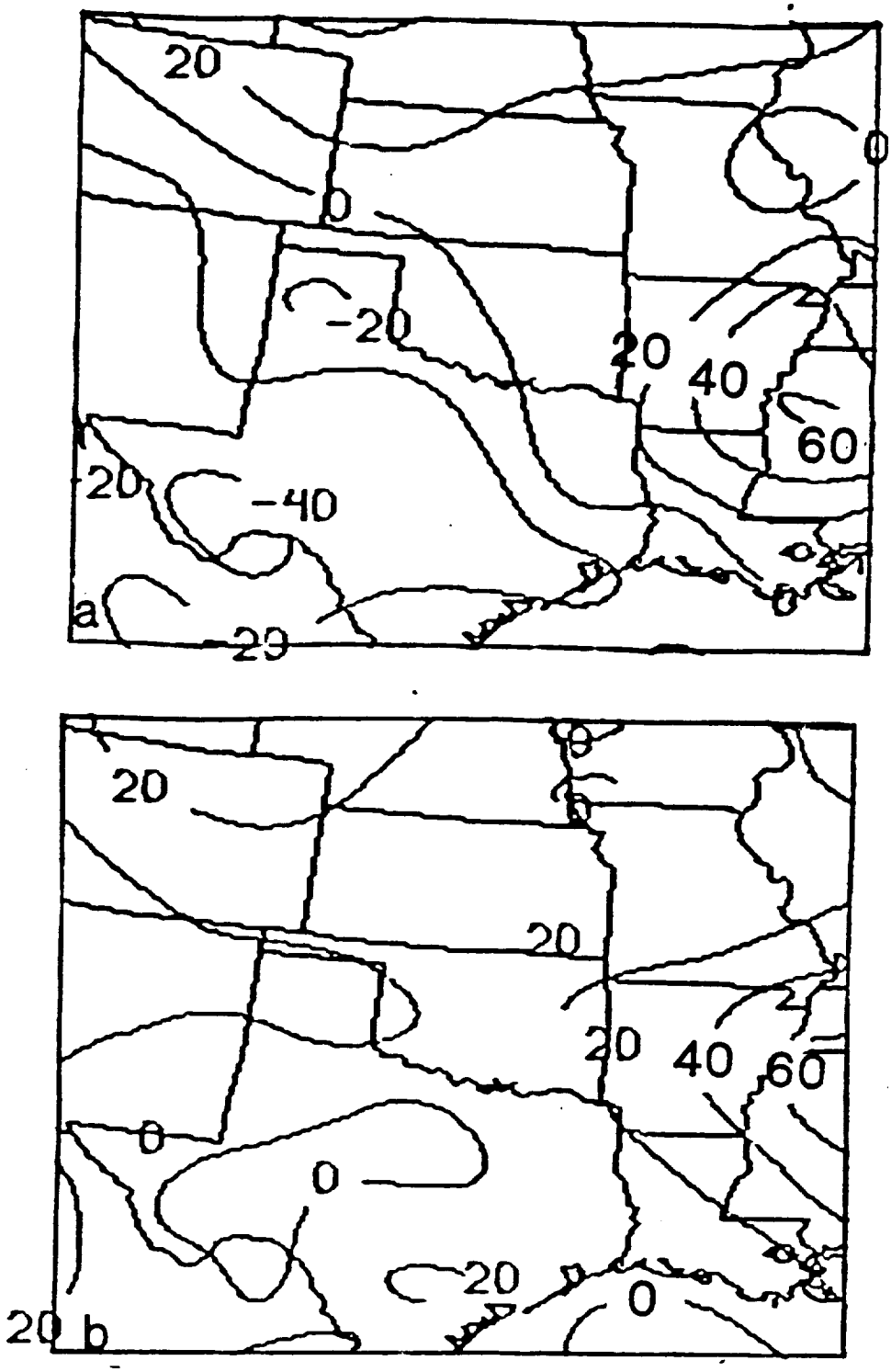

FIG 1

Fig. 1. Errors in 500 mb geopotentials (gpm) for scalar assimilation (1a) and gradient assimilation (1b) of VAS soundings versus special network raob analysis 1500 UTC 6 March 1982.

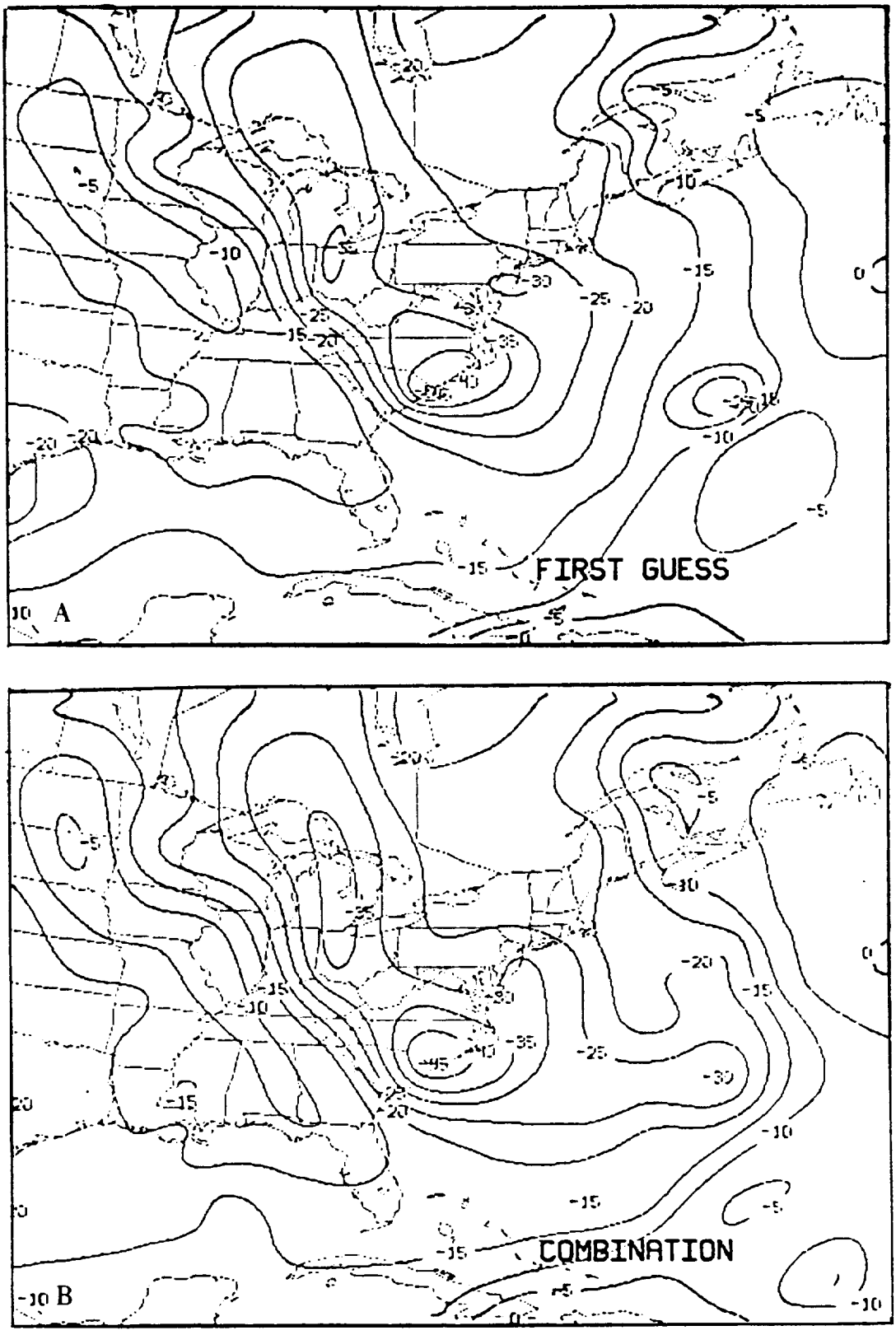

FIG 2

Fig. 2. First guess (radiosonde analysis) of 700 mb dewpoints and combination analysis resulting from variational blending of horizontal gradients from VAS data into first guess.

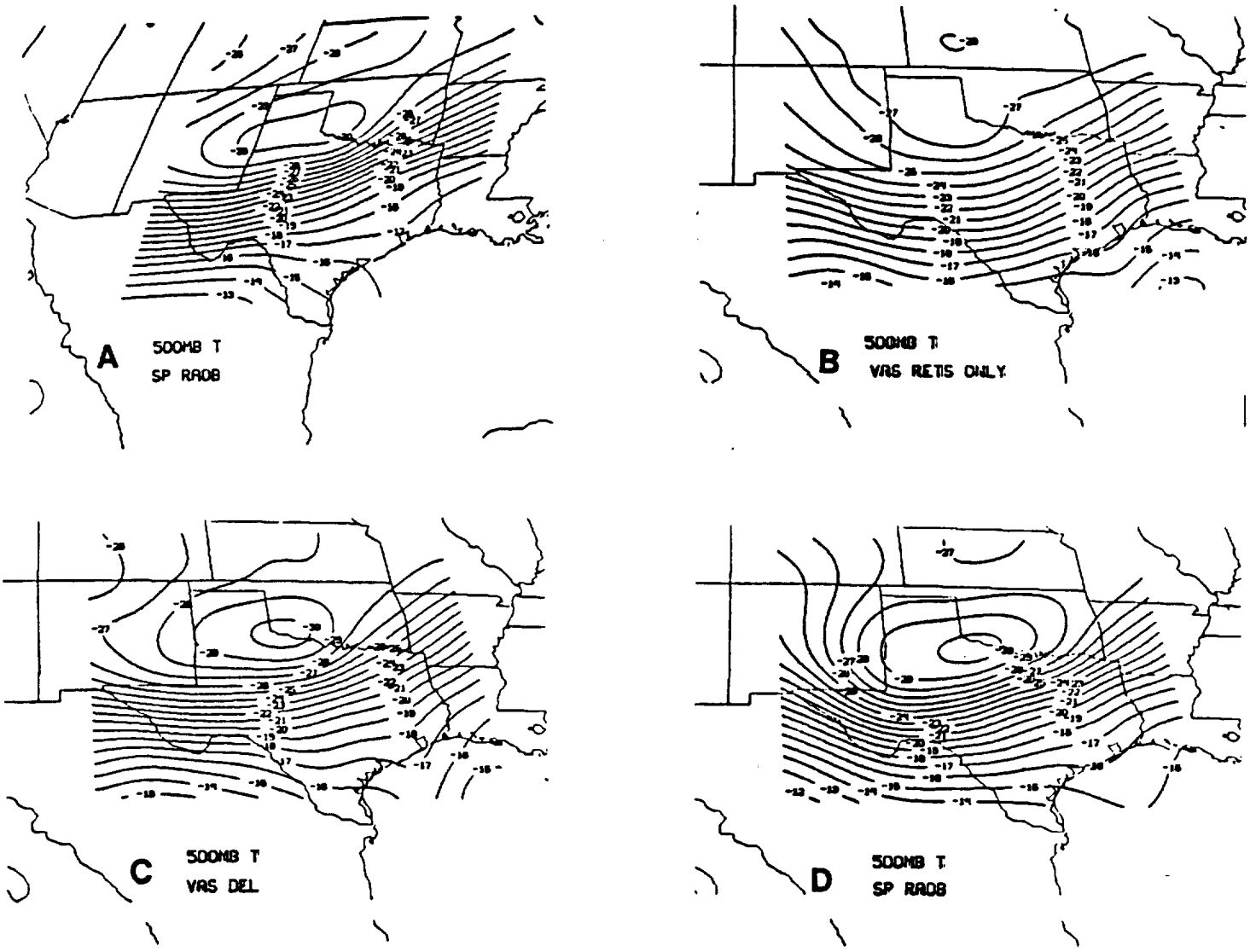

FIG 3

Fig. 3(a). Special network raob analysis of 500 mb temperature (K) 1500 UTC 6 March 1982. (b) Standard analysis of VAS 500 mb temperatures (K) 1800 UTC 6 March 1982. (c) Analysis of 500 mb temperature (K) 1800 UTC 6 March 1982 made using initial state (2a) plus time change of VAS retrievals 1800 minus 1500 UTC. (d) Special network analysis of 500 mb temperature (K) 1800 UTC 6 March 1982.

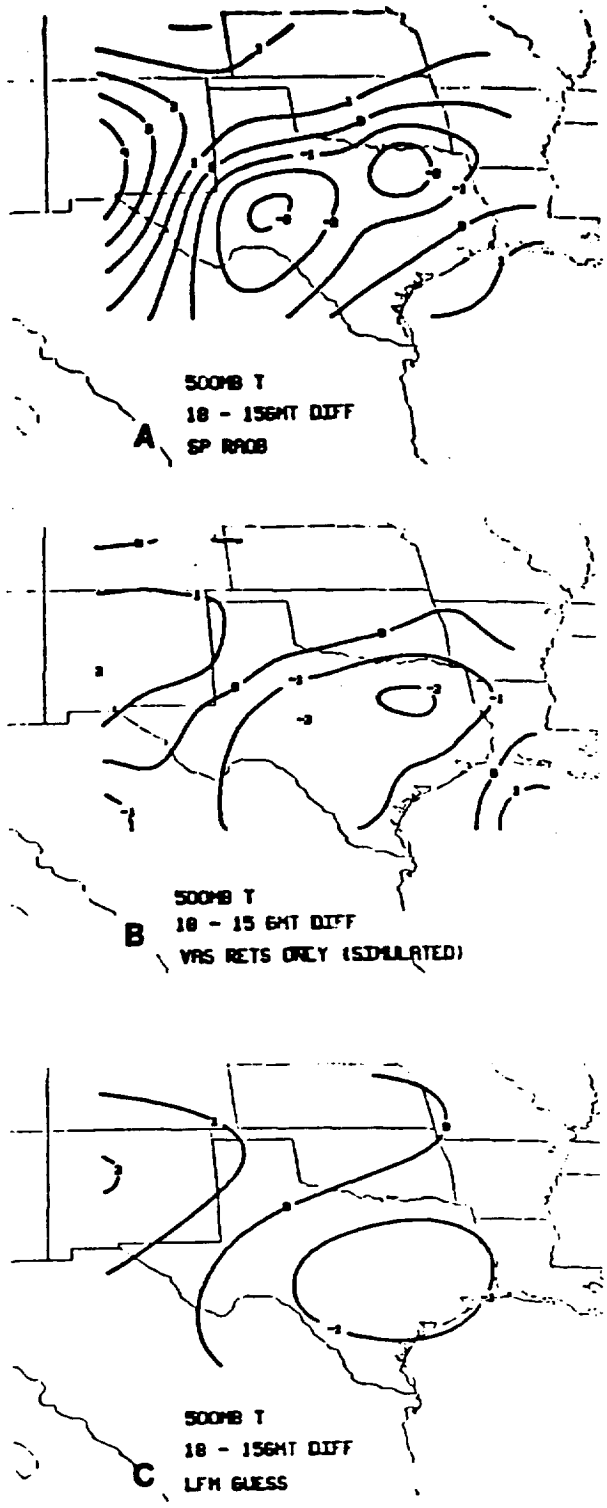

FIG 4

Fig. 4. Time change of 500 mb temperature (K) 1800 minus 1500 UTC 6 March 1982 from special network raobs (3a), VAS (3b), and LFM forecast (3c).

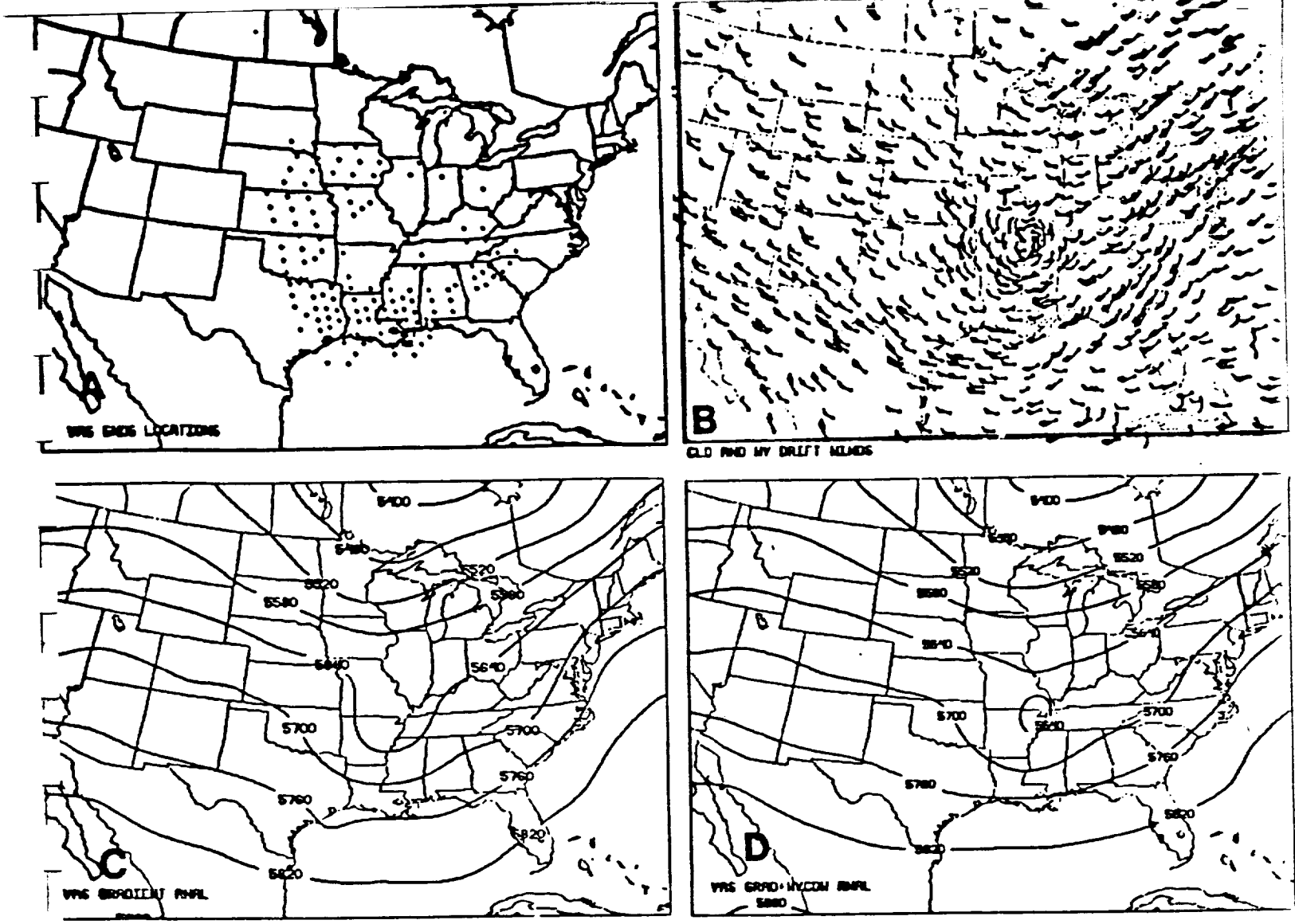

FIG 5

Fig. 5(a). VAS sounding locations 1600 UTC 26 April 1982. (b) CDWVW locations 1600 UTC 26 April 1982. (c) Analysis of 500 mb geopotential (gpm) using VAS soundings 1600 UTC 26 April 1982. (d) Same as (c), only using VAS plus CDWVW.

APPENDIX A: REPRINTS AND ABSTRACTS OF NASA SUPPORTED PUBLICATIONS

Reprinted from JOURNAL OF CLIMATE AND APPLIED METEOROLOGY, Vol. 26, No. 6, June 1987
American Meteorological Society

Assimilation of Scalar Versus Horizontal Gradient Information from the VAS into a Mesoscale Model

GEORGE DIAK

Assimilation of Scalar Versus Horizontal Gradient Information from the VAS into a Mesoscale Model

GEORGE DIAK

Cooperative Institute for Meteorological Satellite Studies, Space Science and Engineering Center, Madison, WI 53706

14 April 1986 and 6 December 1986

ABSTRACT

Comparisons are made between analyses and forecasts which incorporate VAS geopotential data as either scalar or horizontal gradient information for a case study on the AVE/VAS day of 6 March 1982. On this day, incorporating the VAS information in analysis as a variational constraint on horizontal geopotential gradients significantly mitigated the effects of large data biases which made VAS assimilation by standard scalar methods very difficult. A subsequent forecast made from the gradient assimilation was superior to one made from the standard analysis and of comparable quality in geopotentials to a control forecast from synoptic data. Most impact was noted in the forecasts of vertical motion and precipitation in the gradient versus this control simulation.

1. Introduction

During the past several years, the Cooperative Institute of Meteorological Satellite Studies (CIMSS) at the University of Wisconsin-Madison has been developing prototype methodologies for the assimilation of satellite data and products into an analysis/prognosis/display system. The vehicle for the investigations is an analysis/prognosis system developed by the Australian Numerical Meteorological Research Centre (ANMRC) which has been adapted to the United States region and implemented on the Man-computer Interactive Data Access System (McIDAS) facility at the space Science and Engineering Center.

Experiments—to date principally done in a research mode—have involved techniques for the assimilation of soundings from the VISSR Atmospheric Sounder (VAS), cloud and water vapor drift winds and satellite-derived surface energy balance descriptors into the analyses and prognoses.

Several authors have experimented with VAS data as input to numerical prediction models in both Observing System Simulation Experiments (OSSEs) and in real case studies. In general, the positive impact of VAS from these experiments for the relatively data rich continental United States has not been as significant as originally had been hoped. The experiments have been very helpful, however, both in developing a better understanding of the data characteristics and also in motivating improved assimilation techniques. It is fair to say that progress is being made.

While comprehensive investigations of the VAS data (Jedlovec, 1985; Fuelberg and Meyer, 1986) have indicated meso-alpha-scale horizontal gradient information content in the soundings, their reduced vertical resolution, incomplete spatial coverage and certain problematic data characteristics (notably temperature biases) have necessitated new approaches to assimilation. In general, these approaches are designed to preserve the information content of the data and model prediction fields while circumventing problems inherent to the observing system.

One of the formidable limitations of the data source is dictated by its incomplete horizontal coverage (no soundings in cloudy regions). Gal-Chen et al. (1986) demonstrated in a set of OSSEs that the data gaps typical of infrared sounders significantly reduced the impact of VAS soundings in numerical forecasts and suggested a geostationary microwave instrument would be helpful in resolving this problem. In their experiments, it was found that multiple-time data insertion and nudging of the data into the model were instrumental in achieving forecast impact and reducing model shock.

This study is specifically aimed at another of the problematic characteristics of VAS data, the biases in the temperature (geopotential) retrievals which are situation-dependent and can make their assimilation by standard means quite difficult. In these experiments, we compare two methods of assimilation. Both are variational, but the first is "standard" in the sense that scalar VAS thicknesses are used as input to the variational analysis methodology. In the second methodology, horizontal gradients of thickness derived from the VAS soundings are input to the variational analysis scheme.

Cram and Kaplan (1985) have also reported on a variational technique for assimilating VAS gradient information. The methodology described here differs in several respects from their study. Our primary anal-

ysis variable is geopotential height, rather than temperature, to facilitate the later inclusion in the analysis of horizontal geopotential gradients inferred from measured winds. Also, this variational procedure includes vertical structure terms provided from the forecast model (guess field for analyses); the aim is to preserve coherent model-generated vertical detail.

A general problem with the evaluation of satellite information is finding verification data with adequate space and time resolution to compare. The investigation day of 6 March 1982 was one of several AVE/VAS special network days for which a dense space-time network of RAOB observations was available in the Texas region for verification (Hill and Turner, 1983). Also, the VAS temperature data at 1445 UTC on this day exhibited very strong bias characteristics, allowing a meaningful comparison of assimilation techniques.

2. Objective analysis scheme and forecast model

a. Analysis methodology

The three-dimensional objective analysis scheme used is an evolution of the scheme developed in the Australian Numerical Meteorology Research Centre (ANMRC) by Seaman et al. (1977) for limited area analysis over the Australian region and adapted to the United States region. Details and examples of its use in this region can be found in Mills and Hayden (1983) and LeMarshall et al. (1985) and will only be reviewed here as it pertains to this experiment. The scheme combines the successive correction method (SCM) of Cressman (1959) and the variational blending techniques of Sasaki (1970).

The analysis system is based upon principal levels at 1000 and 250 mb, and the calculus of variations is used in an explicitly three-dimensional manner. Estimates of the geopotential ϕ and the geopotential gradient in each coordinate direction are combined at each grid point in the three-dimensional analysis domain.

The basic observational ingredients combined in the blending are observed geopotential thicknesses of each layer and horizontal geopotential gradients either from geopotential measurements or independently derived from wind measurements and a gradient wind law. In this study, however, no wind measurement inputs to the gradient fields are included.

A 1000 mb geopotential field is defined by a SCM analysis using observations of geopotential and a guess field derived hydrostatically from a mean sea level pressure analysis and an assumed lapse rate. The scheme then uses a three-dimensional variational blending of 1000–250 mb thickness and geopotential gradient information at 250 mb to produce a bulk 1000–250 mb atmospheric structure. The variational functional for this gross blending is of the form

$$F_G = \int_x \int_y \left[A(\Delta\phi - \Delta\tilde{\phi})^2 + B\left(\frac{\partial\phi}{\partial x} - \frac{\partial\tilde{\phi}}{\partial x}\right)^2 + C\left(\frac{\partial\phi}{\partial y} - \frac{\partial\tilde{\phi}}{\partial y}\right)^2 \right] dxdy \quad (1)$$

where

F_G	gross blending functional
A, B, C	reliability weights
$\phi, \tilde{\phi}$	adjusted geopotential and observed 250 mb geopotentials (gpm)
$\Delta\phi, \Delta\tilde{\phi}$	adjusted and observed 1000–250 mb geopotential thickness (gpm)
x, y	longitudinal and latitudinal directions.

Once this 1000 to 250 mb thickness has been established, individual level geopotential analyses are then performed by blending the geopotential gradient analysis at a level with the analyzed thickness immediately above and below that level. Thus, at any interior level, the variational functional is of the form

$$F_I = \int_x \int_y \left[D(\Delta\phi_A - \Delta\tilde{\phi}_A)^2 + E(\Delta\phi_B - \Delta\tilde{\phi}_B)^2 + F\left(\frac{\partial\phi}{\partial x} - \frac{\partial\tilde{\phi}}{\partial x}\right)^2 + G\left(\frac{\partial\phi}{\partial y} - \frac{\partial\phi}{\partial y}\right)^2 \right] dxdy \quad (2)$$

where

F_I	interior blending functional
D, E, F, G	reliability weights
$\Delta\phi_A, \Delta\phi_A$	adjusted and observed thickness of layer above an interior level (gpm)
$\Delta\phi_B, \Delta\phi_B$	adjusted and observed thickness of layer below an interior level (gpm).

This procedure is carried out iteratively in the vertical with fixed 1000 and 250 mb geopotentials from the preceding gross blend as upper and lower boundary conditions.

Reliability weights (A–G) for the analyzed geopotential and geopotential gradient fields are determined on the basis of data density and latitude and level-varying standard deviation parameters. In this way, the blended geopotential fields reflect a greater weight to the wind data (when used) in low latitudes and to the thickness information at higher latitudes.

The same type of blending is then carried out for levels above 250 mb with the exception that only the 250 m level is fixed. The Euler–Lagrange type equations which arise from the variational functionals (Equations 1 and 2) are solved through standard over-relaxation techniques.

b. Forecast model

The Subsynoptic Scale Model (SSM) is a ten-level, 67 km resolution primitive equation model written for

the Australian region (McGregor et al., 1978) and adapted for use in the North American region. The model in the form for the United States has been amended with a more complete boundary layer parameterization (Diak et al., 1986), the inclusion of Corby differencing (Corby et al., 1972) to better handle the high topographic regions of the United States and the replacement of the original Arakawa–Schubert convective parameterization with a modified Kuo scheme (Kuo, 1965; Hammarstrand, 1977).

3. VAS data

The success of the VAS experiment as proposed by Suomi et al. (1971) has been the result of close collaboration between scientists and engineers from the University of Wisconsin, NASA, NOAA Santa Barbara Research Center and Westinghouse. The first in a series of instruments was put into geostationary orbit aboard the GOES-D satellite (Smith et al., 1981).

The VAS is a radiometer possessing eight visible channel detectors and six thermal detectors which sense atmospheric radiation in 12 spectral bands whos wavelengths lie between 3.9 and 15 μm. A dwell soun mode of operation was designed to enable the inter pretation of the vertical temperature and moistur structure of the atmosphere. Typical space and tim resolution (in clear areas) are 70 km and 3 h, respec tively. Vertical resolution averages about 4 km fo temperature and moisture.

Soundings for 6 March 1982 were prepared with a physical retrieval scheme (Smith, 1983) using an LFM forecast to provide a first guess.

The characteristics of VAS soundings for this day have been extensively discussed by Jedlovec (1985) and Fuelberg and Meyer (1986) and compared to concurrent RAOB soundings from special network stations. Figure 1a, b shows the mean temperature and geopotential error structure (satellite vs RAOB) as a function of pressure for our investigation time of 1445 UTC. A low-level warm bias (negative values) is evident from the surface to about 800 mb in the satellite retrievals. Above this level a strong cold bias exists to about 600 mb where a moderate warm bias takes over in tropo-

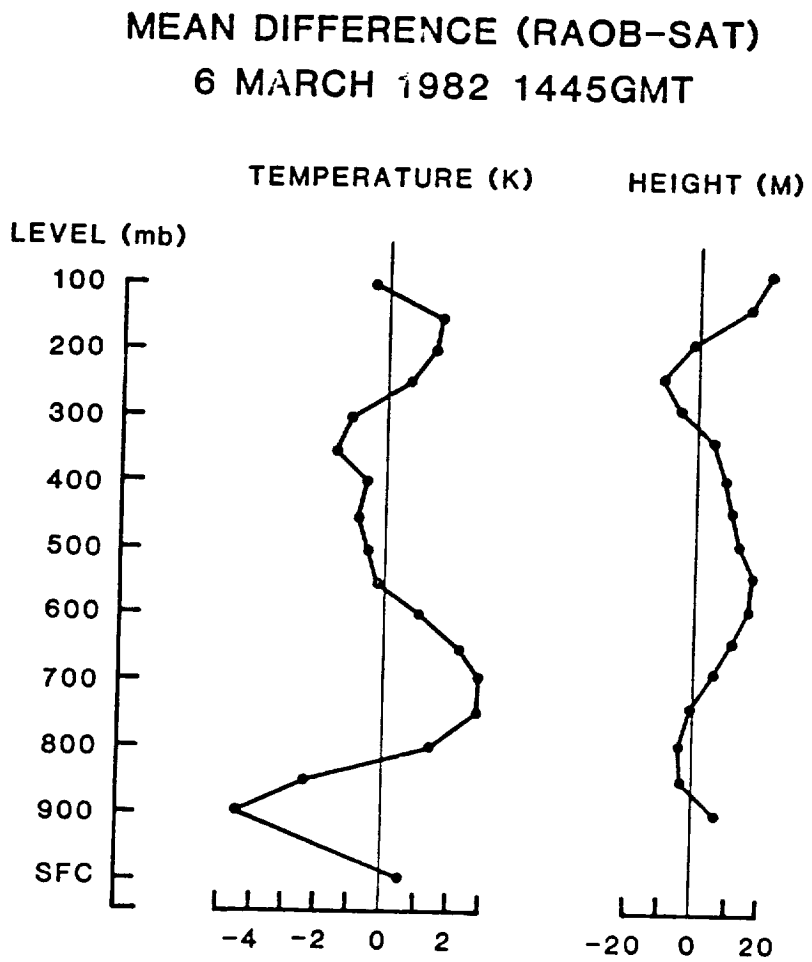

FIG. 1. (a) Mean error structure of temperature (K) for VAS vs special network RAOB for 1445 UTC 6 March 1982; (b) as in (a) except for geopotential (gpm).

pause levels. Geopotential thickness errors (thickness derived from the temperature profiles) may add or cancel depending on the vertically integrated temperature profile. For 1455 UTC we see in Fig. 1 that the dominant feature in geopotential is a negative bias (positive RAOB-satellite values) from 800 to almost 300 mb.

4. Synoptics—6 March 1982

Figure 2a shows a conventional 500 mb RAOB height analysis (also analysis and forecast model domain) for 1200 UTC 6 March; and Figs. 2b and c indicate the corresponding surface and 700 mb dewpoint analyses, respectively. Conditions for this day have been discussed by Jedlovec (1985). The case is marked by a developing frontal wave in the southeast United States with a significant thickness and dewpoint gradient back through the Texas region. The system was the cause of convective activity in the southeast later in the day. Behind this frontal system, a shallow high pressure system was present around western Oklahoma. To the north, a cold front from a low pressure system in Canada was pushing south through the upper plains.

5. The experiments

Two analyses using VAS data were made at the 1445 UTC VAS observation time on 6 March. The first analysis was made incorporating only scalar VAS thicknesses as input into the variational analysis scheme. No horizontal geopotential gradient information, either from VAS measurements or derived from wind information, was used in this analysis. The second analysis for this time was made using only horizontal geopotential gradient information from the VAS as input to the variational functionals (Equations 1 and 2) and no scalar geopotential information. Dewpoint temperatures for these two analyses were identical, both being standard SCM analyses from the scalar VAS information. An analysis was also done at 1500 UTC 6 March using the special network RAOB soundings, to be used as verification for the 1445 UTC VAS analyses. The first-guess fields for the two VAS analyses and the special network analysis were provided by an SSM forecast to 1500 UTC made from a RAOB analysis at 1200 UTC (Fig. 2).

A control forecast of 12 h duration was made from the 1200 UTC RAOB analysis. Two forecasts were made from the 1445 VAS standard and gradient analyses to the same time (0000 UTC 7 March). A third forecast, 1445 to 0000 UTC, was also made using the gradient geopotential analysis with the first-guess (1500 UTC control forecast) moisture field to assess the relative roles of mass versus moisture information on precipitation simulations. Lastly, a RAOB analysis was also done at 0000 UTC to be used as verification for these forecasts.

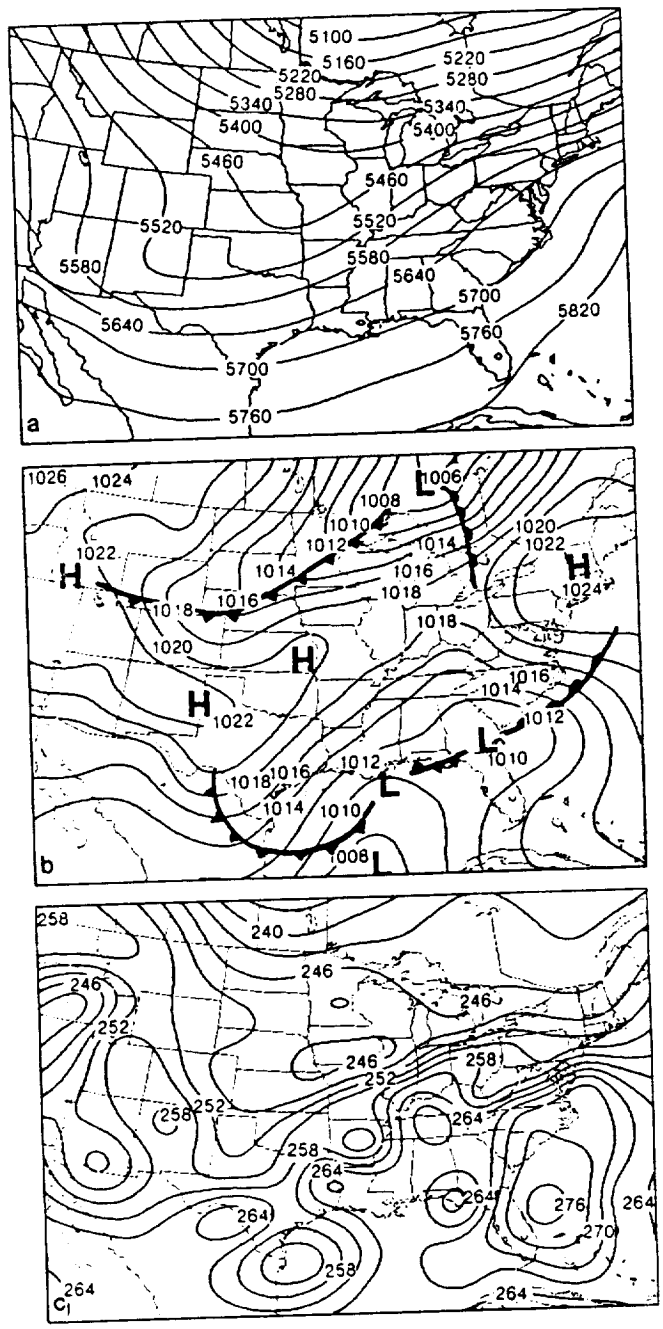

FIG. 2. (a) 500 mb height (gpm) and temperaure (K) analysis from conventional RAOB observations 1200 UTC 6 March 1982; (b) surface analysis 1200 UTC 6 March 1982; (c) dewpoint analysis (K) 1200 UTC 6 March 1982.

6. Results

a. *VAS analyses*

Figure 3a–d shows the VAS standard and gradient analyses at 1445 UTC, the 500 mb special network RAOB analysis at 1500 UTC, and the guess field (1500 UTC control forecast) for these analyses. Data points on Figs. 3a and b are VAS retrieval locations, while those on Fig. 3c are special network sounding locations.

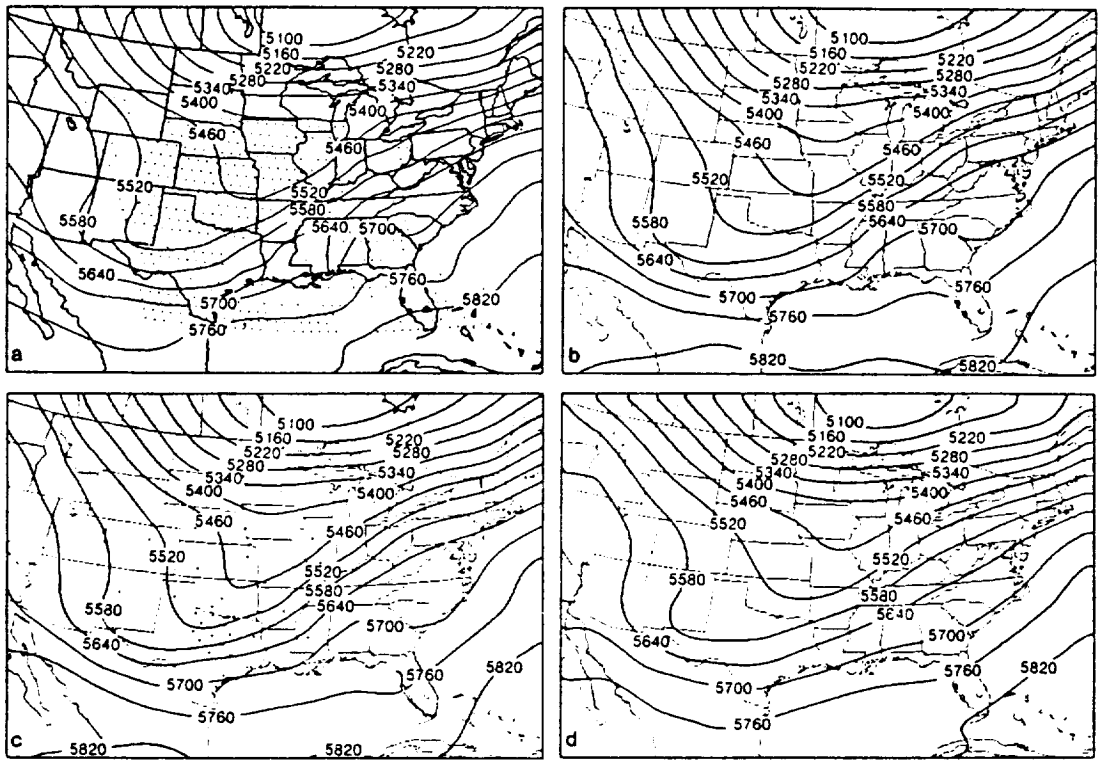

FIG. 3. (a) The VAS standard 500 mb analysis and VAS sounding location 1445 UTC 6 March 1982; (b) VAS gradient 500 mb analysis; (c) 500 mb special network analysis 1500 UTC 6 March 1982 and special network sounding locations; (d) 500 mb 1500 UTC control simulation (first-guess field).

Some of the potential problems in incorporating VAS soundings into synoptic analyses have been discussed by Cram and Kaplan (1985) and others. These include bias errors and potential discontinuities between data and no-data regions. Both of these problems are seen in the standard VAS analysis at 1445 UTC. In the region of the special network data coverage, we see that the VAS standard analysis (Fig. 3a) has 500 mb heights which are biased as much as 30 m low compared with the special network analysis (Fig. 3c). Some evidence of discontinuity (problems of the analysis model in reconciling the data with the guess field) is evident in the Colorado region. The problem is exacerbated by the fact that the first-guess field (Fig. 3d) shows some positive geopotential bias at 500 mb compared to the special network analysis. A stronger discontinuity is evident in the southeastern United States, where the combination of biased VAS data and poor data distribution presents a difficult analysis problem.

Figure 3b is the VAS gradient analysis at 1445 UTC. The discontinuities evident in the VAS standard analysis have been eliminated here, perhaps at the price of somewhat oversmoothing this 500 mb height field. The gradient analysis has modified the guess field in the correct direction in the special network region, reducing the positive bias. Gradients appear fairly well represented although the gradient analysis has produced a flattening of gradients in central Texas and a smoothing of some of the trough features in the Nebraska–Oklahoma region. Jedlovec (1985) has noted a general reduction in horizontal gradients from the VAS compared to special network RAOB data for this day, which is a partial cause of the problem. Also contributing is the inherent smoothing in calculating gradients over finite grid element lengths. A short wave feature has been created in the southeast United States in the gradient analysis which is outside of the special network domain and cannot be verified.

Figure 4a, b shows differences, respectively, between standard and gradient analyses and the special network analysis for the special network verification domain. As shown in this figure for both standard and gradient analyses, the maximum errors in the verifiable region were in the east, where there was a combination of a large VAS data gap and a maximum in the guess field error.

Table 1 shows biases, standard errors and S1 skill scores for the standard and gradient analyses versus the special network analysis over the special network domain. As seen in this table and visually in Fig. 4, the gradient approach to VAS data assimilation has greatly reduced the errors produced by strongly biased information.

b. VAS forecasts

Forecasts of 500 mb geopotential valid at 0000 UTC 7 March are compared in Fig. 5a, d. Figures 5a and b are forecasts from the VAS standard and VAS gradient

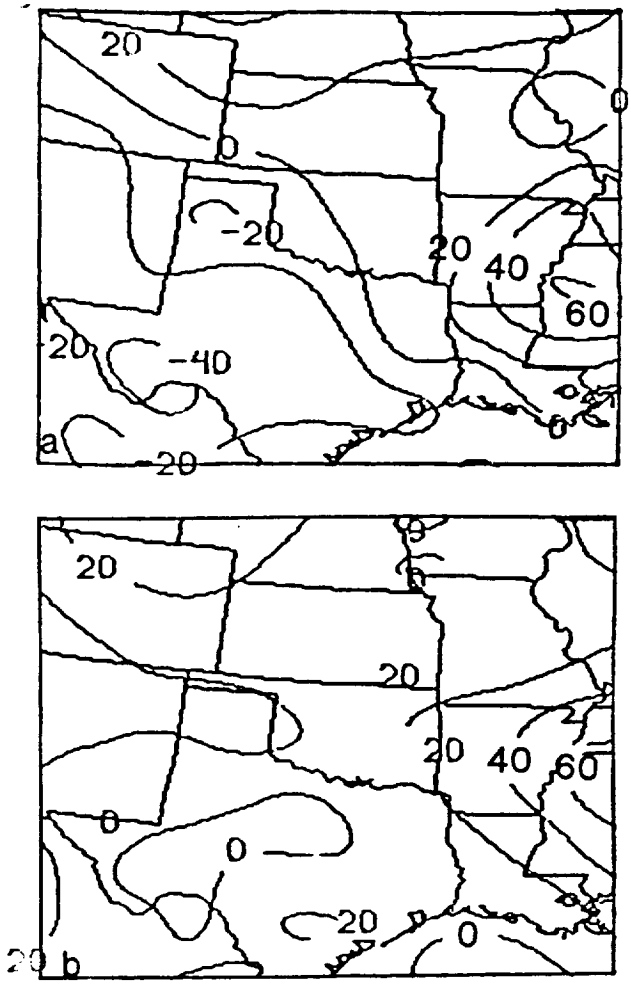

FIG. 4. (a) Difference between VAS standard analysis and special network analysis at 500 mb; (b) difference between VAS gradient analysis and special network analysis at 500 mb.

analyses, respectively, done at 1445 UTC, and Fig. 5c is the control forecast of 12 h duration made from the synoptic analysis at 1200 UTC 6 March. Figure 5d is the verifying synoptic analysis for these forecasts at 0000 UTC 7 March.

Many of the differences evident between gradient and standard analyses have been smoothed out in the subsequent forecast process and only more subtle differences are evident. The wavelength of the trough has been shortened by both VAS forecasts compared to the control and verification. Both have the trough somewhat too deep in the mid-Texas region, with the standard forecast slightly worse, probably due to the negative geopotential biases which existed in its initial analysis. Geopotentials in the southern Illinois and Missouri region appear to be somewhat better in the gradient versus standard forecast.

The control forecast is generally good, but exhibits somewhat weaker gradients than the verification along the trough axis and some positive bias in the northern Texas region. Intuitively, it is difficult to call any one of these forecasts superior to the others.

Biases, standard errors and S1 skill scores for these three forecasts versus the 0000 UTC synoptic analysis are shown in Table 2 for a region encompassing the VAS data points which are shown in Fig. 3a. These statistics bear out the intuitive evaluation of a mixed set of results from these forecasts. For clarity of presentation, the gradient statistics have been marked in Table 2 where they have outperformed the standard and/or control forecasts. As shown, the gradient forecast clearly outperforms the standard forecast, with the most impact being in S1 skill scores and standard error statistics. In the gradient versus control forecast, improvements are noted in biases at many levels, while standard error comparisons between the two are more mixed. The S1 skill scores between gradient and control forecasts are always within about one percentage point of each other; however, at no level is the gradient forecast able to outperform the control in this comparison with a verification analysis made using synoptic-scale data.

Other investigators (Gal-Chen et al., 1986; Cram and Kaplan, 1985; Mills and Hayden, 1983; and others) have similarly found small impact of subsynoptic scale satellite soundings on primary forecast fields for the continental United States. Mills and Hayden (1983), however, found significant impact on forecasts of precipitation, dewpoint and vertical motion and it thus appears worthwhile to examine these fields and their interrelationships also.

Precipitation patterns for the three forecasts for land areas are shown along with verification in Fig. 6a–d, and it can be seen that indeed some significant differences exist. Precipitation in the SSM is produced by a combination of large-scale supersaturation removal and/or convection parameterized with a Kuo-type scheme (Kuo, 1965). In prior sensitivity experiments (Diak et al., 1986), changes in convective precipitation for this model between similar forecasts were shown to be most dependent on changes in surface moisture convergence, which is the forcing term for the Kuo parameterization. In the 6 March experiments described here, while there were some areas of large rel-

TABLE 1. Biases, standard errors, and S1 skill scores for 1445 UTC standard and gradient analyses vs 1500 UTC special network analysis.

	Standard analysis			Gradient analysis		
Level (mb)	Bias (m)	SE (m)	S1	Bias (m)	SE (m)	S1
1000	2.21	7.65	31.18	2.24	7.59	30.41
850	6.25	23.00	65.99	2.32	9.17	33.32
700	−1.38	20.14	40.99	0.57	10.36	25.57
500	−13.69	19.82	26.15	−1.59	10.35	12.96
400	−23.84	20.36	24.88	−2.17	12.38	12.71
300	−32.66	22.62	24.82	−2.14	14.29	11.44
250	−26.63	26.78	26.75	−0.63	14.81	10.32
100	−29.95	29.52	28.17	−2.83	14.17	11.69
150	−49.61	30.14	33.80	−4.06	14.09	13.65
100	−60.48	31.12	46.33	−3.99	13.29	17.89

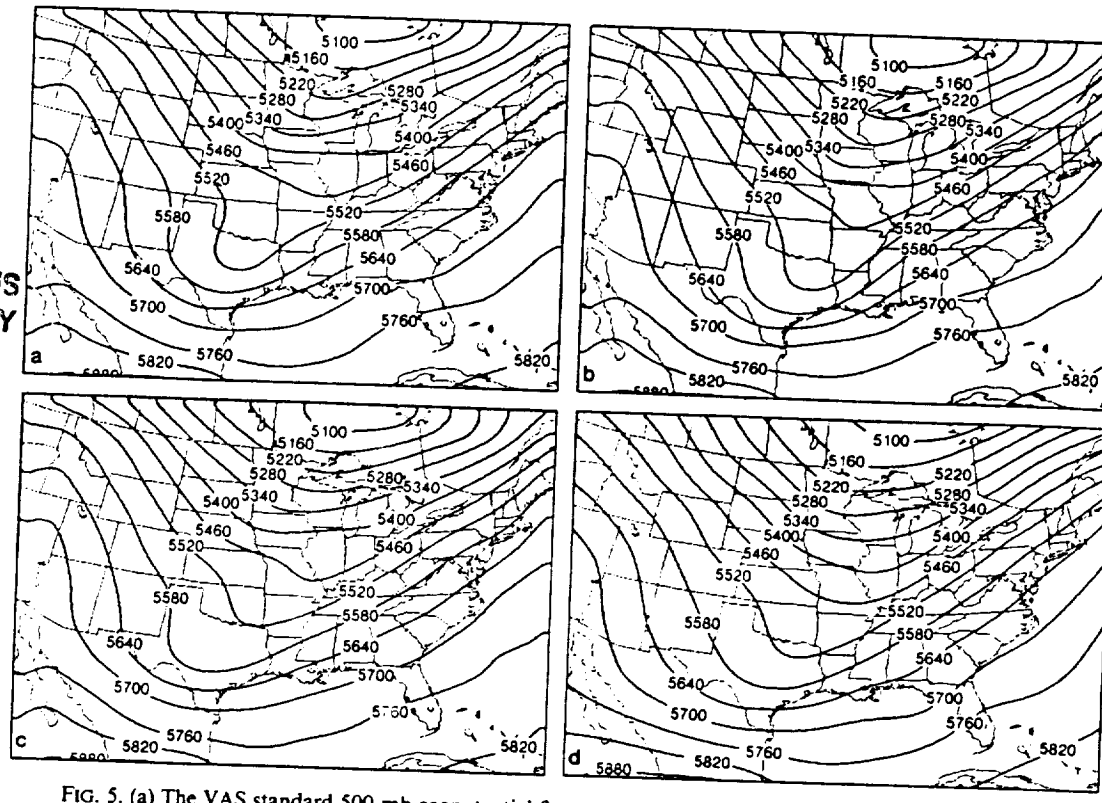

FIG. 5. (a) The VAS standard 500 mb geopotential forecast 1445–0000 UTC; (b) as in 5a, except gradient forecast; (c) as in 5a, except control forecast; (d) synoptic 500 mb analysis 0000 UTC 7 March 1982.

ative changes of convective precipitation between forecasts, it was large-scale precipitation which dominated both regional and overall model totals and produced the patterns shown in Fig. 6. Accordingly, we look to differences in the dewpoint and vertical motion fields as being responsible for these precipitation changes. Vertical motion fields at 1800 UTC ($\dot{\sigma}$ at $\sigma = 0.49$, approximately 500 mb for no terrain) are shown in Fig. 7 for the two satellite forecasts and the control. The dewpoint analysis for the satellite forecasts, the 1500 UTC guess field (control forecast) for this analysis and the 1500 UTC special network dewpoint analysis are shown in Fig. 8a–c.

Precipitation patterns from the control forecast (Fig. 6c) are reasonable, but several deficiencies are evident. South of Lake Erie, large amounts of precipitation are predicted where verification shows a smaller area of lesser accumulation. Precipitation along the southeast front is not as well defined as the verification indicates, and maxima are reduced and somewhat misplaced.

The standard forecast shows a minor reduction in the northeast maximum predicted in the control fore-

TABLE 2. Biases, standard errors, and S1 skill scores for standard, gradient and control forecasts vs verifying 0000 UTC synoptic analysis.

Level (mb)	Standard fcst			Gradient fcst			Control fcst		
	Bias (m)	SE (m)	S1	Bias (m)	SE (m)	S1	Bias (m)	SE (m)	S1 (m)
1000	23.90	20.03	79.29						
850	29.67	16.76	66.32	17.38†*	17.89†	68.26†	17.56	15.57	63.28
700	19.98	16.11	37.57	21.61†*	16.10†	58.76†	22.06	15.23	54.39
500	5.18	16.63	21.38	13.01†*	14.55†*	31.54†	17.18	16.27	31.14
400	−6.54	24.27	23.06	−0.16†*	18.06*	20.91†	11.27	24.52	19.32
300	−17.96	34.03	21.69	−8.85	23.65†*	20.88†	2.63	34.33	19.46
250	−7.49	33.29	21.15	−18.96	32.7†*	19.80†	−8.81	33.62	18.56
200	3.42	31.45	22.01	−7.78	30.96†*	18.92†	0.98	31.79	17.81
150	0.75	28.42	24.37	5.13*	30.26†	19.39†	11.92	24.08	18.50
100	13.99	27.60	30.11	5.68*	25.52†	20.67†	10.13	19.62	19.33
				23.73*	20.85†	22.93†	25.98	9.99	21.56

† Outperformed standard forecast.
* Outperformed control forecast.

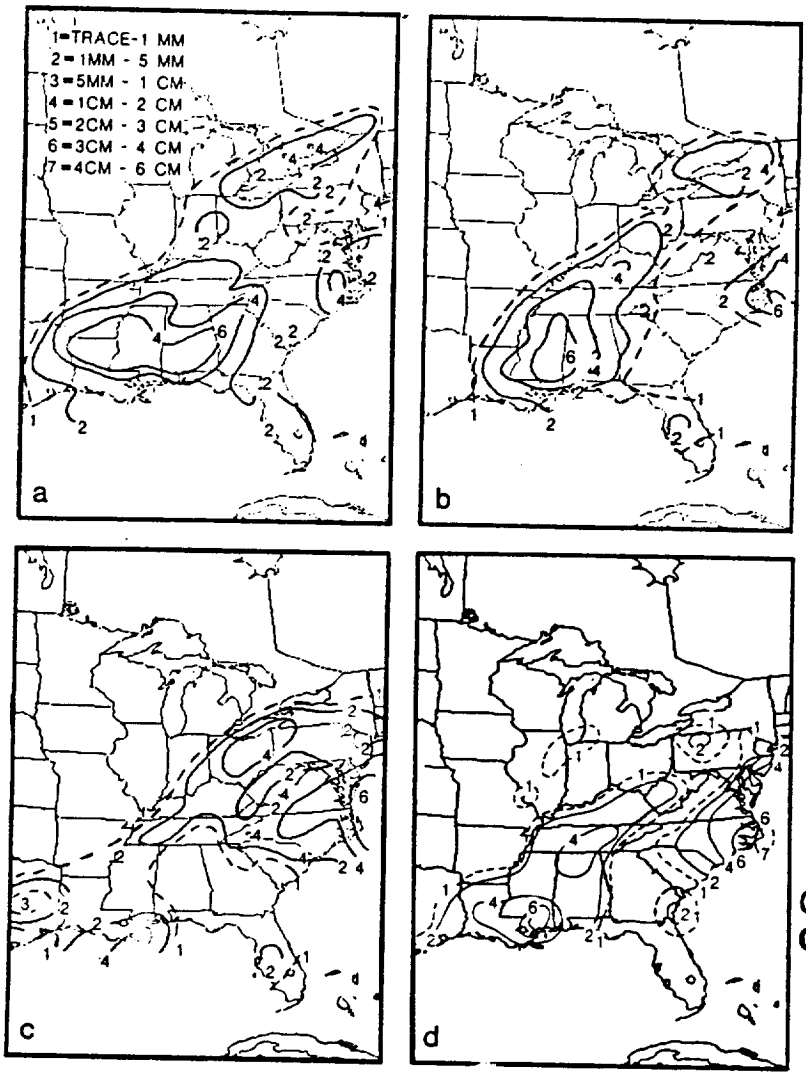

FIG. 6. (a) The VAS standard forecast of precipitation; (b) as in 6a except gradient forecast; (c) as in 6a except control forecast; (d) 1200–0000 UTC Service A precipitation totals.

cast, but the frontal precipitation in the southeast is grossly overpredicted and the axis has been unrealistically elongated due to a spurious maximum in Louisiana through east Texas. As can be seen in Fig. 7a, the precipitation in this area exactly coincides with a large predicted area of intense vertical motion. Recall that in the analysis used to initialize this forecast, this was an area of discontinuity caused by data biases and guess-field error. It is likely that mass adjustments in this presumably sensitive cold frontal region have initiated the vertical motion and precipitation. Evidence of these adjustments was seen in large surface pressure oscillations in the region in the first several hours of this forecast. Similar to Cram and Kaplan (1985) findings, these oscillations were significantly reduced in the gradient assimilation.

The gradient forecast of precipitation (Fig. 6b) is, in general, acceptable with the frontal precipitation sharply defined and bearing a close resemblance to the verification in this region. The vertical motion patterns and precipitation do not show the problem associated with the standard forecast and also appear more well defined than the control simulation. In the northeast, however, the overprediction of precipitation has been only slightly reduced from the control run.

To better clarify the roles of moisture and vertical motion in the changes in precipitation between forecasts, one additional 1445–0000 UTC simulation was made (gradient-1 experiment) using the gradient geopotential analysis at 1445 UTC, but retaining the moisture fields from the first guess (1500 UTC control forecast, Fig. 8b). Thus, this forecast has new satellite mass, but no moisture information.

In the frontal region, the precipitation and vertical motion patterns from this new forecast very closely resembled that of the gradient experiment. It is evident from a comparison of the 1445 UTC satellite moisture analysis with the guess field and the special network

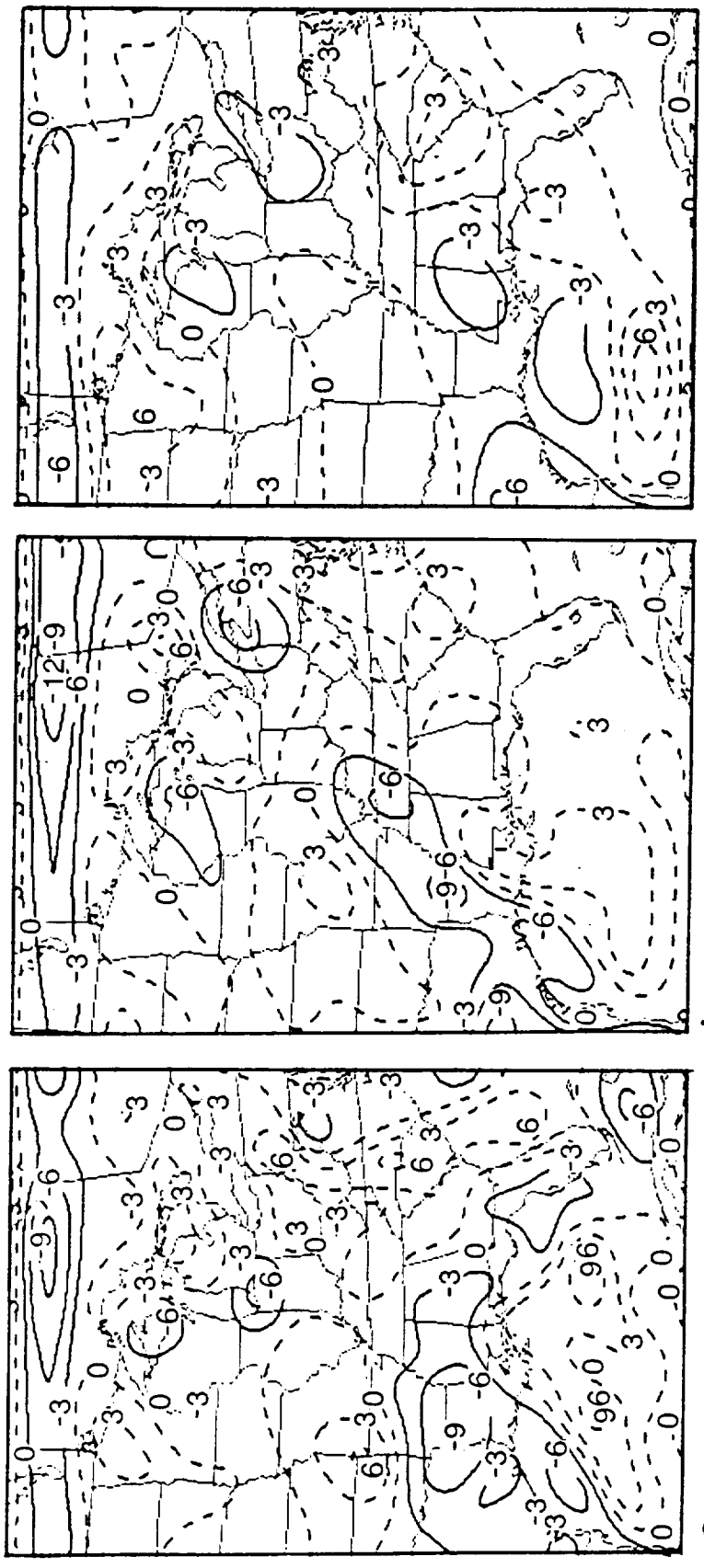

FIG. 7. (a) vertical motion ($\dot{\sigma}$ at $\sigma = 0.49$, approximately 500 mb) 1800 UTC from VAS standard forecast ($sec^{-1} \times 10^6$, negative upward); (b) as in 7a except gradient forecast; (c) as in 7a except control forecast.

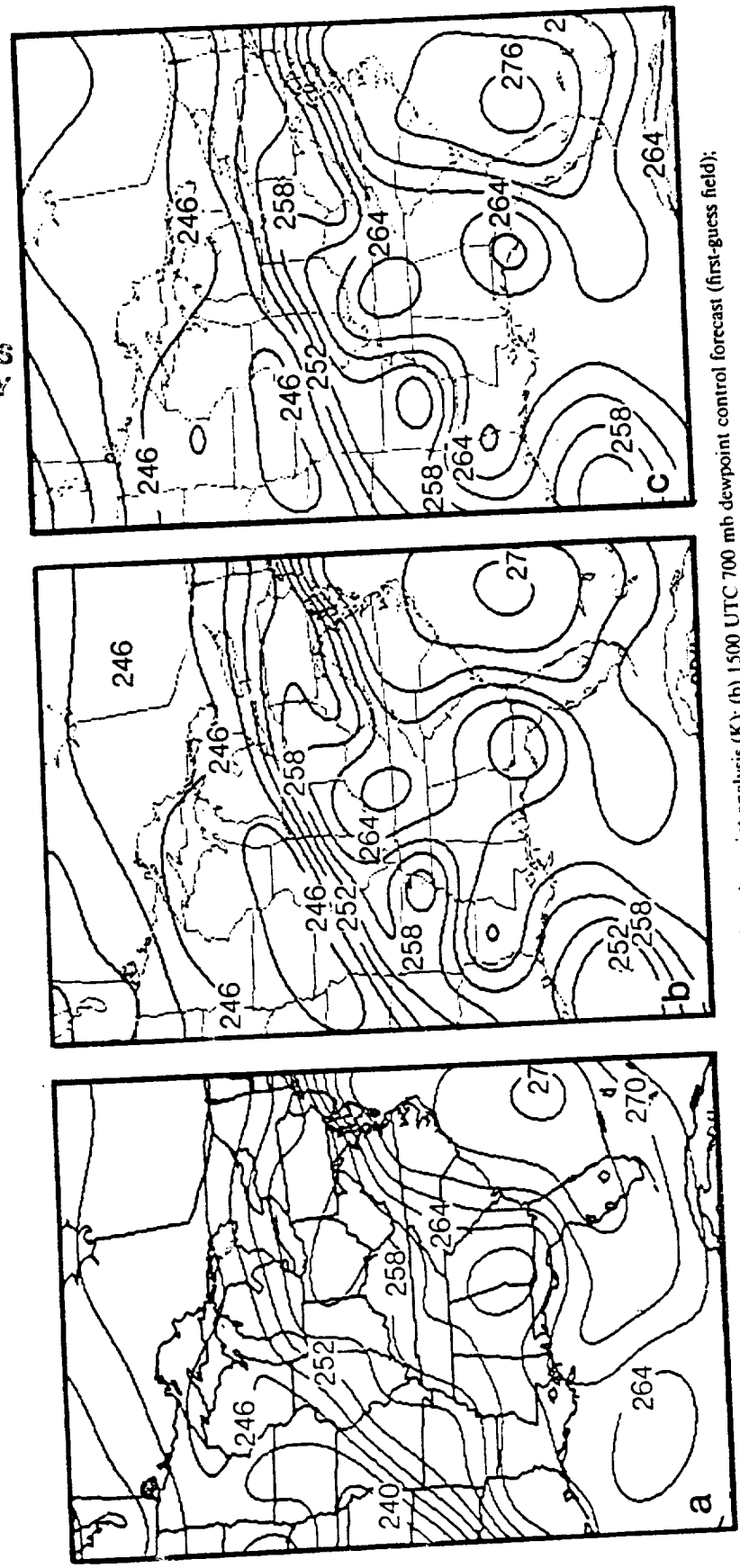

FIG. 8. (a) The 1445 UTC 700 mb standard and gradient dewpoint analysis (K); (b) 1500 UTC 700 mb dewpoint control forecast (first-guess field); (c) 1500 UTC 700 mb dewpoint special network analysis.

analysis moisture (Fig. 8), that the satellite information did improve moisture gradients in this region. The gradient-1 experiment suggests, however, that it was the mass information from VAS and the subsequent vertical motion prediction which were responsible for the well-defined precipitation patterns in the original gradient forecast.

Although VAS soundings in the northeast were sparse and poorly distributed, evidence points here to VAS dewpoint information as the cause for the small reduction in the precipitation maximum in the standard and gradient forecasts versus the control. As shown in Fig. 8, the dewpoint values as well as horizontal gradients in the region have been somewhat reduced in the VAS analysis versus the guess field. The 0000 UTC synoptic analysis showed a similar weakening of dewpoint gradients. While the gradient forecast had upward vertical motion which was as strong as the control in this area (Fig. 7), there was still a reduction in precipitation in this forecast, suggesting predominance of the dewpoint information. Additionally, the gradient-1 forecast, without any satellite moisture information, displayed precipitation in the region which was very similar to the control simulation, adding evidence that moisture information was responsible in this case for the precipitation changes between experiments.

7. Conclusions

A comparison has been made between analyses and forecasts which incorporate VAS geopotential information by scalar and gradient variational assimilation methodologies. For this case of 6 March 1982, a day on which the VAS data exhibited strong biases in geopotential, the gradient methodology clearly outperformed the standard in error statistics for the 1445 UTC comparison of analyses to special network RAOB observations. The gradient forecast outperformed the standard scalar methods in most statistical comparisons and was about the same as a control simulation made without satellite data for overall quality of the geopotential forecast. Effects were noted in the gradient forecast versus both the standard and control forecasts in vertical motion patterns and the prediction of precipitation.

The case is especially encouraging because it is a "worst case scenario" for VAS data—namely, a case in which there were very significant data problems, but in which appropriate assimilation methodologies resulted in an analysis/forecast which was, at worst, not degraded from a control comparison and in some respects was improved. Further work will be aimed at concurrently optimizing the gradient assimilation methodology and the VAS sampling strategy to extract the most information from the observing and assimilation systems.

Results from this study suggest that a potentially powerful observing system may be a combined RAOB and satellite system, with the RAOB observations used to establish synoptic-scale scalar values of observables and satellites defining the mesoscale gradients.

Acknowledgments. This work was supported by the NASA Marshall Space Flight Center Contract NAS8-34732. Thanks to Gary Jedlovec for both helpful discussions and Fig. 1 and to the people in the NESDIS/SDAB at Wisconsin for their assistance and advice.

REFERENCES

Corby, G. A., A. Gilchrist and R. L. Newson, 1972: A general circulation model of the atmosphere suitable for long period integrations. *Quart. J. Roy. Meteor. Soc.*, **98**, 809–832.

Cram, J. M., and M. L. Kaplan, 1985: Variational assimilation of VAS data into a mesoscale model; assimilation method and sensitivity experiments. *Mon. Wea. Rev.*, **113**, 467–484.

Cressman, G., 1959: An operational objective analysis system. *Mon. Wea. Rev.*, **87**, 367–374.

Diak, G. R., S. Heikkinen and J. Bates, 1986: The influence in surface treatment on 24-hour forecasts with a limited area model, including a comparison of modeled and satellite-measured surface temperatures. *Mon. Wea. Rev.*, **114**, 215–232.

Fuelberg, H. E., and P. J. Meyer, 1986: An analysis of mesoscale VAS retrievals using statistical structure functions. *J. Climate Appl. Meteor.*, **25**, 59–76.

Gal-Chen, T., B. D. Schmidt and L. W. Uccellini, 1986: Simulation experiments for testing the assimilation of geostationary satellite temperature retrievals into a numerical prediction model. *Mon. Wea. Rev.*, **114**, 1213–1230.

Hammarstrand, U., 1977: On the parameterization of convection for large scale numerical forecasts at midlatitudes. *Contrib. Atmos. Phys.*, **50**, 78–88.

Hill, C. K., and R. E. Turner, 1983: NASA's AVE/VAS Program. *Bull. Amer. Meteor. Soc.*, **64**, 796–797.

Jedlovec, G. J., 1985: An evaluation and comparison of vertical profile data from the VISSR Atmospheric Sounder (VAS). *J. Atmos. Oceanic Technol.*, **2**, 559–581.

Kuo, H. L., 1965: On the formation and intensification of tropical cyclones through latent heat release by cumulus convection. *J. Atmos. Sci.*, **22**, 40–63.

LeMarshall, J. F., W. L. Smith and G. M. Callan, 1985: Hurricane Debbie—an illustration of the complimentary nature of VAS soundings and cloud and water vapor motion winds. *Bull. Amer. Meteor. Soc.*, **66**, 258–263.

McGregor, J. L., L. M. Leslie and D. J. Gauntlett, 1978: The ANMRC limited area model: Consolidated formulation and operational results. *Mon. Wea. Rev.*, **106**, 427–438.

Mills, G. A., and C. M. Hayden, 1983: The use of high horizontal resolution satellite temperature and moisture profiles to initialize a mesoscale numerical weather prediction model—a severe weather event case study. *J. Climate Appl. Meteor.*, **22**, 649–663.

Sasaki, Y., 1970: Some basic formalisms in numerical variational analysis. *Mon. Wea. Rev.*, **98**, 875–910.

Seaman, R. S., R. L. Falconer and J. Brown, 1977: Application of a variational blending technique to numerical analysis in the Australian region. *Aust. Meteor. Mag.*, **25**, 3–23.

Smith, W. L., 1983: The retrieval of atmospheric profiles from VAS geostationary radiance observations. *J. Atmos. Sci.*, **40**, 2025–2035.

——, V. E. Suomi, W. P. Menzel, H. M. Woolf, L. A. Sromovsky, H. E. Revercomb, C. M. Hayden, D. N. Erickson and F. R. Mosher, 1981: First sounding results from VAS-D. *Bull. Amer. Meteor. Soc.*, **62**, 232–236.

Suomi, V. E., T. Vonder Haar, R. Krauss and A. Stamatin, 1971: Possibilities for sounding the atmosphere from geosynchronous spacecraft. *Space Research IX*, 609–617.

REPRINTED FROM THE SECOND INTERNATIONAL CONVERENCE ON INTERACTIVE INFORMATION AND PROCESSING SYSTEMS FOR METEOROLOGY,OCEANOGRAPHY AND HYDROLOGY
MIAMI,FLORIDA JAN. 14-17,1986

10.11

THE ASSIMILATION OF SATELLITE DATA AND PRODUCTS INTO THE MCIDAS ANALYSIS/PROGNOSIS/DISPLAY SYSTEM

George R. Diak

Cooperative Institute for Meteorological Satellite Studies
Madison, Wisconsin

Graham A. Mills

Bureau of Meteorology Research Centre
Melbourne, Australia

Geary M. Callan

NOAA/NESDIS Systems Design and Applications Branch
Madison, Wisconsin

1. INTRODUCTION

The Man-computer Interactive Data Access System (McIDAS), as its name implies, developed in the 1970's as primarily a satellite data access and display system. Notable contributions were made in areas of cloud and water vapor drift winds, nowcasting products, satellite soundings, earth radiation budgets, planetary atmospheres and many others. The potential of the original system, however, was limited by its computer architecture; that is several smaller computers sharing a data base with each driving several display terminals. Recently the research emphasis has been expanded with a change in computer strategy to one mainframe CPU (IBM 4381) driving all McIDAS terminals.

This availability of the mainframe has allowed expansion into applying some of the research products for synoptic and mesoscale analysis and forecasting. A primary research goal is to determine the potential benefit of satellite data and derived products for such applications. To date, research efforts have concentrated on techniques for assimilation of satellite soundings, cloud drift and water vapor drift winds and satellite-derived surface energy balance descriptors in numerical analyses and prognosis. Concurrent with this research effort is the development of a prototype "4-d" assimilation scheme to examine the feasibility of regular updating of a forecast model with satellite and other asynoptic information; the goal being the best possible continuous description of atmospheric state combining data from all observing systems.

2. DATA AND PRODUCTS

2.1 VAS Soundings

The success of the VISSR Atmospheric Sounder (VAS) experiment as proposed by Suomi et al. (1971) has been the result of close collaboration between scientists and engineers from the University of Wisconsin, NASA, NOAA Santa Barbara Research Center and Westinghouse. The first in a series of instruments was put into geostationary orbit aboard the GOES-D satellite (Smith et al., 1981).

The VAS is a radiometer possessing eight visible channel detectors and six thermal detectors which sense atmospheric radiation in 12 spectral bands whose wavelengths lie between 3.9 and 15 μm. Typical space and time resolution (in clear areas) are 50 km and three hours, respectively. The soundings are produced in real time at the Cooperative Institute for Meteorological Satellite Studies (CIMSS) at the University of Wisconsin using a full physical iterative solution of the radiative transfer equation. The general qualities of similar VAS soundings are described in Velden et al. (1984) and Jedlovec (1984).

2.2 Cloud and Water Vapor Drift Winds

Cloud and water vapor drift winds are also produced at the CIMSS on the McIDAS facility using the technique of Mosher (1978). This data base is generated from GOES half-hourly visible and infrared imagery and hourly water vapor imagery. Wilson and Houghton (1979) have estimated the standard error of the difference between cloud drift winds and rawinsonde reports at about 4.7 ms^{-1} Preliminary statistics for water vapor drift winds (Mosher and Stewart, 1981) show a standard error of about 8 ms^{-1}.

The height assignment of cloud drift winds relies heavily on the bi-spectral method of Mosher (1978). Height assignment of water vapor winds (mid-troposphere level) relies on the use of water vapor brightness temperatures and nearby environmental soundings.

2.3 Surface Energy Balance Descriptors

The description of surface energy budget parameters relies on the time change of

the VAS radiances or soundings from the lower atmosphere being a descriptor of the sensible heating at the surface (i.e., balance of sensible/latent heat). This information, calibrated through use of a surface-boundary layer model, is used to derive surface energy balance descriptors for prognosis models. Fig. 1 shows such a calculation and represents the non-dimensional ratio of sensible heat to net radiation at the surface both calculated from satellite data for a survey done in July 1981.

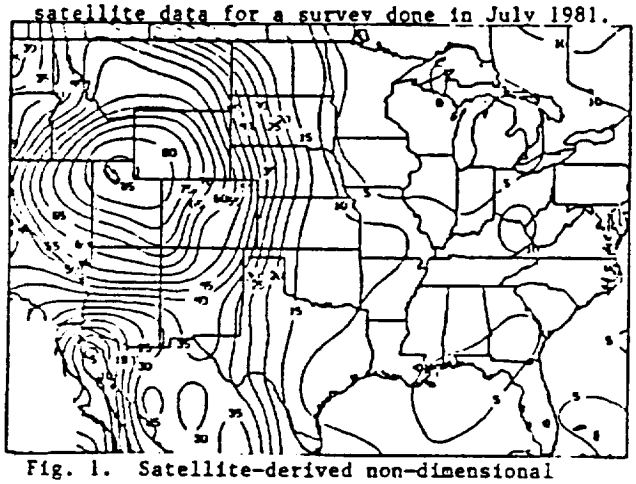

Fig. 1. Satellite-derived non-dimensional ratio of surface sensible heating to net radiation July 20, 1981.(Z X 100)

3. THE ANALYSIS SCHEME AND PROGNOSIS MODEL

The principal characteristics of the analysis scheme and forecast model used in this study are shown in Table 1.

3.1 Analysis Scheme

The analysis scheme uses a 51x61 point grid with a 67 km spacing, on a Lambert Conformal projection covering most of the continental U.S. The scheme is an adaptation to the North American region of the scheme written by R. S. Seaman at the Australian Numerical Meteorology Research Centre and is described in Mills and Hayden (1983). The analysis scheme uses the successive correction technique of Cressman (1959) to generate grid point fields from observations. Subsequent to this the variational blending techniques of Sasaki (1958, 1970) are used to combine fields of geopotential height, thickness and gradient (wind), weighted by their reliability, into an "optimal" analysis. The scheme uses an initial three-dimensional blend of 1000 mb and 250 mb height, gradient and thickness data to produce a bulk atmospheric structure.

Individual level geopotential analysis are then performed by blending the geopotential gradient analyses at a level with the analyzed thickness immediately above or below that level. This scheme is well-suited to the analyses of satellite temperature profiles and water vapor and cloud drift winds because geopotential thickness is a primary analysis variable, facilitating the assimilation of satellite temperature profiles into the objective analysis, while the variational blending ensures a consistent introduction of gradient (wind) information into the analysis. The blended geopotential fields and the gradient/geostrophic relationship are used to produce a wind field from which a stream function field is calculated by a variational blending procedure (Seaman et al., 1977). The forecast model commences its integration from this non-divergent field.

3.2 Prognosis Model

The forecast model is a ten level, 67 km resolution primitive equation model, originally written for the Australian Region (McGregor et al., 1978) and then adapted for use in the North American Region (Mills et al., 1981). The Australian Region version of the model is used operationally by the Australian Bureau of Meteorology. The North American version of this model is different in several respects. It uses the finite differencing scheme of Corby et al. (1972) to minimize truncation errors over steep topography. It uses a Kuo type convective parameterization (Kuo, 1965, 1974) which replaces the Arakawa-Schubert scheme described in McGregor et al. (1978) and it also has a comprehensive boundary layer scheme (Diak et al., 1986) using a similarity-theory surface layer coupled with vertical diffusion of heat, moisture and momentum at the three lower model levels, surface shortwave and longwave radiation modified by cloud and a surface energy balance evaluation.

Table 1

Principle Features of the Analysis Scheme and Prognosis Model

Analysis Scheme
Combination of successive correction method and variational blending in three dimensions.
Ten pressure levels, p = 1000, 850, 700, 500, 400, 300, 250, 200, 150 and 100 mb.
Horizontal resolution: 67 km
Fields analyzed or derived at each pressure level: - geopotential height - temperature - dewpoint - wind components - stream function
Prognosis Model
Primitive equations model in sigma coordinates.
Ten vertical levels at = 0.09, 0.19, 0.29,..0.99
Horizontal resolution: 67 km
Staggered horizontal (Arakawa "C") grid
Semi-implicit time differencing
Surface/boundary layer parameterization
Broad scale precipitation
Kuo-type convective parameterization
Updated boundary conditions

4. INFORMATION POTENTIAL

4.1 VAS Soundings

Fig. 2 (a-c) depicts a series of 500 mb geopotentials for the AVE/VAS day of March 6 1982 when high density space and time radiosonde data was available in the Texas region for confirmation of analyses and prognoses. Fig. 2a shows an analysis (with AVE sounding locations) made from this radiosonde data at 15 GMT. Fig. 2b is an analysis made for 1430 GMT readjusting the guess field (Fig. 2c) to match horizontal height gradient information from the VAS soundings in a version of the variational analysis methodology previously outlined (gradient data points are also depicted on Fig. 2b). The guess field (Fig. 3c) for both analyses is a forecast to 15 GMT made from a conventional network radiosonde analysis at 12 GMT.

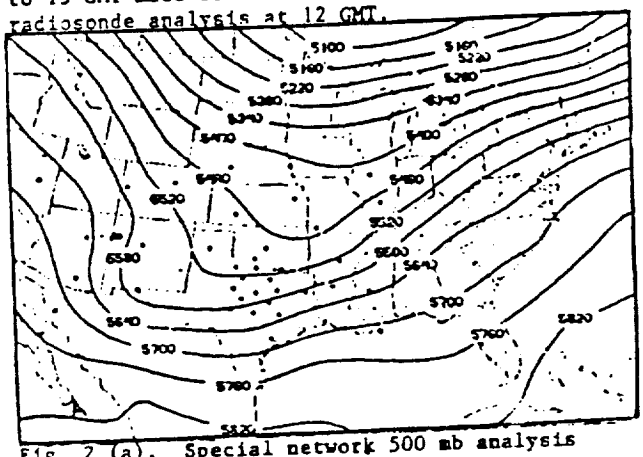

Fig. 2 (a). Special network 500 mb analysis 1430 GMT March 6, 1982.

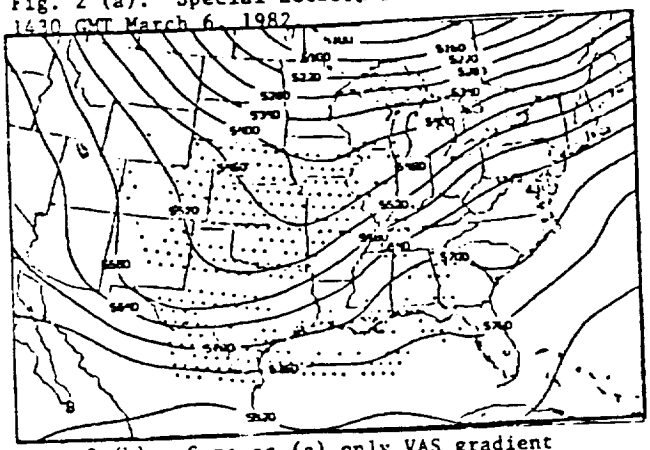

Fig. 2 (b). Same as (a) only VAS gradient analysis.

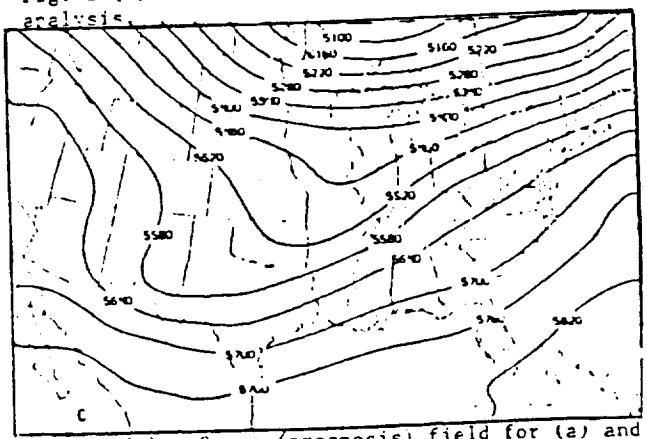

Fig. 2 (c). Guess (prognosis) field for (a) and (b).

Comparing these figures, we see that the VAS gradient analysis has corrected some of the guess field's high geopotential bias within the data domain and brought the fields into better agreement with the special network radiosonde analysis, perhaps at the price of some over-smoothing of the field. While the VAS soundings themselves for this time were significantly biased, the gradient assimilation methodology has greatly reduced these problems for analysis of the data.

A forecast from this VAS analysis (1430-00 GMT) demonstrated similar skill as a control forecast (1200-00 GMT) in geopotentials. Improvements in precipitation patterns were noted in the VAS forecast versus the control.

4.2 Cloud and Water Vapor Drift Winds

Fig. 3 (a-d) shows an analysis situation particularly impacted by the input of cloud and water vapor drift winds for a case study day of April 26, 1982 (Le Marshall et al., 1986). Inspection of satellite imagery for this day showed the presence of a small cut-off low at 500 mb which developed in the southern Illinois region between synoptic stations and synoptic times at about 1600 GMT and gradually weakened during the course of the day. The VAS soundings alone, done only in clear areas, were unable to depict this feature and it did not develop in a control forecast (1200-00 GMT) made from synoptic data. Using cloud and water vapor drift winds, however, in analyses we were able to capture this feature and, in part, its time evolution.

On April 26, Fig. 3 (a-d) shows VAS gradient plus water vapor and cloud drift wind analyses made for 1600, 1700, 1900 and 2000 GMT on this day with the satellite winds also shown. The influence of the wind data is evident and in principle it can be seen that the satellite sounding and wind data have complementary coverage with the former available only in clear areas and the latter mostly in cloudy regions.

5. THE 4-DIMENSIONAL ASSIMILATION SYSTEM

One of the assets of the McIDAS system is the efficient manner in which conventional and satellite data products are routinely ingested and processed. One of the greatest changes which has come about in recent years is the huge increase in volume of satellite products as the spatial and temporal sampling frequency of these instruments has increased, and interactive processing techniques have been refined. The challenge is to provide the best possible four-dimensional specification of the state of the atmosphere, utilizing the information content of these differing information sources, and allowing for the particular strengths and weaknesses of each one. That is, to allow the different data types to complement each other. This problem will be further exacerbated in the near future when an operational ground-based wind profiling network is implemented over the U.S., which will provide specification of the vertical wind profile with a high degree of accuracy, and with a hitherto unavailable sampling frequency.

A four-dimensional data assimilation scheme has been implemented on the McIDAS system, with the aim of (1) providing gridded

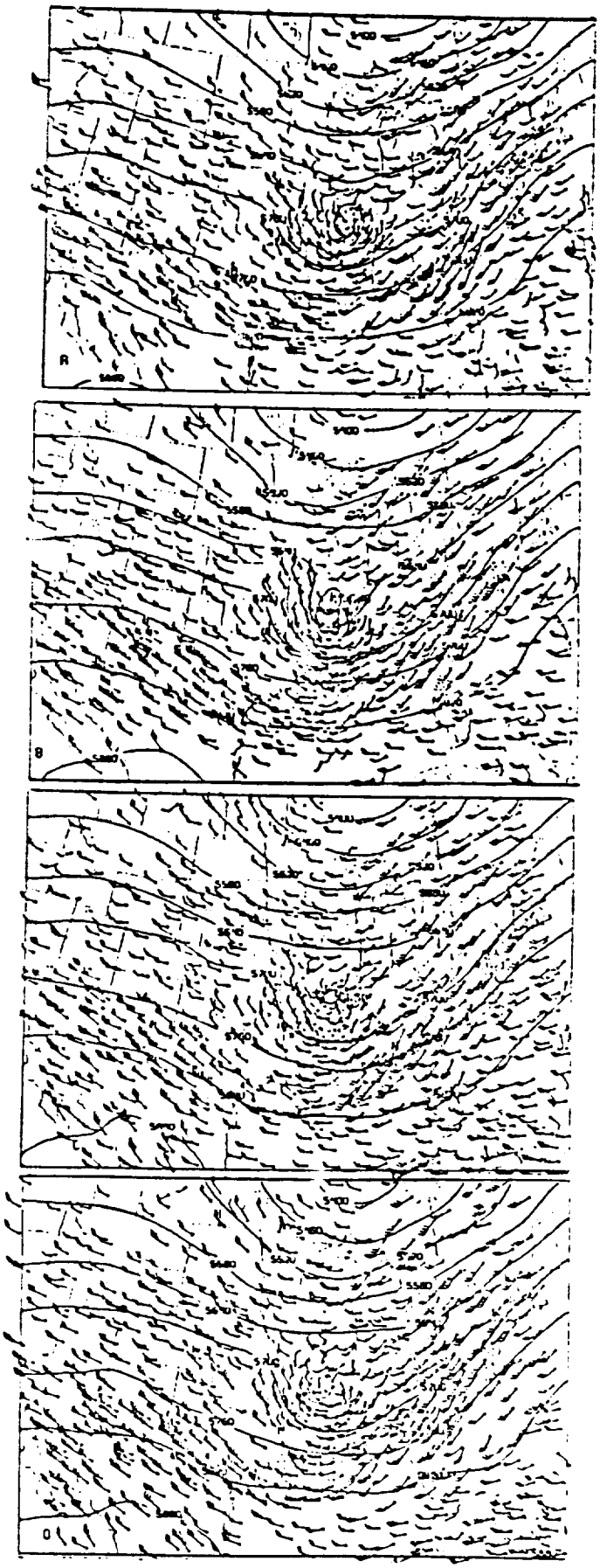

Fig. 3 (a-d). Analyses performed for 1600, 1700, 1900 and 2000 GMT April 26, 1982 with VAS gradient and cloud and water vapor drift wind input.

fields of primary atmospheric variables, utilizing all data available to the McIDAS system, for diagnostic studies, particularly during special effort field experiments such as GALE and STORM; (2) to provide guess fields for satellite retrieval processing during the assimilation; (3) to provide a vehicle for further investigation of the problem of assimilation of data from mixed sources at mesoscale resolution; and (4) to provide initial state specification for NWP data impact studies of significant weather events.

To achieve these aims, the system has been designed to have a variable grid spacing in the meso-α scale (i.e., 50-150 km), a time resolution (that is, analysis update frequency) of 3-12 hours, to have a variable domain, and to have the ability to merge data from all sources available at CIMSS. The chief components of the system are the three-dimensional variational analysis scheme described in Mills and Hayden (1983), but modified to include data-density dependent influence radii, an elliptical influence region for the moisture analysis, and an analysis of wind component deviations from the background field. The forecast model used to link the analyses in time is the new ARPE model (Leslie et al., 1985). The model is nested in a broad-scale forecast, has fully parameterized horizontal and vertical dimensions and includes a full suite of the so-called "physical parameterizations," and a vertical mode initialization scheme. Analysis increments are added to the model fields at each analysis time.

Care has been taken to keep the individual components of the system as modular as possible, so that they may be replaced by test modules for assimilation technique development, and a number of options are available. For example, the particular mix of data required is user specified from that available in McIDAS; the use of divergent or non-divergent winds for model initiation, the choice of wind law used to balance the mass and wind data, the selection of data rejection tolerances, maximum and minimum influence radii for each data type, and a wide range of prognosis model options are user specified.

Output products from the system include fields of mean sea level and surface pressure, surface temperature and dewpoint, and multi-level fields of divergent and non-divergent wind components, temperature, dewpoint, geopotential height, mixing ratio and vertical motion. In addition, a wide variety of diagnostic quantities can be derived from these fields using McIDAS applications software. All products are available on the McIDAS system.

So far, the scheme has been tested in an assimilation mode at three hour update frequency using the VAS temperature and moisture sounding and gradient wind data, the special network radiosonde data and the surface data from the March 6, 1982 situation, and at a 12-hour update frequency during a nine-day period of October 1985 using VAS temperature and moisture profiles and gradient winds, and cloud drift and water vapor winds prepared for the NHC, together with the radiosonde network data. In addition, a number of individual case studies taken from the 1985 hurricane season have been analyzed, with the domain being centered over the particular tropical storm on each day, and the resolution

(i.e., grid spacing) selected to complement the particular data distribution of the case. This domain and resolution selection is interactive. Figures 4 and 5 show examples of analyses produced in real time using the system. The differing domains were selected on the basis of the data distribution and the expected external forcing. Figure 4 shows the 200 mb flow pattern over Hurricane Elena, where the upper level outflow is well-defined by the cloud drift winds. Figure 5 shows the low level flow around Hurricane Bob, again with the cloud-drift winds shown.

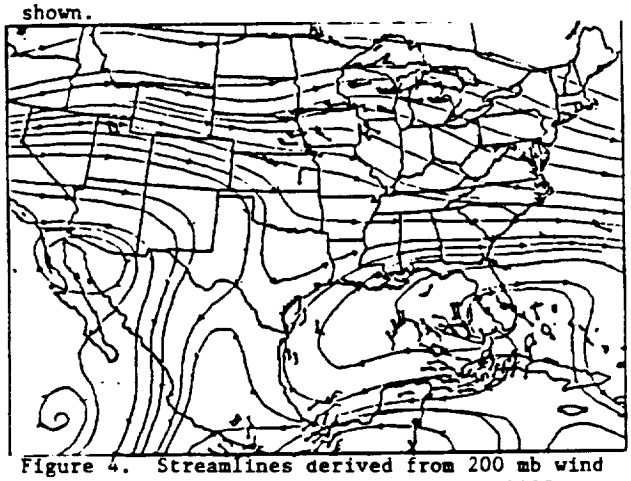

Figure 4. Streamlines derived from 200 mb wind component analyses at 12 GMT 29 August 1985, showing the outflow over Hurricane Elena. The cloud drift data near that level are overlain. Analysis grid spacing 150 km.

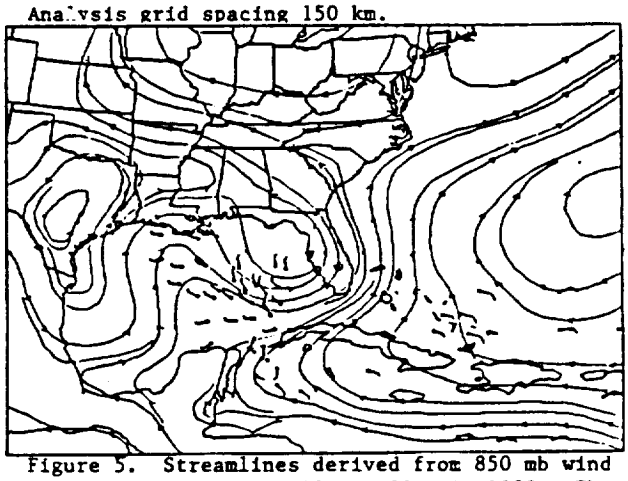

Figure 5. Streamlines derived from 850 mb wind component analyses at 12 GMT 23 July 1985. The cloud drift wind data shown over the Gulf of Mexico complemented the analysis of the low level vortex of Hurricane Bob.

6. ACKNOWLEDGEMENTS

Much of the work on VAS and satellite wind assessment has been funded through the NASA Marshall Space Flight Center Contract NAS8-34732. Surface energy budget work was sponsored by National Science Foundation Grant ATM-8218092.

7. REFERENCES

Corby, G. A., A. Gilchrist, and R. L. Newson, 1972. A general circulation model of the atmosphere suitable for long period integration. Quart. J. Roy. Meteor. Soc., 98, 809-832.

Cressman, G., 1959: An operational objective analysis system. Mon. Wea. Rev., 87, 367-374.

Diak, G. R., S. Heikkinen and J. Bates, 1986: The influence of variations in surface treatment on 24-hour forecasts with a limited-area model, including a comparison of modeled and satellite measured surface temperatures. Accepted for publication, Mon. Wea. Rev., Jan., 1986.

Jedlovec, G. J., 1984: A statistical evaluation and comparison of VISSR Atmospheric Sounder (VAS) data and corresponding rawinsonde measurements. NASA Technical Memorandum No. 82575, 11 pp.

Kuo, H. L., 1965: On formation and intensification of tropical cyclones through latent heat release by cumulus convection. J. Atmos. Sci., 22, 40-63.

Kuo, H. L., 1974: Further studies of the parameterization of the influence of cumulus convection on large scale flow. J. Atmos. Sci., 31, 1232-1240.

Lee, D. K., and D. D. Houghton, 1984: Impact of mesoscale satellite wind data on numerical model simulations: A case study. Mon. Wea. Rev., 112, 1005-1015.

Le Marshall, J. J., G. Diak, W. L. Smith, G. Callan and T. Stewart, 1986: Subsynoptic scale analysis and forecasting using VAS soundings and cloud and water vapor winds. Submitted to Mon. Wea. Rev.

Leslie, L. M., G. A. Mills, L. W. Logan, D. J. Gauntlett, G. A. Kelly, J. L. McGregor and M. J. Manton, 1985. A high resolution primitive equations NWP model for operations and research. Aust. Meteor. Mag., March 1985.

McGregor, J. L., L. M. Leslie, and D. J. Gauntlett, 1978: The ANMRC limited area model: Consolidated formulation and operational results. Mon. Wea. Rev., 106, 427-438.

Mills, G. A., L. M. Leslie, J. L. McGregor, and G. A. M. Kelly, 1981: A high resolution numerical analysis forecast system for short-term prediction over the North American region. Unpublished ANMRC Report, Australian Numerical Meteorology Research Centre, P.O. Box 1289K, GPO, Melbourne, Australia. 76 pp.

Mills, G. A., and C. M. Hayden, 1983: The use of high resolution satellite temperature and moisture profiles to initialize a mesoscale numerical weather prediction model - a severe weather event case study. JCAM, 22, 649-663.

Mills, G. A., G. R. Diak, and C. Hayden, 1983: The subsynoptic scale model and investigations of the value of satellite sounding data in numerical weather prediction. Internal report, Space Science and Engineering Center, University of Wisconsin, Madison, WI, 53706, 227 pp.

Mosher, F. R., 1978: Cloud drift winds from geostationary satellites. Atmos. Tech., 10, 53-60.

Sasaki, Y., 1958: An objective analysis based on the variational method. J. Meteor. Soc. Japan, 36, 77-88.

Sasaki, Y., 1970: Some basic formalisms in numerical variational analysis. Mon. Wea. Rev., 98, 875-910.

Seaman, R. S., R. L. Falconer, and J. Brown, 1977: Application of a variational blending technique to numerical analysis in the Australian region. Aust. Meteor. Mag., 25, 3-23.

Smith, W. L., V. E. Suomi, W. P. Menzel, H. M. Woolf, L. A. Sromovsky, H. E. Revercomb, C. M. Hayden, D. N. Erickson and F. R. Mosher, 1981: First sounding results from VAS-D. Bull. Amer. Meteor. Soc., 62, 232-236.

Smith, W. L., 1983: The retrieval of atmospheric profiles from VAS geostationary radiance observations. J. Atmos. Sci., 40. 2025-2035.

Suomi, V. E., T. Vonder Haar, R. Krauss and A. Stamm, 1971: Possibilities for sounding the atmosphere from geosynchronous spacecraft. Space Research XI, 609-617.

Velden, C. S., W. L. Smith, and M. Mayfield, 1984: Applications of VAS and TOVS to tropical cyclones. Bull. Amer. Meteor. Soc., 65, 1059-1067.

Wilson, T. A., and D. D. Houghton, 1979: Mesoscale wind fields for a severe storm situation determined from SMS cloud observations. Mon. Wea. Rev., 107, 1198-1209.

IMPACT OF THE INITIAL SPECIFICATION OF MOISTURE AND VERTICAL MOTION ON PRECIPITATION FORECASTS WITH A MESOSCALE MODEL

by

PAMELA LYNN EARL

A thesis submitted in partial fulfillment of the requirements for the degree of

MASTER OF SCIENCE
(Meteorology)

at the

UNIVERSITY OF WISCONSIN--MADISON

1985

IMPACT OF THE INITIAL SPECIFICATION OF MOISTURE AND VERTICAL MOTION ON PRECIPITATION FORECASTS WITH A MESOSCALE MODEL

by

Pamela Lynn Earl

Under the supervision of Professor David D. Houghton

ABSTRACT

Four simulations are made with a numerical mesoscale model to determine the effects of suppressing the initial mesoscale information in the moisture and wind fields on the precipitation forecasts. The second half of a 12-hour control forecast represents the ideal reference forecast. This reference forecast can be thought of as being "initialized" with fields from the six-hour control forecast that contain both mesoscale and synoptic scale features. The first experiment is initialized with the same six-hour control forecast, but the moisture fields are smoothed to eliminate the mesoscale component. The horizontal wind fields are replaced with nondivergent winds in the second experiment, but all the other variables come from the six-hour control. This experiment therefore contains only a topographically-induced vertical motion field initially. The third experiment contains both smoothed moisture fields and nondivergent winds initially and is considered the experiment with the most degraded conditions.

All of the experiments' six-hour simulations produce less precipitation than the control forecast. Precipitation rates lag behind the control forecast, and areal coverage is generally less. The third experiment has the worst performance compared to the control, which is expected based on its initial conditions. The smoothed moisture experiment produces less precipitation than the nondivergent experiment in areas over the ocean where moisture magnitudes are reduced by the smoothing process. Over a land area, however, the smoothed moisture experiment forecasts more precipitation than the nondivergent experiment, although moisture magnitudes are reduced in that area also. Generally, the differences between the first two experiments' forecasts are not large enough to conclude whether either mesoscale moisture or initial vertical motion is more essential to precipitation forecasting with a mesoscale model.

A CASE STUDY EVALUATION OF SATELLITE-DERIVED RAINFALL ESTIMATES AND THEIR APPLICATION TO NUMERICAL MODEL PRECIPITATION FORECAST VERIFICATION

by

Glenn Alan Field

Under the supervision of Professor David D. Houghton

ABSTRACT

Satellite-derived precipitation estimates are computed and then evaluated using a dense network of cooperative observer rain gauge reports as the verification. The feasibility of using these satellite rainfall estimates to evaluate numerical model precipitation forecasts is investigated. The correspondence between the numerical model forecast and the observations also is assessed.

The satellite rainfall estimates are produced every half-hour for the 24-hour period starting 1200 GMT, July 20, 1981. They are computed using the operational Scofield-Oliver Convective Rainfall Estimation Technique on the University of Wisconsin's Man-Computer Interactive Data

Access System (McIDAS). (Suomi et. al., 1983) A severe weather outbreak occurred over parts of the southern Midwest during this period and significant rainfall amounts were observed. More than 300 cooperative observer rain gauge observations made during the same time period as the estimates are compiled. The McIDAS analysis procedure provides estimate values assigned to grid points spaced 22 km apart. The rainfall observations, however, are at irregularly located positions. In order to be able to objectively evaluate the estimates, the observations are interpolated to the same grid points as the estimates using a minimum of smoothing. Difference fields then are evaluated.

The numerical model evaluated is an Australian mesoscale model referred to as the Subsynoptic Scale Model (SSM). Its 24-hour precipitation forecast is examined for the same time period as the satellite estimates and ground-based observations. The horizontal resolution (134 km) and map projection of the SSM are much different than for the estimates and observations. A regridding and interpolation scheme is employed, which allows the SSM model to be objectively evaluated on a common grid with the estimates and observations.

The results show that the satellite estimates compare very favorably with the observations, especially with regard to location of rainfall maxima. It is shown that the orientation of the maxima and minima axes in the contoured estimate field is in good agreement with the observations and radar reports. As would be expected, this agreement improves with higher amounts of smoothing. There are many apparent overestimates, for which several plausible explanations are given. Some displacement errors are observed and it is shown how small location errors can lead to large errors in a gridded difference field.

By using satellite estimates as part of the SSM model verification, this study suggests a new application for the use of the Scofield-Oliver technique. Unfortunately, the SSM model fails to accurately predict convective precipitation in this case study. Its forecast precipitation area is too far to the north and the amounts are much too small. Nevertheless, the feasibility of using satellite estimates to verify the model is demonstrated. It is shown that the potential exists for operational numerical (mesoscale) modeling to benefit by having such satellite verification information for precipitation which can be produced in near real-time.

REPRINTED FROM THE SECOND CONFERENCE ON SATELLITE METEOROLOGY/
P4.11 REMOTE SENSING AND APPLICATIONS, MAY 13-16 , 1986,WILLIAMSBURG,VA.

ANALYSIS AND FORECAST EXPERIMENTS INCORPORATING SATELLITE SOUNDINGS AND CLOUD AND WATER VAPOR DRIFT WIND INFORMATION

Brian M. Goodman

George R. Diak

Cooperative Institute for Meteorological Satellite Studies
Space Science and Engineering Center
Madison, Wisconsin

Graham A. Mills

Bureau of Meteorology Research Center
Melbourne, Australia

1. INTRODUCTION

The Man-computer Interactive Data Access System (McIDAS) (Suomi et al., 1983) has extensive capability to ingest conventional surface and upper air meteorological data, in addition to satellite-derived data which can be processed and edited in the McIDAS environment. These satellite products routinely consist of temperature and moisture profiles from both orbiting (Smith et al., 1979) and geostationary (Smith, 1983) satellites, as well as cloud drift and water vapor winds derived from geostationary satellite imagery (Mosher, 1979, Stewart et al., 1985), and gradient winds estimated from VAS temperature soundings (Hayden, 1985).

While large amounts of application software exists to analyze and process these data for specific case studies, including advanced objective analysis and numerical weather prediction models (Mills and Hayden, 1983, LeMarshall et al., 1985), no formal mechanism has hitherto existed to perform routine assimilation of these mixed data types with the aim of producing four-dimensional gridded data sets of the primary atmospheric variables which can be used to periodically update limited area forecast models. While most national weather centers use global forecast model products to provide the first guess for the analyses used to initialize their limited area forecast models, there is no reason why an equivalent data assimilation system should not be operated on a limited area domain, provided care is taken in the specification of the lateral boundary conditions. Mills (1981) has demonstrated a stable analysis/forecast cycling system using FGGE data sets over a limited area domain in the Australian region.

The essential phases of data assimilation scheme are a model forecast to the data insertion time, the correction of the forecast fields to fit the observed data (the analysis phase), and an initialization phase to balance the adjusted fields prior to the next forecast stage. Lorenc (1984) lists the following desirable principles of such a scheme: (1) the analysis must fit the observations to within their estimated observational errors; (2) the analyzed fields must be internally consistent, matching the structure, scale, and balance of the atmosphere; and (3) the anlysis must be near the forecast based on earlier observations unless current observations indicate otherwise.

Two further requirements were made. First, the system should be computationally efficient and geographically portable. Second, the system should be as robust as possible, without excessively compromising the quality of the output product. That is, minimal manual intervention should be needed in the operation of the system. This is, however, to some extent at the expense of maintaining maximum detail in the analysis, and a variety of options exist to relax these constraints in development and testing of this system.

It was decided to base the first generation of this system on existing analysis and forecast modules, with which some experience and expertise was available, and to modify these pre-existing components to improve their suitability as assimilation vehicles. The basic modules which are used in the scheme are the three-dimensional variational analysis scheme of R. S. Seaman (e.g. Mills, 1981) and the new Australian Region Primitive Equation (ARPE) model which has been extensively described by Leslie et al. (1985). The interface programs have been extensively modified so that the system should approach satisfying Lorenc's condition (3) above. The range of available options is summarized in Table 1. The basic and incremental assimilation cycles are schematically represented in Figs. 1 and 2, respectively. The analysis scheme, the forecast model, the interface codes, and how they are linked together to perform an assimilation sequence in the McIDAS environment will be discussed in detail in a forthcoming paper.

The assimilation system was initially tested in a case study mode using a mixture of VAS soundings and special network radiosonde data at 1430 and 1730 GMT on March 1982 (Diak, et al., 1986). To adequately test the

Table 1

Options To Be Selected

Data mix:	
Radiosonde	
Special network	
Satellite temperature retrievals/gradient winds (either/or)	
Cloud and water vapor drift winds	
SVCA/buoys	
Assimilation type:	
Basic	
Incremental	
Analysis:	
Weight of geostrophic/gradient wind	
Rejection tolerance	
Minimum pass radii for first pass	
Pre-processor:	
Sigma level disposition	
Divergent or non-divergent winds	
Topography enhancement factor	
Model:	
Timestep	
Boundary conditions	- fixed
	- updated
Initialization	- none
	- free VMI
	- pressure constrained VMI
Physics options	- surface T, T_D prediction
	- convective pptn
	- large scale pptn
	- vertical diffusion

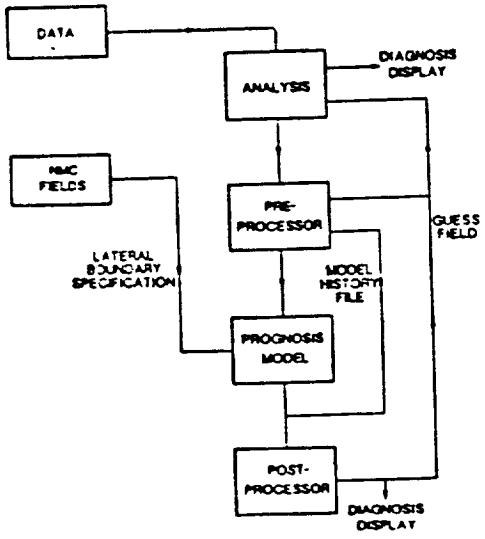

Fig. 1. Basic (or cold start) case study configuration.

assimilation system using data from more extended periods of time, advantage was taken of CIMSS support of the National Hurricane Center to assimilate radiosonde, buoy, VAS temperature and dewpoint (Smith, 1983) and gradient wind data (Hayden, 1985), and cloud drift and water

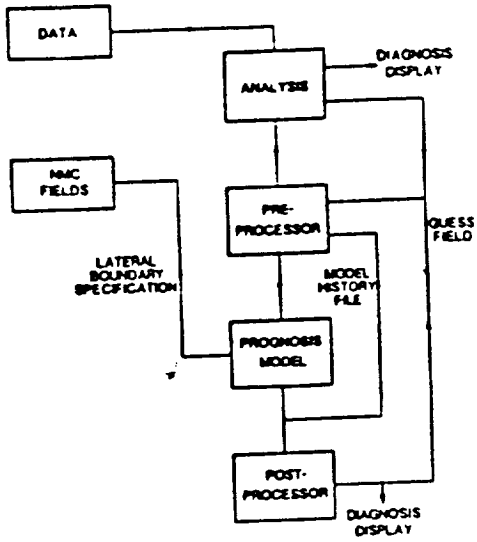

Fig. 2. Incremental assimilation sequence configuration.

vapor motion winds (Stewart, et al., 1985). A 12 hour assimilation interval run at 00 and 12 GMT was performed in a quasi-real-time mode from 12 GMT on 8 October 1985 to 12 GMT on 18 October 1985. No VAS or cloud and water vapor drift winds were available during the weekend. For convenience, the domain was chosen to be the same as the March 6 assimilation: 26x31 grid with a 125 km grid spacing centered on longitude 95W and between latitudes 20 and 50N.

A significant amount of day-to-day fluctuation was noted during this period of time, and some interesting situations did occur. For example, at 12 GMT on day 283, the initialization makes very large changes to almost all fields, and clearly there was considerable imbalance in the initial state, which was then followed by the largest 1000-500mb thickness errors in any of the 12-hour forecasts (Fig. 3). It was encouraging, at this stage of development of the system, to find that this did not destabilize the system. There is a considerable degree of oscillation in the skill of the 1000-500mb thickness forecasts based at 12 GMT and those based at 00 GMT. The cause of this may be due to the differing mixes of satellite and conventional data at the different times, or may be due to more subtle factors needing further investigation.

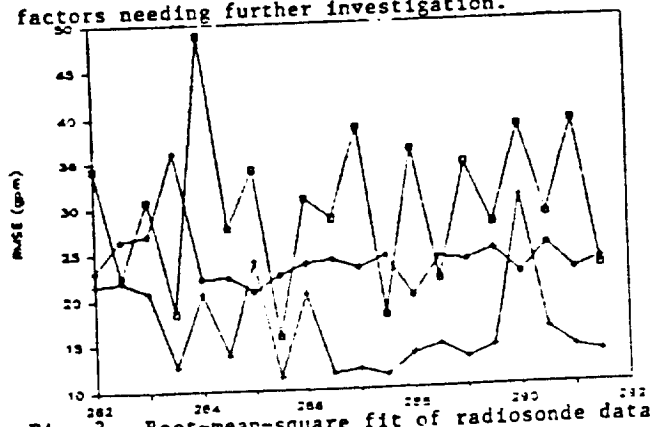

Fig. 3. Root-mean-square fit of radiosonde data 1000-500 mb thickness to assimilation cycle analyses, initialized fields, and 12 hour prognoses at 12-hour intervals from 00 GMT 9 October 1985 (day 282) to 12 GMT 18 October 1985 (day 291).

When looking at the RMS vector errors in Fig. 4, it must be remembered that the wind fields input to the prognosis model are non-divergent increments added to the model forecast wind fields, and thus the RMSVE statistics have a greater magnitude than would be expected from a scalar analysis of wind components. The RMSVE of the radiosonde data to these wind fields are also included for comparison, and are substantially lower than the statistics for the winds used for model initiation.

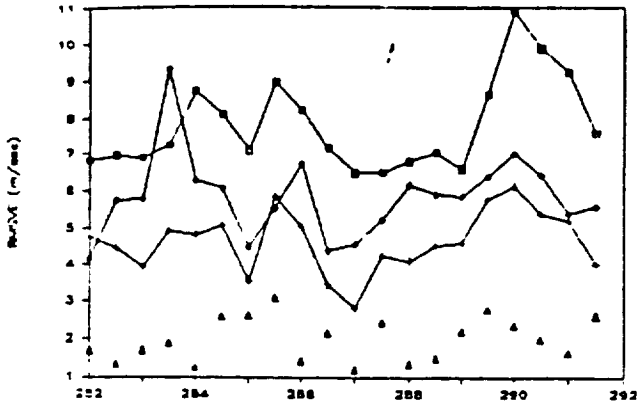

Fig. 4. Root-mean-square vector error at 500 mb of 12-hour prognoses, analyses with non-divergent wind increments, analyses with divergent wind increments (triangles), initialized fields, and 12-hour prognoses at 12-hour intervals from 00 GMT 9 October 1985 (day 292) to 12 GMT 18 October 1985 (day 291).

To a large extent, Lorenc's condition (3) is met by correcting the first guess forecast in the anlysis. Of equal desirability is that information from the prognosis model which is not resolved by the observations or the analysis scheme be preserved through the analysis (correction) and initialization phases of the assimilation. One such field is the vertical motion structure. The 500 mb omega field ($\partial p/\partial t$) were compared before the analysis and after initialization at each data insertion time and, in general, the major features and structure were preserved which was very encouraging. Two examples for the 12-hour forecast vertical motion and the after initialization vertical motion at 00 GMT 10 October and 00 GMT 16 October 1985 are shown in Fig. 5. In each case, it is clear that substantial continuity of these fields has been preserved, even though there has been significant changes to the prognosis fields during the analysis. These patterns are quite typical of the synoptic sequence during this period, with an area of upward vertical motion toward the northwest of the grid, associated with an advancing trough, and another weaker, elongated southwest-northeast area of upward motion which has propagated southeastward in association with the eastward passage of the preceeding middle latitude trough.

This period was not synoptically very active. A powerful anticyclonic circulation covered the southeastern part of the U.S. throughout the entire period, with a sequence of advancing troughs which entered the analysis domain from the west and northwest and were forced northward by the anticyclone as they moved eastward. The assimilation sequence clearly demonstrates a synoptic continuity

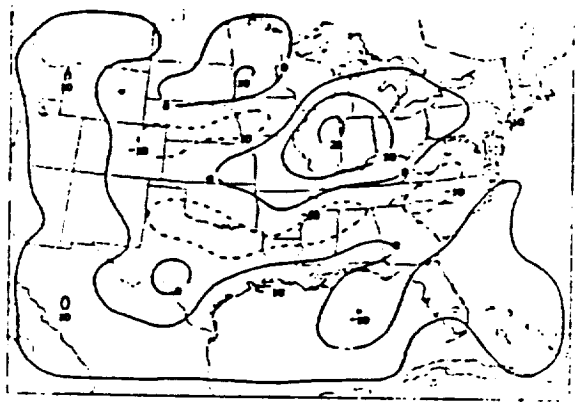

Fig. 5. Before analysis and after initialization 500 mb vertical motion ($\partial p/\partial t$) fields at 00 GMT 16 October 1985 (units mb/hr).

throughout the entire assimilation period for all variables, as would be expected from a robust analysis/prognosis system. Figure 6 shows an example of four assimilation analyses of 500 mb heights and winds for the two-day period 00 GMT 15 October to 12 GMT 16 October 1985.

Development of a functional, stable assimilation system is being continued in a delayed real-time mode in association with the special GALE observing networks at 12 and 6 hour analysis/prognosis assimilation cycles, and in a quasi-real-time mode on a 3 hour assimilation interval during the special observing periods.

2. ACKNOWLEDGEMENTS

Much of the work on VAS and satellite wind assessment has been funded through the NASA Marshall Space Flight Center Contract NAS8-34732.

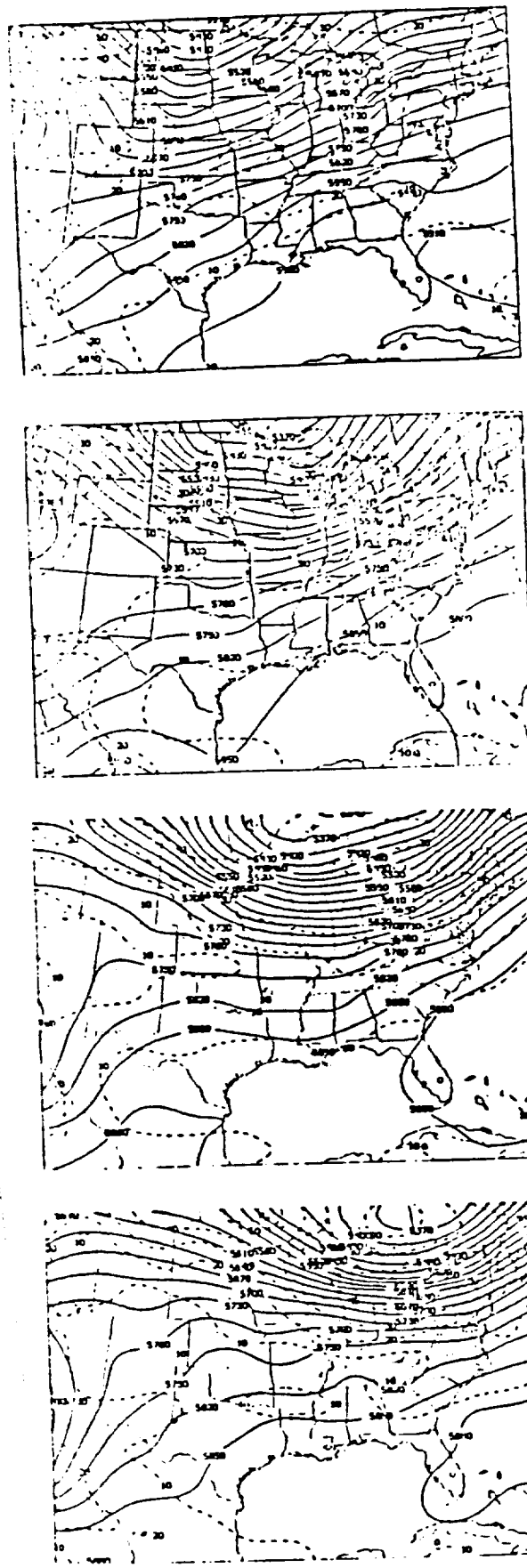

Fig. 6. 500 mb geopotential height/isotach patterns from 00 GMT 15 October 1985 to 12 GMT October 1985.

3. REFERENCES

Diak, G., S. Heikkinen and J. Bates, 1986: The influence of variations in surface treatment on 24-hour forecast with a limited area model, including a comparison of modelled and satellite-measured surface temperatures. Accepted by Mon. Wea. Rev.

Hayden, C. M., 1985: Estimating the wind field from VAS temperature soundings. Submitted to J. Clim. Appl. Meteor.

LeMarshall, J. F., W. L. Smith and G. M. Callan, 1985: Hurricane Debby - An illustration of the complementary nature of VAS soundings and cloud and water vapor motion winds. Bull. Amer. Meteor. Soc., 66, 268-263.

Leslie, L. M., G. A. Mills, L. W. Logan, D. J. Gauntlett, G. A. Kelly, J. L. McGregor and M. J. Manton, 1985. A high resolution primitive equations NWP model for operations and research. Aust. Meteor. Mag., March 1985.

Lorenc, A. C., 1984: Data assimilation by repeated insertion into a forecast model - principles, practice, problems and plans. ECMWF Seminar/Workshop. Data assimilation systems and observing system experiments with particular emphasis on FGGE. Vol. 2, pp. 181-214.

Mills, G. A., 1981: An objective limited area analysis/prognosis experiment using FGGE data in the Australian region. Mon. Wea. Rev., 109, 1898-1913.

Mills, G. A. and C. M. Hayden, 1983: The use of high horizontal resolution satellite temperature and moisture profiles to initialize a mesoscale numerical weather prediction model - severe weather event case study. J. Clim. Appl. Meteor., 22, 649-663.

Mosher, F. R., 1979: Cloud drift winds from geostationary satellites. Atmos. Tech., 10, 53-60.

Smith, W. L., 1983: The retrieval of atmospheric profiles from VAS geostationary radiance observations. J. Atmos. Sci., 40, 2025-2035.

Smith, W. L., H. M. Woolf, C. M. Hayden, D. Q. Wark, and L. M. McMillin, 1979: The TIROS-N operational vertical sounder. Bull. Amer. Meteor. Soc., 60, 1177-1187.

Stewart, T. R., C. M. Hayden and W. L. Smith, 1985: A note on water vapor wind tracking using VAS data on McIDAS. Bull. Amer. Meteor. Soc., 66, 1111-1115.

Suomi, V. E., R. Fox, S. S. Limaye and W. L. Smith, 1983: McIDAS III: A modern interactive data access and analysis system. J. Clim. Appl. Meteor., 22, 766-778.

NASA Technical Memorandum

NASA TM-86565

THE MULTISPECTRAL ATMOSPHERIC MAPPING SENSOR (MAMS): Instrument Description, Calibration, and Data Quality

By Gary J. Jedlovec, W. Paul Menzel, Robert Atkinson, Gregory S. Wilson, and John Arvesen

Systems Dynamics Laboratory
Science and Engineering Directorate

August 1986

National Aeronautics and Space Administration

George C. Marshall Space Flight Center

MSFC - Form 3190 (Rev. May 1983)

TECHNICAL REPORT STANDARD TITLE PAGE

1. REPORT NO.	2. GOVERNMENT ACCESSION NO.	3. RECIPIENT'S CATALOG NO.
NASA TM -86565		

4. TITLE AND SUBTITLE	5. REPORT DATE
The Multispectral Atmospheric Mapping Sensor (MAMS): Instrument Description, Calibration, and Data Quality	August 1986
	6. PERFORMING ORGANIZATION CODE
7. AUTHOR(S) Gary J. Jedlovec,* W. Paul Menzel,** Robert Atkinson,*** Gregory S. Wilson, and John Arvesen****	8. PERFORMING ORGANIZATION REPORT #
9. PERFORMING ORGANIZATION NAME AND ADDRESS	10. WORK UNIT NO.
George C. Marshall Space Flight Center Marshall Space Flight Center, Alabama 35812	11. CONTRACT OR GRANT NO.
	13. TYPE OF REPORT & PERIOD COVERED
12. SPONSORING AGENCY NAME AND ADDRESS	Technical Memorandum
National Aeronautics and Space Administration Washington, D.C. 20546	14. SPONSORING AGENCY CODE

15. SUPPLEMENTARY NOTES

Prepared by Atmospheric Sciences Division, Systems Dynamics Laboratory, Science and Engineering Directorate.

16. ABSTRACT

A new instrument has been developed to produce high resolution imagery in eight visible and three infrared spectral bands from an aircraft platform. An analysis of the data and calibration procedures has shown that useful data can be obtained at up to 50 m resolution with a 2.5 milliradian aperture. Single sample standard errors for the measurements are 0.5, 0.2, and 0.9°K for the 6.5, 11.1, and 12.3 μm spectral bands, respectively. These errors are halved when a 5.0 milliradian aperture is used to obtain 100 m resolution data. Intercomparisons with VAS and AVHRR measurements show good relative calibration. MAMS development is part of a larger program to develop multispectral Earth imaging capabilities from space platforms during the 1990s.

*University of Wisconsin-Madison, Space and Engineering Center.
**NOAA/NESDIS Advanced Satellite Products Project, Madison, Wisconsin.
***General Electric Co.
****NASA Ames Research Center, Moffett Field, California.

17. KEY WORDS	18. DISTRIBUTION STATEMENT
Multispectral imagery Radiometric calibration Blackbody temperatures Radiances Single sample noise, Coherent noise, Spectral response, Sensitivity	Unclassified – Unlimited

19. SECURITY CLASSIF. (of this report)	20. SECURITY CLASSIF. (of this page)	21. NO. OF PAGES	22. PRICE
Unclassified	Unclassified	41	NTIS

DETECTION OF MOUNTAIN-INDUCED MESOSCALE WAVE STRUCTURES WITH HIGH RESOLUTION MOISTURE IMAGERY

Gary J. Jedlovec
CIMSS, Univ. of Wisc.
Madison, Wisc.

W. Paul Menzel
NOAA/ASPP
Madison, Wisc.

Gregory S. Wilson
NASA/MSFC
Huntsville, Al.

Robert J. Atkinson
General Electric Co.
Huntsville, Al.

1. INTRODUCTION

Radiosonde observations near the surface and aloft often detect pressure, temperature, and wind patterns associated with large scale atmospheric wave features which govern our daily weather conditions. The detection of small scale waves such as gravity and bouyancy oscillations however, usually require special observations to measure the perturbations directly. These waves need not always be measured or sensed directly and their observable signatures (i.e., clouds) can be detected in visible photography or satellite imagery.

The detection of mountain and lee wave structures is often done by observing cloud signatures in regions where vertical oscillations are forced by terrain. Satellite observations of these small scale clouds are possible with high resolution visible sensors. Direct observation of wind and thermodynamic parameters is achieved by instrumented aircraft, lidar, and radar measurements. From these observations, quantitative information is available about mountain and lee waves, their formation and three dimensional structure. However, because a moist environment is not necessary, many wave features may go undetected by these conventional measurements because of the absence of clouds.

During one of the flights of the Multispectral Atmospheric Mapping Sensor (MAMS) on a NASA U2 high altitude aircraft in 1985, wave features were found in water vapor channel imagery in close proximity to the Sierra Nevada mountains of California (Fig. 1). Visible channel imagery from the flight was examined for cloud features but none were found. This paper presents evidence that the waves in the imagery reflect changes in the vertical temperature and moisture distribution produced by the vertical oscillations. These features on the downwind or lee side on the mountains are called lee waves.

2. BACKGROUND

2.1 Instrument Characteristics

The MAMS is a multispectral scanner capable of producing high resolution imagery in visible and infrared bands with detailed spectral resolution. Table 1 summaries the characteristics of the instrument and its spectral bands. The MAMS is flown on a NASA U2/ER2 at an altitude of 20km providing a resolution cell of 50-100m on the ground.

Table 1

MAMS: The Multispectral Atmospheric Mapping Sensor

Provides high resolution visible and IR scanning capabilities from a high altitude aircraft platform.

Scan rate	6.25 or 12.50 rps
Instantaneous field-of-view	2.5 or 5.0 mrad
Ground resolution (nadir,19.8km)	50m or 100m
Total field-of-view	86°
Roll correction	±15°
Calibration sources	IR, 2 controllable bbs
Pixels per scan line	716

Spectral Bands

Channel	Wavelength (microns)	Spectral Region	Single Sample Noise(1) 2.5/5.0@6.25rps
1	.42 - .45	blue	1.0
2	.45 - .52	blue/green	.5
3	.52 - .60	green	.4
4	.60 - .62	yellow/orange	.5
5	.63 - .69	red	.5
6	.69 - .75	red/near IR	.4
7	.76 - .90	near IR	.4
8	.90 -1.05	near IR	.4
9	6.20 - 6.90	water vapor	.40/.20
10	10.32 - 12.02	window (cold)	.15/.10
11	10.32 - 12.02	window (warm)	.15/.10
12	12.20 - 12.56	water vapor	.75/.40

(1) NEΔT (mw/ster/m^2/cm^{-1}) for 1-8, NEΔT (°C) for 9-12.

The width of the entire cross track field-of-view is 40km, providing detailed resolution over a relatively large area.

Eight channels of the instrument are used to separate the visible and near-infrared radiation into narrow bands which sense reflected solar energy from the earth's surface and clouds. The three infrared channels (one of which is redundant) cover selected regions where infrared emission from the earth and atmosphere are of interest. These bands

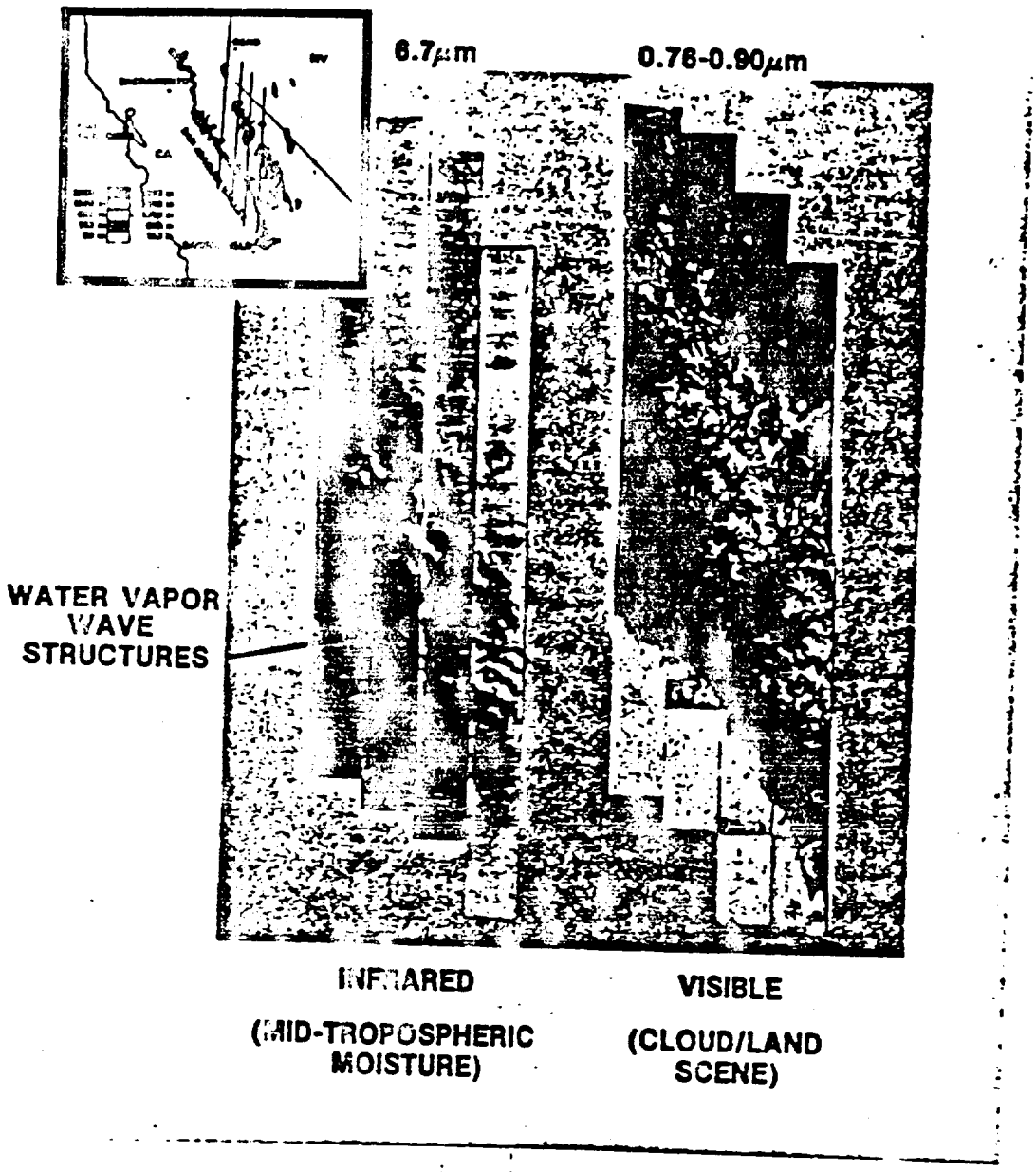

Figure 1. MAMS water vapor and visible channel composite imagery from four adjacent flight tracks on 22 January 1985 from 1942-2109 GMT. The inset shows the major terrain features of the Sierra Nevada mountains over which the imagery was collected.

include the mid-tropospheric (channel 9, 6.5 microns) and low-tropospheric (channel 12, 12.3 microns) water vapor region, and a window region (channel 10/11, 11 microns) where the atmosphere is relatively transparent. The 11 and 12 micron bands form what has become known as the split window channels (Chesters et al., 1983). Further details about the instrument and spectral bands may be found in Jedlovec et al. (1986).

2.2 Structure of Lee Waves

Stationary waves such as mountain or lee waves are a local phenomena which may have significant effect on local weather conditions because of their associated cloud patterns and wind distributions. They may also feedback to the larger scales of motion. The presence of either mountain or lee waves is due to vertical oscillations of air parcels as air is forced over the mountain. Mountain waves usually consist of one vertical oscillation of the flow pattern between two mountain peaks and are mainly governed in size by the spacing of the ridges. Lee waves, although forced by mountains, are not restricted in size to one or two vertical oscillations as with the mountain waves. In fact, the overshooting of the downward flow (the restoring force is gravity) on the lee side of the obstacle produces vertical oscillations which may extend for many wavelengths downstream.

The water vapor image in Fig. 1 shows wave structures in the lee of the Sierra Nevada mountains. Three or four waves are discernable, each having an estimated wavelength of 15-20km. The waves extend away from the face of the mountain range for about 70km and along the face for at least

.0km. The waves appear somewhat irregular, possibly due to variations in the mountain peaks, tangental distortion from the scanner geometry (Jedlovec et al., 1986), limb brightening (due to increased water vapor path length at the edges of the flight track), as well as other unknown causes.

The nature of the vertical oscillation producing lee waves was studied in detail by Brunt(1927) who derived a set of equations which can be used to describe this flow pattern. From Brunt's work, a simple vertical oscillation in the atmosphere has a period given by

$$\tau = \frac{2\pi}{\left[\frac{g}{T}(\Gamma - \gamma)\right]^{\frac{1}{2}}} \qquad (1)$$

where

γ is the environmental lapse rate,
Γ the dry adiabatic lapse rate,
g the gravitational acceleration, and
T the environmental temperature.

An air parcel moving horizontally with a velocity of V and under this vertical oscillation will complete one cycle over a distance of

$$\lambda = v\tau = \frac{2\pi v}{\left[\frac{g}{T}(\Gamma - \gamma)\right]^{\frac{1}{2}}}. \qquad (2)$$

Upon examining this equation, it becomes apparent that the horizontal wavelength (λ) is governed by the wind speed and atmospheric stability. Strong winds and low stability favor long wavelengths, while weak winds and strong stability favor shorter ones.

A number of investigators have studied lee waves by observing their visible signatures and with direct measurements of temperature and wind velocity. Atkinson (1981) presents a fairly extensive review of this research. The characteristics of these waves vary from occurance to occurance but representative values are presented below. The wavelengths of lee waves range from 2-70km but most occurances are in the range of 5-20km. The wavelengths tend to increase with height and seem to be related to the mean wind speed. Corby (1957) performed a linear regression of wind speed on wavelength and suggested that a high enough correlation existed for the wavelength to be determined from the wind speed alone.

Another feature which is of interest is the wave amplitude, defined as the vertical distance between the peak and trough of a streamline. This is more difficult to determine from the cloud itself and requires a number of special measurements of the wind field. From the available empirical data, these wave amplitudes are typically about 1km but amplitudes of 7km have been measured. The larger amplitudes may occur when the wavelength closely matches the size of the obstacle forcing the wave.

From these studies, it appears that two parameters control the appearance and size of lee waves; namely, stability and wind. Of course the obstacle (mountain) is necessary to initiate the vertical oscillation and may have some control over the wave amplitude. Stability and wind are also important parameters in (1), however, the importance of stability in determining wavelength seems less important than indicated by (2). A typical environmental temperature and wind profile would consist of layers of varying stability and an absence of horizontal wind shear. In the lowest layer, the atmosphere would be neutral with a strong layer of stability aloft. This stable layer is necessary for the formation of the waves and should occur near the level of the mountain peak. A layer of weaker stability usually exists above this level. The flow should be perpendicular to the mountain at all levels and increase in speed with height. Significant horizontal shear reduces the liklihood for the development of lee waves.

2.3 Atmospheric Conditions

In the previous section, the atmospheric conditions required for the development of lee waves were summarized. Although they are local conditions, they are governed by the large scale atmospheric patterns. Thus, a discussion of the large scale features on 22 January 1985 corresponding to the MAMS observations is necessary. The upper air data (Fig. 2) exhibited a pronounced ridge of high pressure over the eastern Pacific ocean and over the northwestern portion of the U. S. A trough was positioned over the central part of the country with a portion of it hanging back into Utah and the southern portions of Nevada and California. This set up a prevailing flow pattern from the northeast over much of the Sierra Nevada mountains.

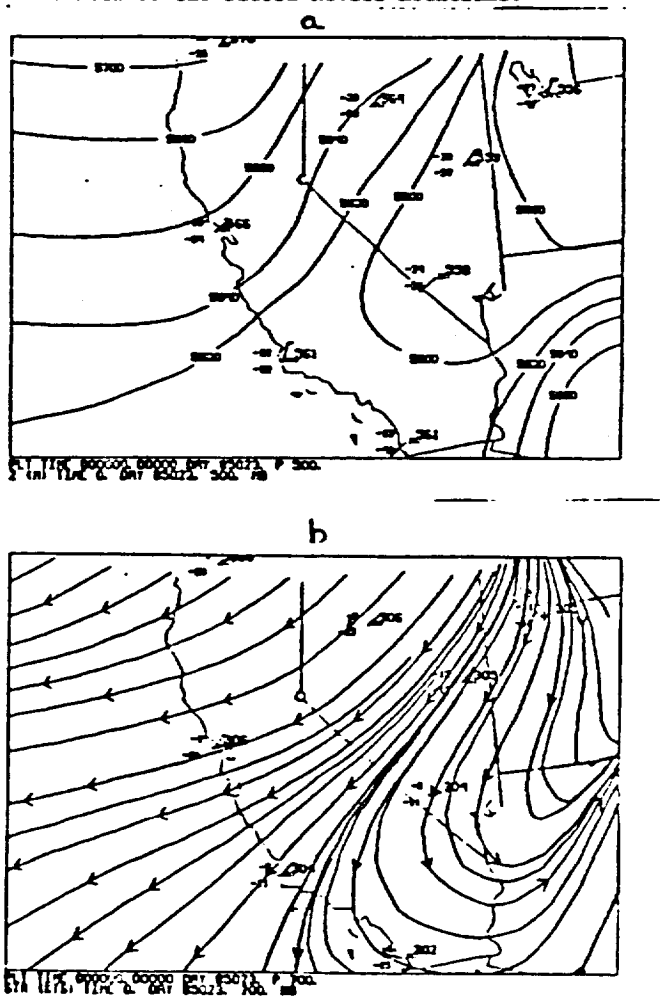

Figure 2. a) 500mb rawinsonde station plots and height analysis, and b) 700mb plots and streamlines for 23 Jan 1985 at 0000 GMT. Plots and analyses are in their standard units.

The region of interest (the Sierras) is in a void region of the rawinsonde observing network. However, since only 3h difference exists between the MAMS and radiosonde observations, and on the stationarity of the weather systems, a reasonable estimation of the temperature, moisture, and wind profile may be available from the upwind sites. For this reason, data from two Nevada locations is presented in Fig. 3. A moderate to strong inversion exists around 700mb in both soundings. The atmosphere is quite dry above and below this level. The nearly saturated layer at the level of the inversion indicates a shallow layer of clouds. Clouds are not observed over the Sierras so the actual dewpoint will be somewhat colder. The winds are weaker at 72486 but both profiles indicate flow from the northeast without much directional shear with height. From these diagrams, it seems reasonable to assume that conditions would be favorable for lee waves over the Sierras.

3. DISCUSSION

Although Fig. 1 was briefly discussed in previous sections, further discussion seems appropriate at this time. The MAMS 6.5 micron and visible/near-infrared channel imagery is displayed from four adjacent flight tracks on 22 January 1985. The data were collected from 1942-2109 GMT over the plateau region of Nevada, the Sierra Nevada mountains and the central valley of California as indicated by the inset map. The peaks of the Sierras climb to about 4000m and drop sharply to the southwest. Each flight track is about 40km wide making the entire ground distance of the west-east extent 160km. The north-south extent is roughly 400km. For display purposes, the resolution has been degraded to about 400m.

Many very small scale features are apparent in the water vapor imagery. In the center of this imagery, alternating bright (cold/moist) and dark (warm/dry) features exist in wave-like patterns. They are orientated in a northwest-southeast direction parallel to the mountains. It is not possible to determine the position of the waves with respect to the position of the mountains from this image alone. The accompanying flight tracks of visible data capture the cloud/land features at the same instant as the water vapor imagery. Therefore this data can be overlaid and used to determine the exact position of the waves. Several landmarks are visible in the scene, the best being the quasi-circular Lake Mono in the right hand flight track. The bright regions in the lower portion of the visible image are fog and low clouds over the central valley. The bright areas in the center represent snow in the mountains above the 2400m level. Thus the snow region can be used to outline the major mountain features. From this and the terrain map, it is clear that most of the water vapor wave features reside on the downwind side of the mountains where surface elevations are below 2000m. It should also be noted that no clouds are present in the visible imagery over this region.

The estimated wavelengths of these waves (described in section 2.2) can be compared to that obtained from (2) or estimated from the mean tropospheric wind speed. The environmental lapse rate, temperature, and wind speed used in (2) is somewhat arbitrary. A value of γ of 0°K/km (T=250°K), and V of 10 m/s, yields 3.2 km, a rather short wavelength. Since the wave structures occupy more than a single level in the vertical, it may be more appropriate to uses values representative of a layer of the atmosphere. Using values from the 800-400mb layer (T=250°, γ= 6.5, and V=20), a wavelength of 10.7 km is obtained. This is somewhat less than the estimated length of 15-20km. As previously mentioned, Corby (1957) used an empirical relationship between wind speed and wavelength with a good correlation. The linear fit of his data (wavelength versus wind speed) produced a slope of roughly 0.45. For a mean environmental wind speed of 20m/s, a wavelength of 9km is predicted. In either case, a stronger wind speed would be needed to match the one estimated from the water vapor imagery. Considering that the actual wind profile over the Sierras is somewhat uncertain, these calculations are relatively close to the estimates from the observed data.

It is much more difficult to estimate the amplitude of these lee wave features without direct in situ measurements. However, the next section describes an approach to estimate the amplitude by simulating the MAMS water vapor channel radiances.

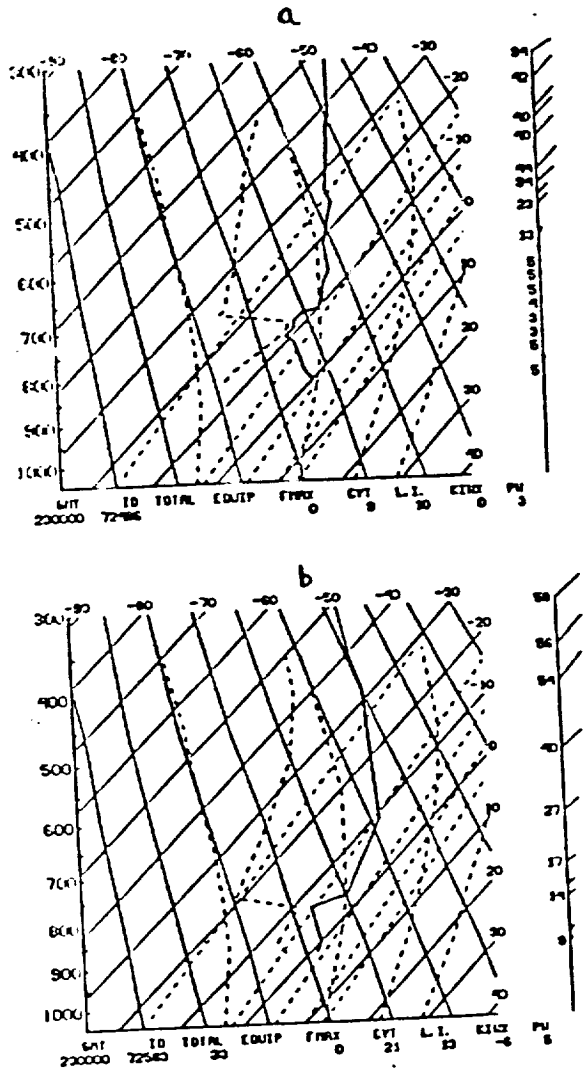

Figure 3. SkewT-LogP diagrams for two Nevada rawinsonde sites a) 72486, and b) 72583 at 0000 GMT 23 Jan 1985. Winds are plotted in knots.

4. RADIATIVE TRANSFER SIMULATIONS

The water vapor image presented in Fig. 1 represents energy emitted by atmospheric water vapor somewhere in the mid-troposphere. The procedure to determine this layer or level has been the subject of investigation by researchers for many years. In the case of cloud height determinations using window channel radiances, the altitude of the cloud can be estimated by comparing the measured blackbody temperature to a local rawinsonde. The water vapor signal does not come from a single level but actually a layer of the atmosphere (Jedlovec, 1984), and depends on the amount, vertical distribution, and temperature of the vapor itself. It is unclear whether blackbody temperatures in this channel can be used directly to infer a mean height from which the signal originates.

In an attempt to estimate the amplitude of the lee waves observed in Fig. 1, several approaches were considered. Table 2 presents the observed blackbody temperatures measure in the peaks and troughs of the lee wave features. Typical values indicate a 6° temperature difference from the peak to the trough of the wave. It is difficult to use one of the soundings in Fig. 3 to directly infer the levels of the peak and trough of the lee waves. It may be reasonable to assume that the level of the neutral point of the wave is 246°K (-27°C) and the peak and trough occuring at the level of their measured temperature (Table 2), however. If this is done, the estimated wave amplitude is about 1km. While this is consistent with the amplitudes of a typical lee wave, it depends heavily on the lapse rate of the sounding used. Because of the lifting of the lower level inversion by the mountains, a smaller lapse rate of temperature probably existed over the Sierras, producing a greater vertical amplitude for the lee wave.

Another approach to estimate the lee wave amplitude used a composite of the two soundings in Fig. 3. From the composite sounding, MAMS water vapor channel radiances were simulated (McMillan and Fleming, 1976; Fleming and McMillan, 1977; and Weinreb and Neuendorffer, 1973). In order to obtain a representative profile in both the peak and trough of the waves, the inversion layer near 700mb and the accompanying moisture distribution were raised and lowered adiabatically in increments of 1 km. Blackbody temperatures were computed from the channel radiances. Temperature differences of 6°K were observed (similar to the measure values from Fig. 1) as well as the appropriate blackbody temperatures when the inversion was at 2 and 6km level for the trough and peak, respectively. This 4km vertical amplitude, while larger than most lee wave amplitudes, is more consistent with the level of the mountain peaks which produce them.

Table 2

Observed and simulated blackbody temperatures for the lee waves. Units are in degrees°K.

Observed Blackbody Temperatures	mean	extreme
Wave peak	243.5	242.0
Wave trough	249.5	251.0
Simulated Blackbody Temperatures (4km)		
Wave peak	243.9	
Wave trough	249.5	

5. CONCLUSIONS

The above work has presented evidence for the existence of lee waves in the absence of clouds using high resolution MAMS moisture imagery. Although verifying measurements do not exist, an evaluation of wind profiles and stability in the surrounding region support the existence of these waves. Estimations of the horizontal wavelengths of the observed lee wave features are not inconsistent with those from previous studies. The estimated vertical amplitude, although less certain, seems realistic for the setting. Further work is necessary to more accurately determine this vertical amplitude.

Acknowledgements. This work was performed in part by the lead author while affiliated with several organizations. Support from the Universities Space Research Association through a NASA contract and from the Space Science and Engineering Center at the University of Wisconsin was appreciated. Mr. John Arvesen of NASA/Ames and Jeff Myers also contributed in the collection and data reduction of the MAMS flight data. Their efforts are also appreciated.

REFERENCES

Atkinson, B. W., 1981: Meso-scale Atmospheric Circulations. Academic Press, New York, 495p.

Brunt, D., 1927: The period of simple vertical oscillations in the atmosphere. Q. J. Royal Meteor. Soc., 53, 30-31.

Chesters, D., L. W. Uccellini, and W. D., Robinson, 1983: Low-level water vapor fields from the VISSR Atmospheric Sounder (VAS) "split window" channels. J. Climo. Appl. Meteor., 22, 725-743.

Corby, G. A., 1957: Preliminary study of atmospheric waves using radiosonde data. Q. J. Royal Meteor. Soc., 83, 49-60.

Fleming, H. E., and L. M. McMillan, 1977: Atmospheric transmittance of an absorbing gas. 2. A computationally fast and accurate transmittance model for slant paths at different zenith angles. Appl. Opt., 16, 1366-1370.

Jedlovec, G. J., W. P. Menzel, G. S. Wilson, R. J. Atkinson, and J. Arvesen, 1986: The Multispectral Atmospheric Mapping Sensor (MAMS): Instrument description and data quality. (in press).

Jedlovec, G. J., 1984: Mesoscale analysis of 6.7μm image data from the VISSR Atmospheric Sounder (VAS) for several case studies. Preprints, Conf. on Satellite/Remote Sensing and Appl. AMS, Boston, 185-190.

McMillan, L. M., and H. E. Fleming, 1976: Atmospheric transmittance of an absorbing gas: A computationally fast and accurate transmittance model for absorbing gases with constant mixing ratios in inhomogeneous atmospheres. Appl. Opt., 15, 358-363.

Wienreb, M. P., and A. C. Neuendorffer, 1973: Method to apply homogeneous-path transmittance models to inhomogeneous atmospheres. J. Atmos. Sci., 30, 662-666.

[Reprinted from BULLETIN OF THE AMERICAN METEOROLOGICAL SOCIETY, Vol. 66, No. 3, March 1985]
Printed in U. S. A.

Hurricane Debby—An Illustration of the Complementary Nature of VAS Soundings and Cloud and Water Vapor Motion Winds

John F. Le Marshall[1], William L. Smith[2], and Geary M. Callan[3]

Abstract

The utility of VISSR Atmospheric Sounder (VAS) temperature and moisture soundings and cloud and water vapor motion winds in defining a storm and its surroundings at subsynoptic scales has been examined using a numerical analysis and prognosis system. It is shown that the VAS temperature and moisture data, which specify temperature and moisture well in cloud-free areas, are complemented by cloud and water vapor motion data generated in the cloudy areas. The cloud and water vapor "winds" provide thermal gradient information for interpolating the soundings across cloudy regions. The loss of analysis integrity due to the reduction of VAS sounding density in the cloudy regions associated with synoptic activity is ameliorated by using cloud and water vapor motion winds. The improvement in numerical forecasts resulting from the addition of these data to the numerical analysis is recorded.

1. Introduction

Between 14 September 1982 and 20 September 1982, Hurricane Debby moved through the western Atlantic Ocean, 500 miles from the east coast of the United States providing a first opportunity for the VAS instrument on GOES-5 to observe a hurricane and its environment. During this period, a data base was established from the usual conventional observations, VAS observations from GOES-5, HIRS and MSU observations from NOAA-6 and NOAA-7, cloud and water vapor motion "wind" observations, and National Hurricane Research Laboratory aircraft dropwindsonde measurements. The utility of the various components of this data base in defining the storm and its surrounding environment has been examined. This study concentrates on the utility of the GOES-5, VAS temperature and moisture sounding data, and cloud and water vapor motion data. The timeliness, density, and coverage of GOES sounding and wind data make them well-suited for analysis and forecast purposes in the western Atlantic Ocean.

2. The data base

The data base used in this study had three components: the usual conventional observations without ship reports, AIREPS, and the satellite components. These data were received in real time at the Space Science and Engineering Center (SSEC) at the University of Wisconsin in Madison.

VAS sounding data from GOES-5 were processed using the physical retrieval scheme developed at the NESDIS Development Laboratory in the Space Science and Engineering Center at Madison (Smith, 1983). This scheme provides soundings that represent a full physical solution of the radiative transfer equation. Surface data are used to reduce sounding errors near the lower boundary, and the temperature and moisture retrievals are made in a fully interactive Man-computer Interactive Data Access System (McIDAS) environment (Suomi *et al.*, 1983), which among other things, facilitates the removal of errors due to cloud contamination and noise. The first guess field used in the retrieval scheme was a 12-hour National Meteorological Center (NMC) global forecast, and the retrievals were made approximately every 150 km. The quality of these VAS soundings is discussed in detail in Velden *et al.* (1984) and shows that the RMS temperature difference between these soundings and radiosondes is between 1 K and 2 K through the troposphere.

Cloud and water vapor motion winds were also produced at the SSEC on the McIDAS using the technique described by Mosher (1978), which was applied to GOES-5 half-hourly visible and infrared imagery and hourly water vapor imagery. This technique is based on manual selection of suitable cloud and water vapor tracers from which pursuant programs generate wind vectors, using a correlation technique to determine the final position of the tracers selected. The quality of these cloud drift and water vapor winds is discussed in Mosher (1978) and Mosher and Stewart (1981), respectively. The height assignment for the cloud drift winds was done using the bi-spectral method, while the water vapor winds relied on the use of the water vapor brightness temperature and nearby temperature-pressure soundings. A most important advantage of the latter remotely sensed data types was that when some areas appeared to be data-sparse during analysis, a quick reexamination of the VAS radiance and cloud and water vapor image fields often allowed generation of supplementary sounding or wind data where they were required.

3. The analysis-prognosis system

The chief characteristics of both the analysis and prognosis schemes are listed in Table 1. The analysis and prognosis schemes have a horizontal grid spacing of either 67 km or 134 km (51 × 61 or 24 × 29 elements) on a Lambert Conformal Conic Projection. For this study, the prognosis model inte-

[1] Visiting Scientist from Bureau of Meteorology, Australia. Present affiliation: Cooperative Institute for Meteorological Satellite Studies, 1225 West Dayton St., Madison, WI 53706.
[2] NOAA/NESDIS Development Laboratory, 1225 West Dayton St., Madison, WI 53706.
[3] NOAA/NESDIS Development Laboratory, Systems Design and Applications Branch, 1225 West Dayton St., Madison, WI 53706.

TABLE 1. Principle features of the analysis scheme and prognosis model.

Analysis System
Combination of successive correction method and variational blending in three dimensions
Ten pressure levels, p = 1000, 850, 700, 500, 400, 300, 250, 200, 150, and 100 mb
Horizontal resolution: 67 km
Fields analyzed or derived at each pressure level:
• geopotential height
• temperature
• dewpoint
• wind components
• stream function

Prognosis Model
Primitive equations model in σ–coordinates
Ten vertical levels at σ = 0.05, 0.15, 0.25, . . . , 0.95
Horizontal resolution (67 km) 134 km
Staggered horizontal grid (Arakawa "C" grid)
Semi-implicit time differencing
Surface/boundary layer parameterization
Broad scale precipitation
Kuo-type convective parameterization
Updated boundary conditions

grations have been run at 134 km resolution. The model also has the option to update boundary conditions using tendencies provided by a larger scale model. A brief summary of both the analysis and prognosis schemes are given below.

a. The analysis scheme

The objective analysis scheme used in this study is an adaptation of a scheme written at the Australian Numerical Meteorology Research Centre (ANMRC) by R. S. Seaman for limited area objective analysis over the Australian region (Mills *et al.*, 1981). The scheme uses a combination of the successive correction method (SCM) of Cressman (1959), which generates fields of geopotential height, thickness, gradient, and dewpoint from observations, and the variational blending techniques of Sasaki (1958, 1970). The variational blending uses the calculus of variations to combine fields of geopotential height, thickness, and gradient, weighted by their reliability into an "optimal" analysis, a method well-suited to analysis of satellite temperature profiles and cloud and water vapor motion winds. It relies on an initial three-dimensional blend of 1000 mb and 250 mb height, gradient, and thickness data to specify the bulk atmospheric structure. Subsequent to this, individual level geopotential analyses are performed by blending the geopotential gradient analyses at that level and the analyzed thicknesses immediately above and below the level in question. Geopotential thickness being a primary analysis variable facilitates assimilation of satellite temperature profiles into the objective analysis, while the variational blending procedure ensures a consistent introduction of gradient information into the analysis. Different weights can also be given to scalar and gradient information in the blending procedure that determines geopotentials, allowing the geopotential gradient information inherent in satellite temperature data sets to be utilized more effectively than would be the case in a simple SCM analysis.

The wind fields are derived from the blended geopotential fields using the gradient/geostrophic wind relationship, and these wind components are used as input to a variational blending procedure (Seaman *et al.*, 1977) to derive a stream function field at each analysis level. The model commences its integration using this non-divergent field.

b. The forecast model

The forecast model is a primitive equation model originally written for the Australian region (McGregor *et al.*, 1978) and later adapted to the North American region (NA) (Mills *et al.*, 1981). The model has been used operationally by the Australian Bureau of Meteorology at a resolution of 250 km, and in a research mode within the ANMRC at 125 km. The model for use over the NA region differs from the Australian version in three important respects. First, the finite differencing scheme of Corby *et al.* (1972) has been included to minimize truncation error over regions of steep topography. Second, a Kuo-type convective parameterization scheme (Kuo 1965, 1974) has replaced the Arakawa-Shubert scheme described in McGregor *et al.* (1978). A comprehensive boundary layer scheme has also been added to the model (Mills *et al.*, 1983), using similarity theory at the surface coupled with vertical diffusion of heat, moisture and momentum at the three lower model levels.

4. The analyses

Three analyses have been done for each of the following time periods: 0000 GMT and 1200 GMT on 16 September 1982, and 0000 GMT on 17 September 1982. These analyses used conventional data (C), conventional plus VAS sounding data (C + V), and conventional plus VAS sounding plus cloud and water vapor drift wind data (C + V + CDW). The first guess fields for the 0000 GMT 16 September 1982 analysis were a combination of the National Meteorological Center (NMC) global and Limited Fine Mesh (LFM) analyses. The LFM grid data were used by the analysis scheme to modify a global analysis first-guess field. The global analyses alone were used as first-guess fields for the other analyses due to problems generated by the proximity of the storm to the LFM boundary and the better quality of the global analysis in the region of the storm, and because the later cut-off time of the global analysis permitted the inclusion of satellite and other data.

The mean sea level pressure (MSLP) analyses for the latter two analyses were very slightly altered by the addition of "bogus observations," so that the analyzed cyclone center fitted the observed "best track" reconnaissance data for the storm. By using these MSLP fields it was felt the study in some ways gauged the impact of VAS and CDW data used in conjunction with an "operational" MSLP analysis. The MSLP field was the same for each set of analyses done at a particular time.

Figs. 1(a) and (b) show the conventional (C), conventional plus VAS sounding (C + V) and conventional plus VAS sounding plus cloud and water vapor drift wind analyses (C + V + CDW) at 500 mb and 250 mb at 0000 GMT on 16

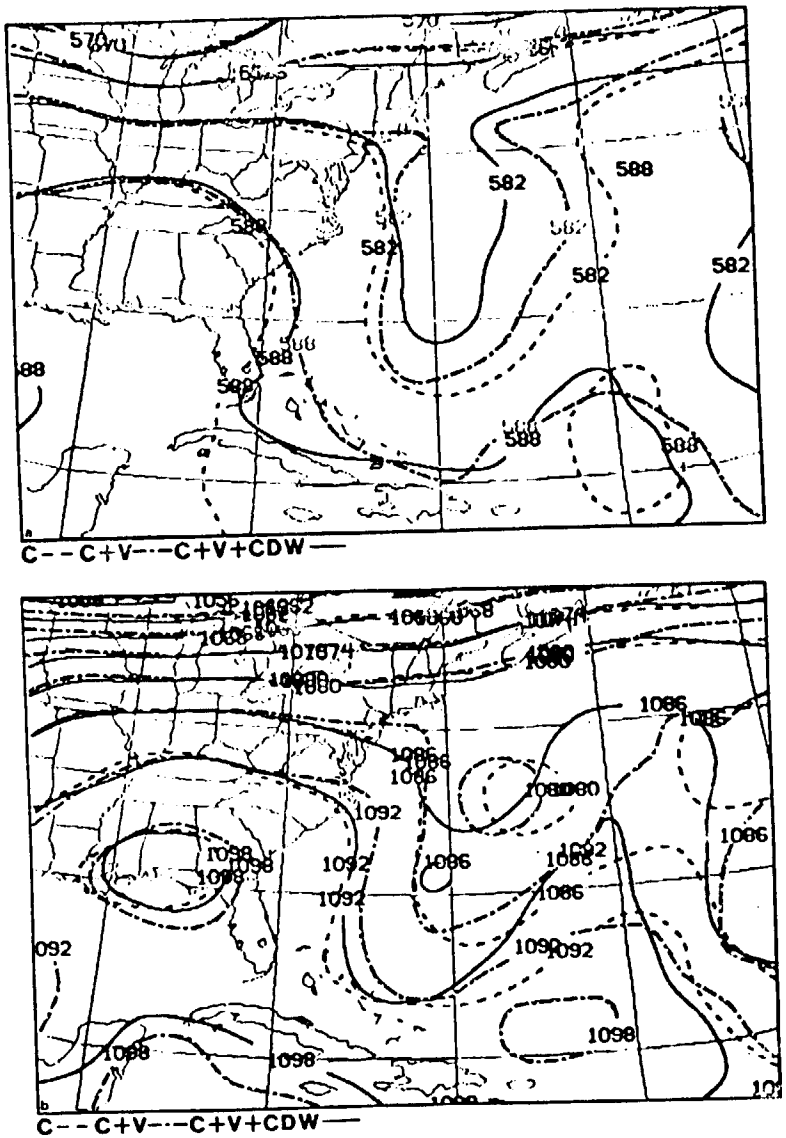

FIG. 1. (a) Comparison of 500 mb geopotential analyses at 0000 GMT on 16 September 1982 using conventional (C), conventional plus VAS (C + V), and conventional plus VAS plus cloud and water vapor drift wind observations (C + V + CDW). (b) Comparison of 250 mb geopotential analyses at 0000 GMT on 16 September 1982 using conventional (C), conventional plus VAS (C + V), and conventional plus VAS plus cloud and water vapor drift wind observations (C + V + CDW).

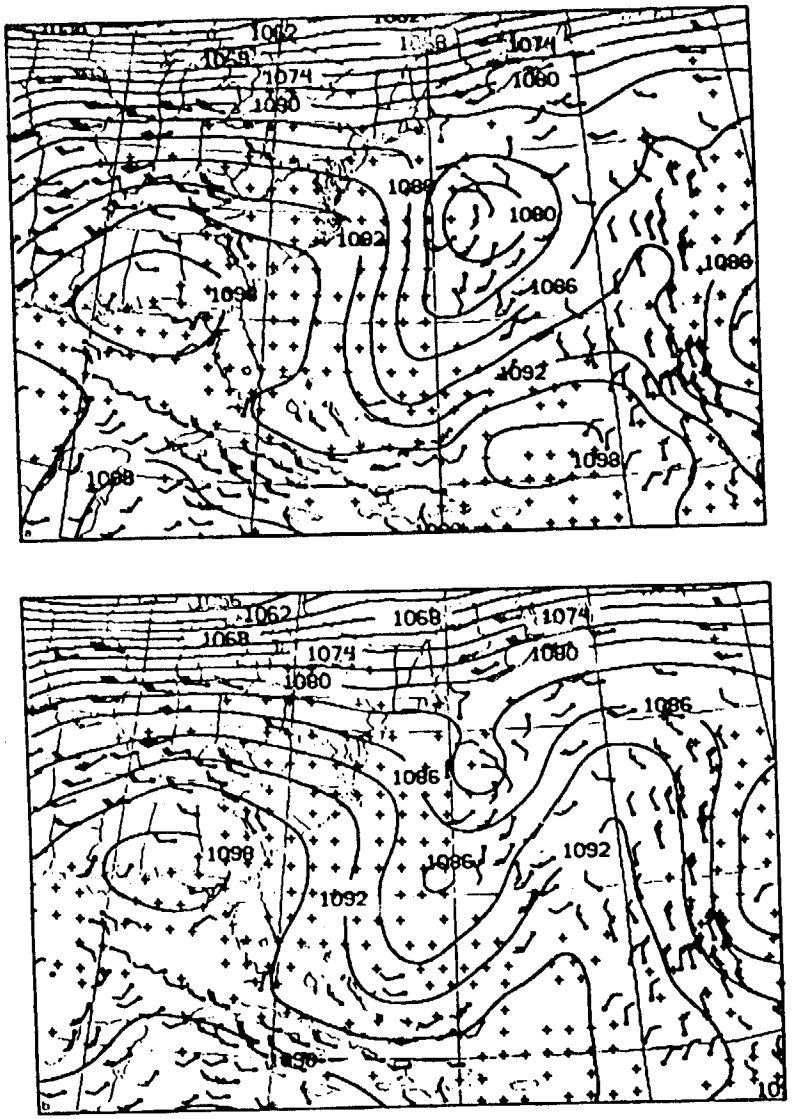

FIG. 2. (a) The 250 mb geopotential analysis at 0000 GMT 16 September 1982 using conventional and VAS observations (C + V). Cloud drift winds and VAS sounding positions superimposed. (b) The 250 mb geopotential analysis at 0000 GMT on 16 September 1982 using conventional, VAS, and cloud drift wind observations (C + V + CDW). Cloud drift winds and VAS sounding positions superimposed.

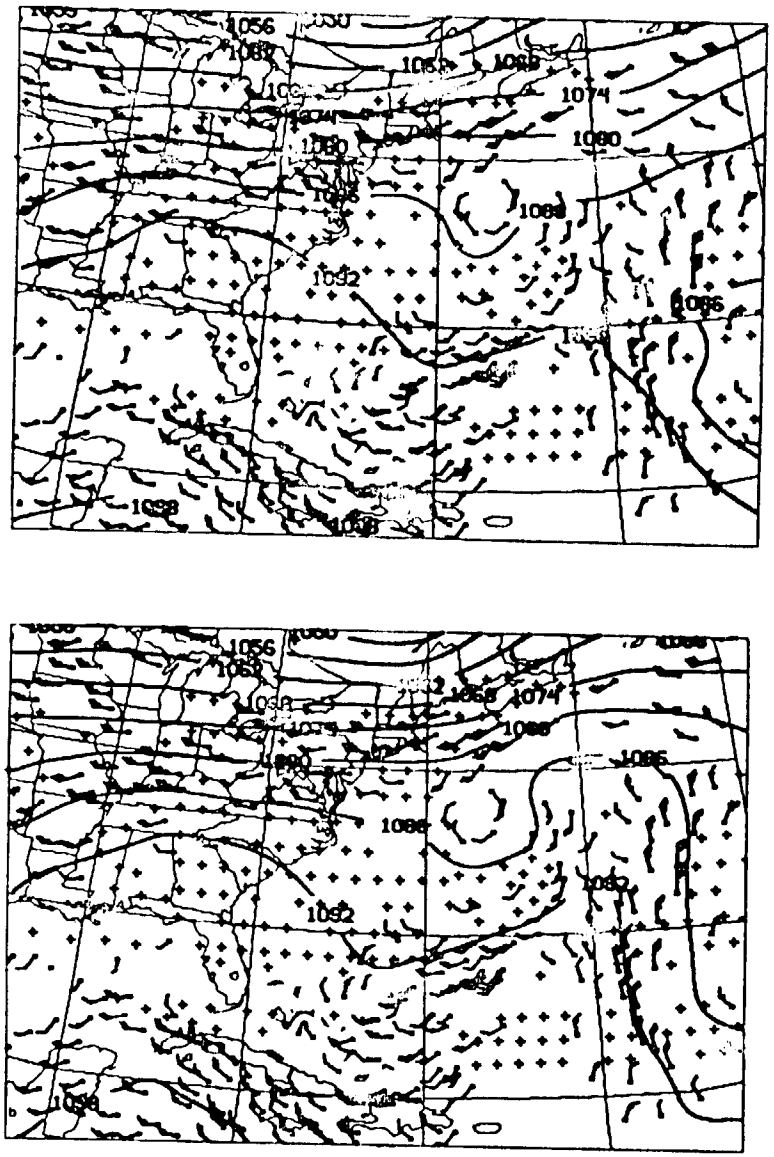

FIG. 3. (a) The 250 mb geopotential analysis at 0000 GMT 17 September 1982 using conventional and VAS observations (C + V). Cloud drift winds and VAS sounding positions superimposed. (b) The 250 mb geopotential analysis at 0000 GMT 17 September 1982 using conventional, VAS, and cloud drift wind observations (C + V + CDW). Cloud drift winds and VAS sounding positions superimposed.

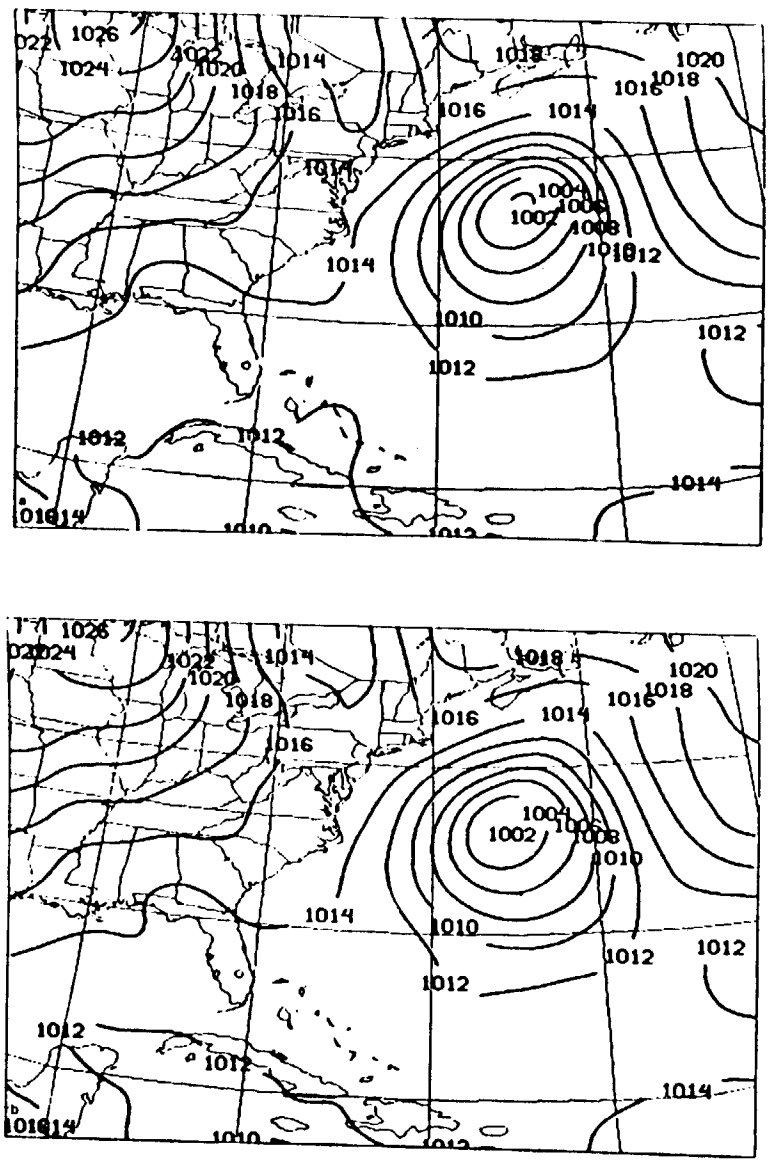

FIG. 4. (a) The 12-hour MSLP prognosis valid 0000 GMT 17 September 1982 from the C analysis. (b) The 12-hour MSLP prognosis valid 0000 GMT 17 September 1982 from the C + V + CDW analysis.

September 1982. They illustrate the impact of increasing the data base and show a gradual correction of the geopotential fields to what one would expect to be an optimum analysis with all data being used. Figs 2(a) and (b) show the 250 mb C + V and C + V + CDW analyses for 0000 GMT in a little more detail, with the VAS sounding positions (+) and cloud and water vapor motion wind data plotted. Fig. 2 illustrates two salient features of these analyses. The first is that the VAS sounding distribution and the cloud and water vapor motion wind distribution are complementary and provide a quite uniform data base over the western Atlantic. This is anticipated, as the VAS sounder provides soundings in the cloud-free areas, while suitable cloud tracers can often be found in the remaining areas. The second is that although the VAS data improve on the conventional analysis, the loss of VAS data caused by the intense cloudiness associated with Hurricane Debby has masked two significant features in the analysis (Fig. 2(a)): the exact positions of the cyclonic circulation centers near 70°W, and the strength of the ridge at 60°W. It can be seen that the addition of cloud drift wind data to this analysis (Fig. 2(b)) has ameliorated the problem. Similarly, in the 0000 GMT analyses on 17 September 1982 at 250 mb, the VAS sounding and cloud drift wind distribution was again uniform (Figs. 3(a) and (b)), while the addition of cloud drift wind data again ameliorated the problem of defining ridge and trough positions in an otherwise data-sparse region. It should also be pointed out that during the 0000 GMT analysis on 17 September 1982, additional cloud drift wind data were generated from imagery in a matter of minutes after it was found a data void was present near 38°N, 67°W.

5. The forecasts

The analyses using C, C + V, and C + V + CDW data at 0000 GMT and 1200 GMT on 16 September 1982 have been used to initialize the primitive equation model, described in Section 3b, over the analysis domain. The forecasts have been run at 137 km resolution. The integrations were run for a period of 12 hours, were non-nested, and the C + V + CDW analyses were used for verification. It should be noted that with analyses and forecasts at this resolution, we can examine only the larger-scale features associated with the hurricane.

The central position of the storm system has been measured from the 12-hour MSLP forecast and compared to the estimated best track position. The results are shown in Table 2. No great significance is intended to be fixed to the magnitude of these position errors, but the relative magnitude gives an indication of the positive impact of both VAS sounding and cloud and water vapor wind data on the analyses. The MSLP 12-hour forecast fields from the C and C + V + CDW analyses at 1200 GMT 16 September 1982 are shown in Figs 4(a) and (b).

TABLE 2. Storm central position error compared to estimated best track position for the 12-hour forecasts.

Forecast valid	ERRORS (N.M.) C	C + V	C + V + CDW
1200 GMT 16 Sept 1982	91	30	28
0000 GMT 17 Sept 1983	59	23	11
Mean Error (N.M.)	75	27	20

TABLE 3. S1 skill scores of the 12-hour forecasts delineated according to the data base of the original analyses.

Level	C	C + V	C + V + CDW
MSLP	48.6	46.4	46.2
1000	49.9	47.6	46.5
500	49.9	49.1	49.8
250	51.1	43.8	41.7

S1 skill scores (Teweles and Wobus, 1954) where $S1 = 100\Sigma e_g/\Sigma g_e$, e_g is the error in the forecast variable gradient, and g_e is the observed or forecast variable gradient (whichever is larger) have also been calculated for each of the model integrations and are presented in Table 3. When examining these scores, it appears the difference in skill shown in the positioning of the center of the storm is partially reflected in the S1 scores at MSLP and 1000 mb. It must be noted, however, that the surface analyses have been constructed without surface reports over much of the analysis area, hence the comparison of gradients in these regions must be viewed with some degree of caution. It is significant that the 250 mb level is the level that contains the most data, and forecasts at this level have shown a steady increase in skill as the data base increases.

6. Concluding remarks

From this example, it can be seen that VAS and CDW observations form complementary data bases. In areas of extensive cloudiness, CDW data allowed full subsynoptic scale analysis at cloud-tracer level by adding gradient information in areas devoid of VAS data. This often significantly changed the numerical analysis that had previously been interpolated through the area. It can also be seen that the use of VAS sounding and cloud and water vapor wind data, in conjunction with an "operational" MSLP analysis, appeared to have a positive impact on 12-hour numerical forecasts, although it is recognized that two sets of forecasts do not provide a statistically significant conclusion. An important point noted in this study is that through the use of McIDAS, wind vectors and VAS retrievals could be generated in association with the analysis process to allow selective augmenting of the analysis data base in a time frame of minutes when data voids were encountered. This capability is one most operational analysts would find very useful.

As a result of the analysis improvements seen in this study, full resolution model integrations (67 km) are now being undertaken on a number of tropical storms in order to further quantify the impact of VAS sounding and cloud and water vapor motion data in a variety of cases. Similar studies have already been done over the mainland, where careful account needs to be made of the relative quality of VAS temperature

gradients and absolute values. Again the complementary nature of the VAS soundings and cloud and water vapor drift "wind" data has been evident, with the cloud and water vapor motion wind data providing the information needed for the positioning of trough and ridge lines and circulation centers in cloud areas devoid of VAS soundings. This has permitted detailed subsynoptic scale analysis between the more widely spaced soundings of the conventional network.

Finally, it should be noted that the study was done with a data base available in "real time" when the VAS instrument is operational. Thus, it would appear that the prospects of a quasi-continuous 100-km resolution upper air data base at one- to three-hour frequency with a timeliness suitable for operational weather forecasting in the North American region are excellent.

Acknowledgments. Many thanks are due to Tod Stewart for generating cloud and water vapor motion winds, and to Mrs. Gail Turluck for her efforts in producing the manuscript. This work was supported under NASA Contract NAS8-34732. We acknowledge the enthusiastic support from personnel of the NASA/Marshall Space Flight Center.

References

Corby, G. A., A. Gilchrist, and R. L. Newson, 1972: A general circulation model of the atmosphere suitable for long period integrations. *Quart. J. Roy. Meteor. Soc.*, **98**, 809–832.

Cressman, G., 1959: An operational objective analysis system. *Mon. Wea. Rev.*, **87**, 367–374.

Kuo, H. L., 1965: On formation and intensification of tropical cyclones through latent heat release by cumulus convection. *J. Atmos. Sci.*, **22**, 40–63.

——, 1974: Further studies of the parameterization of the influence of cumulus convection on large scale flow. *J. Atmos. Sci.*, **31**, 1232–1240.

McGregor, J. L., L. M. Leslie, and D. J. Gauntlett, 1978: The ANMRC limited area model: Consolidated formulation and operational results. *Mon. Wea. Rev.*, **106**, 427–438.

Mills, G. A., L. M. Leslie, J. L. McGregor, and G. A. M. Kelly, 1981: A high resolution numerical analysis/forecast system for short term prediction over the North American region. Unpublished ANMRC Report, Australian Numerical Meteorology Research Centre, P.O. Box 1289K, G.P.O., Melbourne, Australia, 76 pp.

——, G. R. Diak, and C. Hayden, 1983: The subsynoptic scale model and investigations of the value of satellite sounding data in numerical weather prediction. Internal report, Space Science and Engineering Center, University of Wisconsin, Madison, WI 53706, 27 pp.

Mosher, F. R., 1978: Cloud drift winds from geostationary satellites. *Atmos. Tech.*, **10**, 53–60.

——, and T. R. Stewart, 1981: Characteristics of water vapor tracked winds. *NAVENVPREDRSCHFAC Contractor Report, CR 81-06*, 51 pp.

Sasaki, Y., 1958: An objective analysis based on the variational method. *J. Meteor. Soc. Japan*, **36**, 77–88.

——, 1970: Some basic formalisms in numerical variational analysis. *Mon. Wea. Rev.*, **98**, 875–910.

Seaman, R. S., R. L. Flaconer, and J. Brown, 1977: Application of a variational blending technique to numerical analysis in the Australian region. *Aust. Meteor. Mag.*, **25**, 3–23.

Smith, W. L., 1983: The retrieval of atmospheric profiles from VAS geostationary radiance observations. *J. Atmos. Sci.*, **40**, 2025–2035.

Suomi, V. E., R. Fox, S. S. Limaye, and W. L. Smith, 1983: McIDAS III: A modern interactive data access and analysis system. *J. Climate Appl. Meteor.*, **22**, 766–778.

Teweles, S., and H. Wobus, 1954: Verification of prognostic charts. *Bull. Amer. Meteor. Soc.*, **35**, 455–463.

Velden, C. S., W. L. Smith, and M. Mayfield, 1984: Applications of VAS and TOVS to Tropical Cyclones. *Bull. Amer. Meteor. Soc.*, **65**, 1059–1067.

Reprinted from Preprint Volume, Second Conference on Satellite Meteorology/Remote Sensing and Applications, May 13-16, 1986, Williamsburg, Va. Published by the American Meteorological Society, Boston, Mass.

P4.3

VERIFICATION OF SMALL-SCALE WATER VAPOR FEATURES IN VAS IMAGERY USING HIGH RESOLUTION MAMS IMAGERY

W. Paul Menzel

NOAA/NESDIS Advanced Satellite Products Project
Madison, Wisconsin

Gary Jedlovec

Cooperative Institute for Meteorological Satellite Studies
Madison, Wisconsin

Gregory Wilson

Marshall Space Flight Center
Huntsville, Alabama

1. INTRODUCTION

The Multispectral Atmospheric Mapping Sensor (MAMS) is a new instrument designed to produce high resolution imagery in eight visible and three infrared spectral bands from an aircraft platform. Thermal emission from the earth's surface, clouds, and atmospheric water vapor is measured at 12.3, 11.2, and 6.5 microns at up to 50 meter horizontal resolution. Similar infrared spectral bands are part of the VISSR Atmospheric Sounder (VAS) which is capable of 6.9 km horizontal resolution from its geostationary orbit. Sequences of 6.7 micron VAS images have been used to track water vapor structures and to infer atmospheric motion vectors (Stewart et al., 1985). They have also been used to investigate small scale atmospheric moisture variability (Jedlovec, 1984). The high resolution MAMS data give credence to the small scale variations in the VAS water vapor imagery.

The purpose of this paper is two-fold. We shall (1) describe the MAMS instrument and the radiance characteristics, and (2) intercompare some VAS and MAMS radiances and images.

2. MAMS INSTRUMENT CHARACTERISTICS

The MAMS is a modification of NASA's Airborne Thematic Mapper (Daedalus, 1982). The MAMS has two major components, the scan head and the spectrometer (Fig. 1). The scan head consists of the primary collecting telescope, a rotating scan mirror, a motor encoder assembly, and two controlled thermal sources. The field of view is defined by the aperture which is available in two different sizes, 2.5 mrad and 5.0 mrad. The spectrometer consists of optical elements which spectrally separate the polychromatic input energy, lenses which focus the separated energy onto sensors, detectors which convert optical energy to an electrical signal, and pre-amplifiers which condition the signal. The energy collected by the spectrometer is separated into four distinct optical paths using dichroic filters; three paths for the infrared data (one for each spectral band) and one for the visible and near infrared data. The spectrometer detectors are silicon for the visible radiation and mercury cadmium telluride for the thermal infrared radiation. The visible detector is an eight element array which converts optical energy to electrical energy. The spectral response of each band is determined by the dispersion characteristics of the prism placed in the optical path and the location of the array in the dispersed beam. The thermal infrared detectors are each housed in a vacuum dewar which contains a cooled long wave filter which defines the particular spectral band. Each infrared detector has an associated pre-amplifier to process the electrical signal. The spectral bands are summarized in Table 1. The spectral response functions for the three infrared channels of the MAMS (Fig. 2) were specified to be similar to the 6.7, 11.2, and 12.7 micron channels on VAS (also shown in Fig. 2).

The MAMS produces high resolution imagery in these visible and infrared spectral bands from a high altitude aircraft at 20 km as shown in Fig. 3. The horizontal ground resolution, GR, of each individual field of view is 100

Table 1

Rangle of MAMS Spectral Bands

8 visible (microns)	3 infrared (microns)
.42- .45	6.20- 6.85 (upper level water vapor)
.45- .52	10.32-12.02 (window)
.52- .60	12.20-12.56 (lower level water vapor)
.60- .62	
.63- .69	
.69- .75	
.76- .90	
.90-1.05	

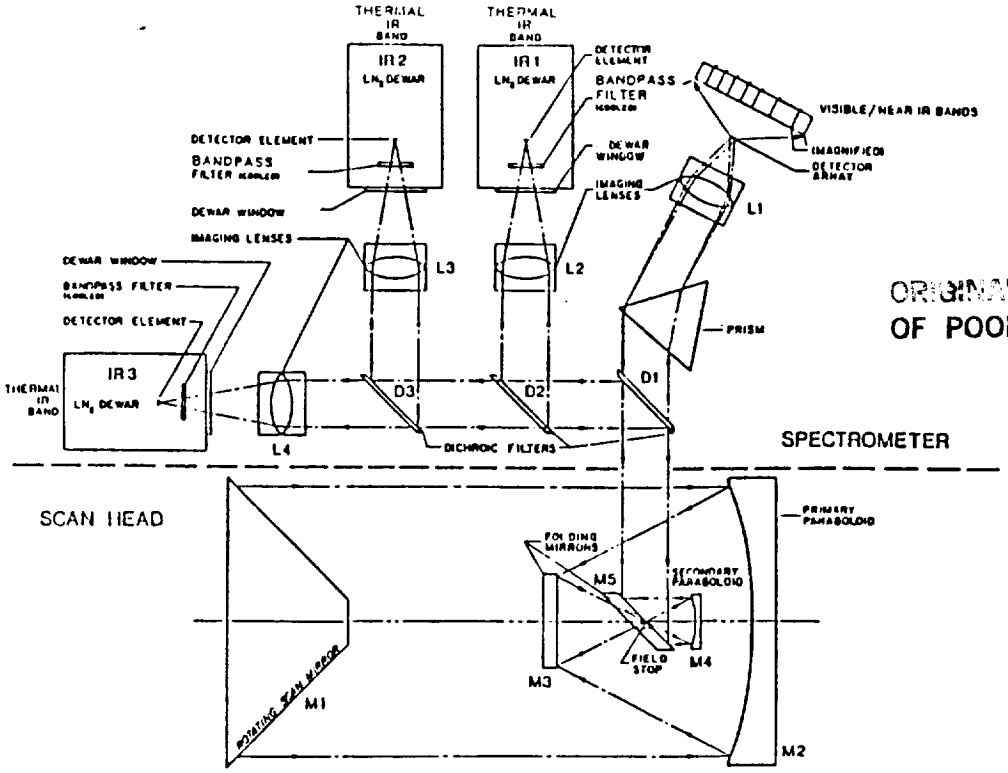

Fig. 1. Schematic of MAMS spectrometer and scan head.

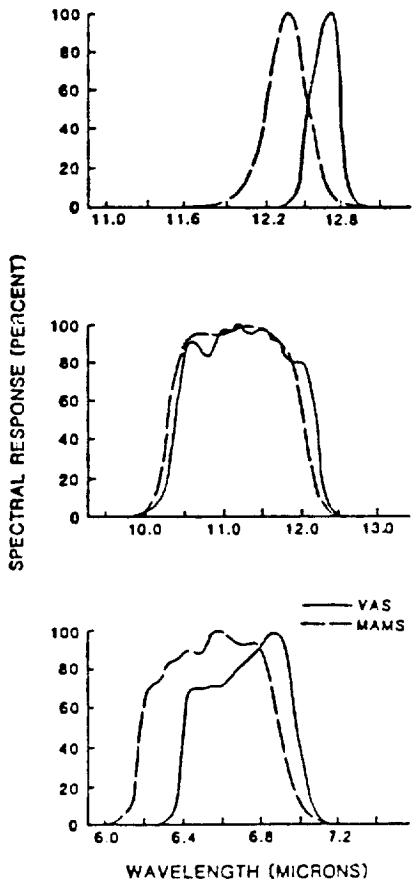

Fig. 2. Spectral response curves indicating the sensitivity of the MAMS and VAS instruments in the 12 micron, 11 micron, and 6 micron regions.

meters (50 meters if the smaller 2.5 mrad optics are used). The total field of view for one scan is 86° which covers the width, w, of the entire cross path of roughly 40 km. The scan rate is 6.25 revolutions per second (12.50 when the 2.5 mrad optics are used) and produces 67% overlap, 1-P, of each scan line with the previous one for nominal aircraft speed (740 km/hr). On each scan line 716 samples are taken so that there is 52% overlap of neighboring pixels along a scan line (4% when the 2.5 mrad optics are used). These overlaps can be used to good advantage to reduce the noise in the scene by spatial averaging.

Radiometric calibration of the infrared data is accomplished by viewing two blackbody sources and by assuming the detector response is linear with respect to radiance (a fractional nonlinearity of less than 5×10^{-4} is observed). Calibration occurs every scan line by viewing a warm and then a cold blackbody of known temperature. For a given spectral band, the radiance is determined from the temperature through the convolution of the normalized spectral response and the Planck function. The calibrated radiances are transformed back into temperatures using the inverse Planck relation with the nominal spectral band center wavelength.

Prior to flight, the gain and offset for each spectral band are adjusted electronically in order to minimize the likelihood of saturation over hot scenes and to maximize the effective operating range. The 6.5 micron band is adjusted to cover 210 to 280°K, while the 11.2 and 12.3 micron bands operate from 220 to 340°K. An eight bit digitizer is used so that for the 6.5 micron band the gain is approximately .3°K per count, and for the remaining surface viewing bands it is approximately .5°K per count.

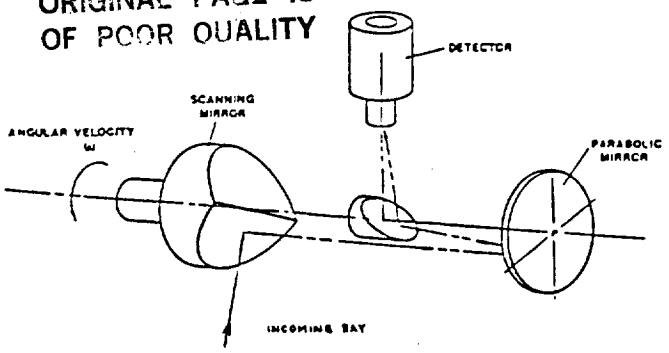

Fig. 3a. A simplified schematic of the inflight configuration of the optical elements of the MAMS.

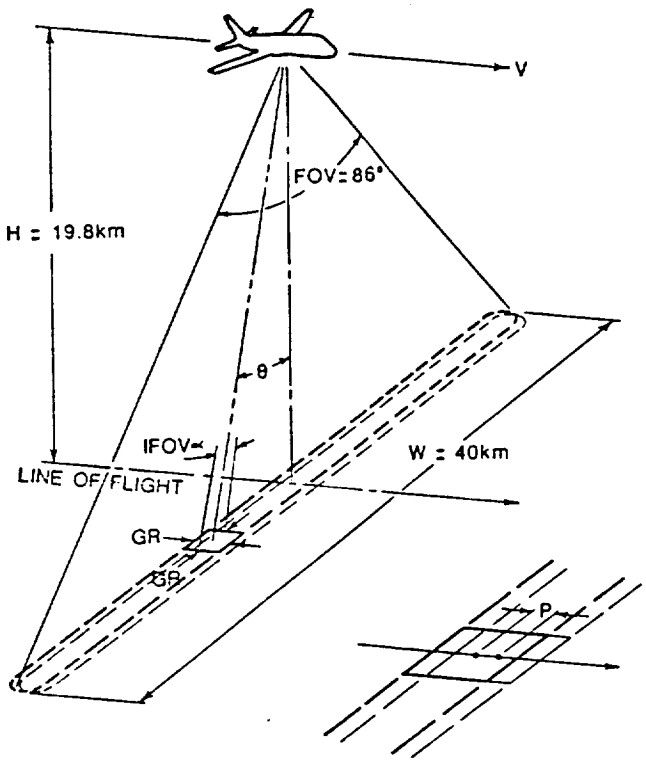

Fig. 3b. Scanning geometry for the MAMS instrument onboard a NASA U2/ER2 aircraft. Lower insert shows position of the center of the nadir ifov for two adjacent scans.

Truncation errors are assumed to be roughly half these values.

The infrared detectors on MAMS exhibit some low frequency noise so that samples taken at 52 microsecond intervals for the spin rate of 6.25 revolutions per second (26 microsecond sampling occurs at 12.5 rps) experience noise contributions with significant correlation. An analysis of covariance (Menzel, 1980) of the noise with the 5 mrad aperture reveals that after averaging ten consecutive samples noise is reduced by a factor of .54, .52, and .37, respectively, in the three infrared spectral bands in order of increasing wavelength (uncorrelated noise would have a factor of $1/\sqrt{10}$ or .32).

Inflight single sample noise values were determined from multiple samples over a uniform portion of the ocean. For a sample size of 100, the single sample noise values with the 5 mrad aperture were found to be .2, .1, and .4°K, respectively, for the spectral bands in order of increasing wavelength (for the 2.5 mrad aperture the values were .5, .2, and .9°K).

3. DATA INTERCOMPARISONS

Radiances for the MAMS and VAS spectral responses were simulated for each band and sensor in a radiative transfer calculation. A representative atmospheric transmittance was computed using a band model and radiosonde temperature and moisture profiles. Table 2 shows that the MAMS detects radiances within one to two mW/ster/m^2/cm^{-1} of the VAS detected radiances. The MAMS spectral responses are shifted to shorter wavelengths (as shown in Fig. 2), hence less radiance is detected. This translates into brightness temperature differences of less than a degree Kelvin.

Table 2

Intercomparison of Simulated Data

	6 micron	11 micron	12 micron
R(MAMS)	7.86	96.5	109.5
T(MAMS)	254.8	287.3	286.0
R(VAS)	8.73	97.5	111.6
T(VAS)	253.9	287.3	285.4
$\Delta T_{MAMS-VAS}$	0.9°K	0.0	0.6

radiances in mW/ster/m^2/cm^{-1}, temperatures in °K

Radiances from the MAMS and VAS were collected simultaneously over a relatively isothermal area of ocean off the California coast on 18 May 1985. Table 3 presents the comparison. After compensating for the inherent spectral differences of the two instruments, the MAMS data is within .5, 2.5, and 1.5°K of the VAS data, respectively, for the spectral bands in order of increasing wavelength. The observed split window channel differences (11 micron less 12 micron) are comparable, 2.5°K for MAMS and 2.1°K for VAS and thus showing similar low level moisture concentrations. The observed water vapor channel data (6 micron) show MAMS detecting upper level moisture concentrations very much like VAS, with MAMS showing somewhat less attenuation than VAS. These comparisons

Table 3

Intercomparison of Observed Data

	6 micron	11 micron	12 micron
R(MAMS)	6.01	99.9	111.1
T(MAMS)	247.1	289.5	287.0
R(VAS)	6.80	97.0	111.1
T(VAS)	246.5	287.1	285.0
$\Delta T_{MAMS-VAS}$	.6°K	2.4	2.0

radiances in mW/ster/m^2/cm^{-1}, temperatures in °K

are quite reasonable, since the spatial resolution of each sensor is very different (VAS at 7 km and MAMS at .05 km at nadir), the navigation of the MAMS data is from visual siting of landmarks only, and non-nadir viewing of the MAMS has not yet been taken into account.

Imagery from the MAMS and VAS were compared from flights over Oklahoma and Kansas on 12 May 1985. The goal of the intercomparison is to verify small scale features observed in the VAS water vapor images with the higher resolution MAMS data. These water vapor inhomogeneities in the VAS data have been used to obtain motion vectors when several images are considered in sequence. While the imagery is often too amorphous to track winds reliably with a correlation technique, it has produced good wind fields by single pixel tracking (Stewart et al., 1985). The MAMS data tends to verify that small scale gradients (down to several single pixels) in the VAS data are real. Fig. 4a shows the VAS 6.7 micron images with the MAMS flight track superimposed while Fig. 4b shows the 6.3 micron MAMS data (at 400m resolution for display) gathered in flight from G to H. These images were enhanced to delineate the moisture features. Brighter (colder) regions represent clouds or relatively high water vapor content and darker (warmer) areas represent drier air in the middle layer of the atmosphere. The MAMS images are not limb corrected and, therefore, images appear brighter (colder) toward the edges. The moisture features compare very nicely; starting at G, MAMS shows a dry tongue giving way to a moist ridge which becomes less moist at H. Fig. 5a shows single pixel resolution of the VAS image covering the MAMS track from E to F of Fig. 4a; Fig. 5b displays the MAMS data covering the boxed region of Fig. 5a. The temperatures from brightest to darkest pixels within the boxed-in area differ by 5°K indicating that these fluctuations are not instrument noise, but real atmospheric features. Six of the VAS features are corroborated nicely by the MAMS image. This lends credence to the assertion that the VAS distinguishes moisture features which are small enough to represent a wind vector, yet large enough to exist in several successive images. The features we are examining were discernible for at least two hours in the VAS images.

4. CONCLUSION

The MAMS measures thermal emission from the earth atmosphere system in eight visible and three infrared spectral bands (12.3, 11.2, and 6.5 microns) at up to 50m horizontal resolution. These infrared bands are very similar to three of the VAS infrared spectral bands. The instrument was flown aboard a NASA U-2 in May-June 1985 and corresponding VAS data was collected. MAMS radiometric performance is comparable to that of VAS. The MAMS exhibits somewhat less attenuation from water vapor than VAS because its spectral bands are shifted to shorter wavelengths away from the absorption band center. Intercomparisons of these images give credence to small scale variations in the VAS water vapor imagery. Attempts are underway to identify the scales of which these features must be tracked to depict the preconvective environment.

The MAMS has been developed to combine high resolution visible and infrared measurements to study small scale atmospheric moisture variability, to monitor and classify clouds, and to investigate the role of surface characteristics in the production of clouds, precipitation, and severe storms. As part of the Cooperative Huntsville Meteorological Experiment (COHMEX), the MAMS will be flying this summer to gather data for these studies.

5. ACKNOWLEDGEMENTS

This work was performed on the University of Wisconsin Man-computer Interactive Data Access System (McIDAS) under NASA support. Mr. John Arvesen and Mr. Jeff Myers at NASA/Ames contributed to the MAMS data collection and processing. Mr. Bob Atkinson at NASA/MSFC assisted in the calibration of the flight data.

6. REFERENCES

Daedalus, 1982: Operator's Manual: AADS1268 digital multi-spectral scanner system. Daedalus Enterprises, Ann Arbor, MI.

Jedlovec, G. J., 1984: Mesoscale analysis of 6.7 micron image data from the VISSR Atmospheric Sounder (VAS) for several case studies. Conf. on Satellite/Remote Sensing and Appl. AMS, Boston, 185-190.

Menzel, W. P., 1980: Prelaunch study report of VAS-D performance. Repot on NASA contract NAS5-21965, Space Science and Engineering Center, University of Wisconsin, Madison, WI.

Stewart, T. R., C. M. Hayden, and W. L. Smith, 1985: A note on water-vapor wind tracking using VAS data on McIDAS. BAMS, 66, 9, 1111-1115.

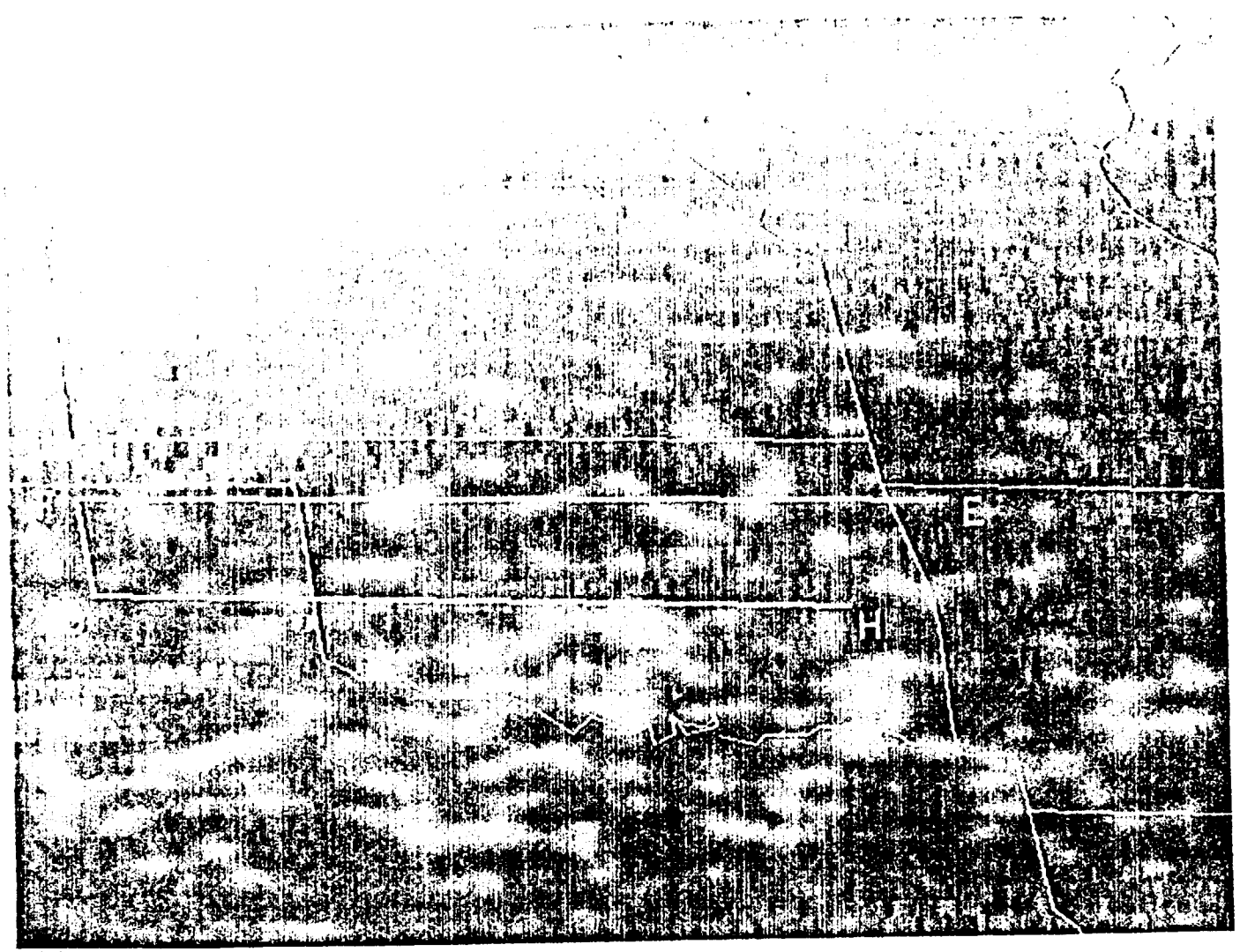

(A)

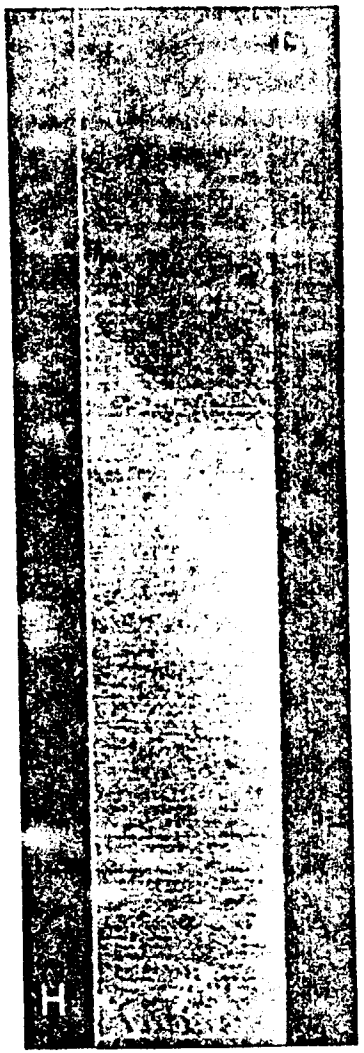

(B)

Fig. 4a. Enhanced VAS water vapor image with the MAMS flight track superimposed for 18 May 1985 at 1701 GMT.
Fig. 4b. Corresponding MAMS 6.3 micron enhanced image gathered in flight from G to H on 18 May 1985 at 1707 GMT.

P4.10 REPRINTED FROM THE SECOND CONFERENCE ON SATELLITE METEOROLOGY/ REMOTE SENSING AND APPLICATIONS, MAY 13-16 ,1986 WILLIAMSBURG,VA.

IMPACT OF THE INITIAL SPECIFICATION OF MOISTURE AND VERTICAL MOTION ON PRECIPITATION FORECASTS WITH A MESOSCALE MODEL— IMPLICATIONS FOR A SATELLITE MESOSCALE DATA BASE

Pamela E. Mlynczak

Department of Meteorology
University of Wisconsin-Madison

George R. Diak

Cooperative Institute for Meteorological Satellite Studies
University of Wisconsin-Madison

David D. Houghton

Department of Meteorology
University of Wisconsin-Madison

1. INTRODUCTION

Over the years, a number of regional numerical weather prediction models have been developed in an attempt to forecast not only synoptic scale events, but the mesoscale phenomena that are associated with or even independent of synoptic scale systems. One problem with regional models, however, involves the forecast of precipitation, which is a mesoscale event itself. The onset of precipitation in model forecasts commonly lags behind the observations, even when precipitation is observed at the initial time. To understand the nature of precipitation forecast deficiencies, two key related variables, namely moisture and vertical motion, their initialization in a model, and their evolution during the forecast must be examined. In this study, model simulations with modifications of the initial specifications of moisture and vertical motion will be examined to determine the relative impact of the mesoscale component of each parameter on the subsequent quantative precipitation forecast.

2. MESOSCALE MODEL

2.1 Analysis System

The analysis system and the forecast model have a grid of 51 east-west rows and 61 north-south columns on a Lambert conformal projection, with a horizontal grid increment of 67 km at the standard latitudes of 20 and 50 degrees north latitude. The domain is shown in Fig. 2. The principal characteristics of the analysis system are found in Table 1.

The objective analysis scheme is a version of the analysis system which is used by the Australian Numerical Meteorology Research Centre (ANMRC). This research analysis system was developed from the analysis scheme used operationally by Australia's Bureau of Meteorology (Seaman et al., 1977). The scheme is a combination of the successive correction method (SCM) of Cressman (1959) and the variational blending technique of Sasaki (1958, 1970). The research version contains three-dimensional variational blending of geopotential. Mills (1981) presents a qualitative discussion of the analysis sequence.

Table 1

Principal Characteristics of the Analysis System and Model

Analysis System
Combination of successive correction method and variational blending in three dimensions
Ten pressure levels, p=1000, 850, 700, 500, 400, 300, 250, 200, 150, and 100 mb
Horizontal resolution: 67 km
Fields analyzed or derived at each pressure level: - geopotential height - temperature - dewpoint - horizontal wind components - streamfunction
Forecast Model
Primitive equations model in σ-coordinates
Ten vertical levels at σ=0.09, 0.19, 0.29, ..., 0.99
Horizontal resolution: 67 km
Staggered horizontal grid (Arakawa "C" grid)
Semi-implicit time differencing (Δt=5 min)
Similarity theory surface layer
Stability-dependent vertical diffusion of momentum, heat, moisture above surface layer through depth of boundary layer
Surface shortwave and longwave flux modified by cloudiness
Surface energy balance equation
Large-scale precipitation
Kuo-type convective parameterization
Updated boundary conditions

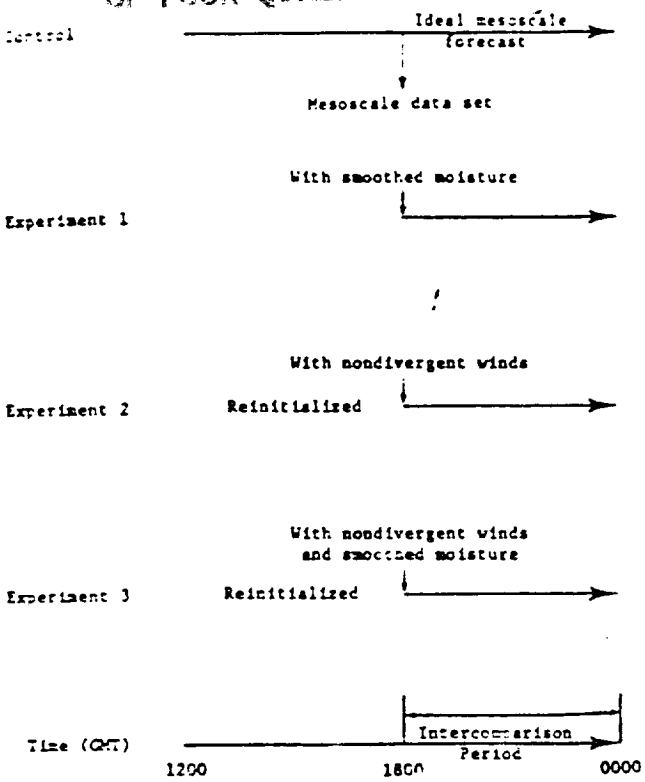

Fig. 1. Schematic summary of experimental design. The duration for each simulation is indicated by horizontal arrows.

2.2 Forecast Model

The forecast model was developed from the Australian Region Primitive Equations (ARPE) model (McGregor et al., 1978). The subsynoptic Scale Model (SSM) of the Space Science and Engineering Center at the University of Wisconsin-Madison used in this study is an adaptation of the ARPE model to the North American region. In this adaptation on Kuo-type convective parameterization (Kuo, 1965, 1974) and a comprehensive planetary boundary layer scheme were incorporated into the model. Also, a finite differencing scheme discussed by Corby et al. (1972) which lessens truncation effects in regions of steep topography has been added. Further characteristics are found in Table 1.

3. EXPERIMENTAL DESIGN

Four simulations are made with the SSM to determine the impact of the initial moisture and vertical motion fields on the evolution of the precipitation forecasts. These are a control forecast 12-hour simulation that begins at 1200 GMT 6 March 1982 and three experiment simulations with modifications to the moisture and vertical motion fields incorporated at 1800 GMT. The experiment forecasts from 1800 GMT are compared to the second half of the control forecast. The experimental design is given in Fig. 1.

The 12-hour control simulation begins at 1200 GMT 6 March 1982 and develops precipitation by 1300 GMT. The model is still producing precipitation at 1800 GMT the time a data set is extracted for use in the three experiments.

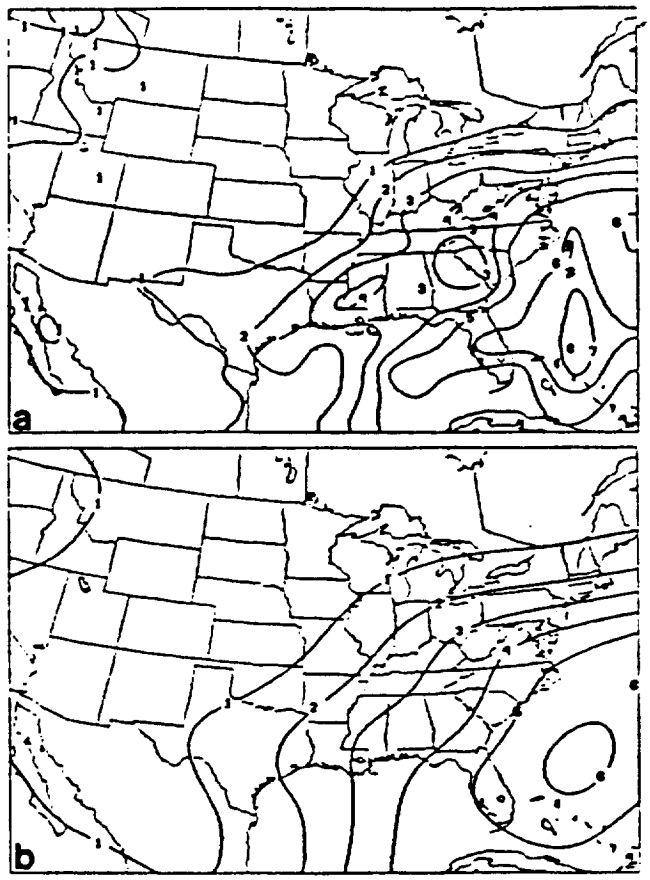

Fig. 2. Mixing ratio from the control forecast at 1800 GMT for the sigma level of 0.69; a) unsmoothed, b) smoothed. Contour interval is 1 g kg^{-1}.

Beginning at this time, changes in the precipitation rates and accumulations due to changes in the initial specifications will be most accentuated. The six-hour control forecast from 1800 GMT 6 March to 0000 GMT 7 March 1972 provides the "ideal forecast"—one that contains mesoscale moisture and vertical motion information from beginning to end.

Experiment 1 is run like the control forecast, except that at 1800 GMT, smoothed moisture fields replace the mesoscale moisture fields in the model. The moisture fields are smoothed to make them representative of fields that would be obtained from analyzed radiosonde data, usually considered to be at the synoptic scale. Fig. 2 shows the original and the smoothed mixed ratio fields for the sigma level of 0.69. Experiment 1 provides the precipitation forecast for the initial state with only a synoptic scale moisture field.

Experiment 2 is like the control forecast except that the initial wind fields are constrained to be nondivergent at 1800 GMT. The nondivergent wind components are derived from the model winds extracted from the control forecast data set and are inserted into the model. All of the other variables remain unchanged. Because the winds are nondivergent, the initial vertical motion is suppressed, particularly away from areas of significant topography (Fig. 3). Experiment 2 shows the effect of a nondivergent initialization of winds on the subsequent quantitative precipitation forecast.

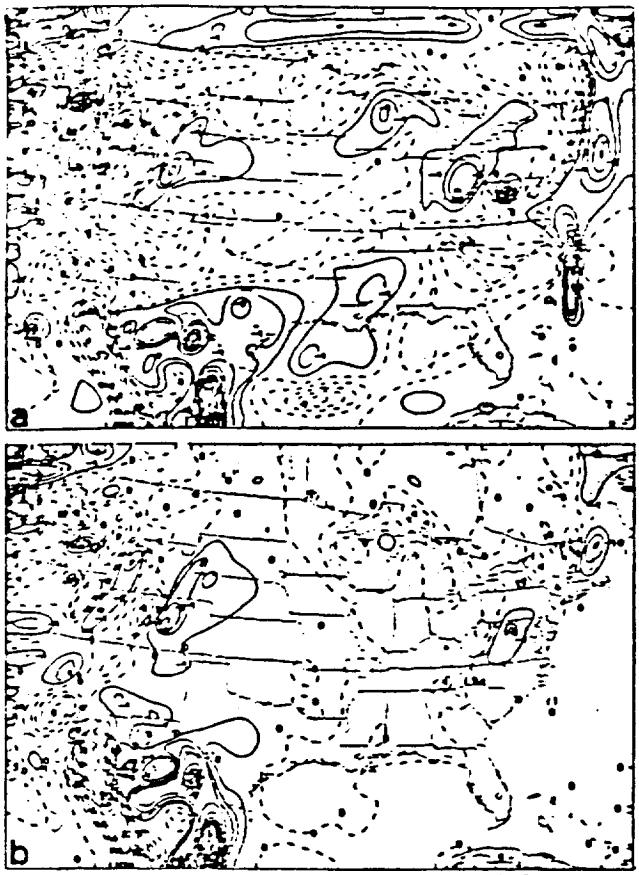

Fig. 3. Vertical motion $\dot{\sigma}$ at 1800 GMT for sigma level of 0.49; a) control, b) experiment 2. Negative values (upward motion) are solid. Contour interval is $2X10^{-6}$ s^{-1}.

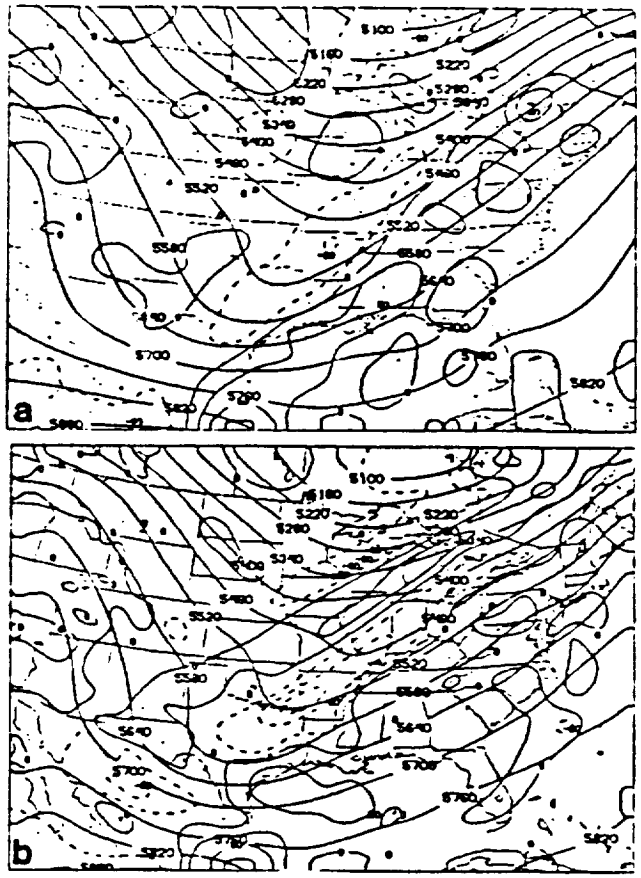

Fig. 4. 500-mb geopotential heights (m) and 500-mb relative vorticity (contour interval $40X10^{-6}$ s^{-1}, negative values dashed) at 0000 GMT; a) observed, b) control.

Experiment 3 is a combination of Experiments 1 and 2, containing both the initial smoothed moisture and nondivergent wind fields. This experiment is the most representative of a forecast beginning with synoptic analyses. It should be noted, however, that mesoscale and synoptic scale information from the six-hour control forecast remained in the height and temperature fields.

4. CONTROL CASE OF 6 MARCH 1982

The purpose of this research to study the changes made to a precipitation forecast due to modifications of the initial moisture and vertical motion fields is achieved by comparing simulation of the three experiments to the control forecast. The performance of the control itself is discussed very briefly here, although its accuracy in terms of the observations is not central to the analysis.

The model performed well at 500-mb level, as shown in Fig. 4. The forecasted trough over the central U.S. is slightly behind that of the analysis, but the intensity is simulated well. The forecast, however, does not capture the short wave trough observed west of Florida. The forecast of mean sea level pressure was excellent, with accurate placement and strength of the features (not shown).

The precipitation forecast from the model was not as satisfactory as the height and mean sea level pressure forecasts. The model's placement of copious rainfall east of Virginia and North Carolina seems accurate, based upon comparing Figs. 5 and 6 with radar maps (not shown). Precipitation output from the model is shown in hundredths of centimeters. The development of the precipitation area over Ohio and Pennsylvania lagged four hours behind the observations, yet the model greatly overforecasted the amounts in this region, producing as much as 2.00 cm (0.75 in.) while the observations were all less than 0.25 in. The model's performance in the Gulf region compared much less favorably to the observations than did the forecast off the East Coast and over the northeastern United States. The precipitation band observed over Louisiana, Mississippi, and Alabama was not forecasted at all. No rainfall greater than 0.25 in. was forecasted over the land. Instead, the model generated precipitation out over the Gulf of Mexico, but not until 1700 GMT. The validity of this feature is questionable because of the lack of verification data; however, satellite imagery did suggest that precipitation had developed here earlier before moving eastward. The forecasted feature, however, remained stationary.

It is unfortunate that the precipitation forecast produced by the control simulation was not more accurate. The purpose of this study, however, is to discuss changes in the forecasts brought about by modifications to the initial conditions. It is expected that the comparisons between the control and the experiments will be meaningful, regardless of the simulation deficiencies in the control forecast.

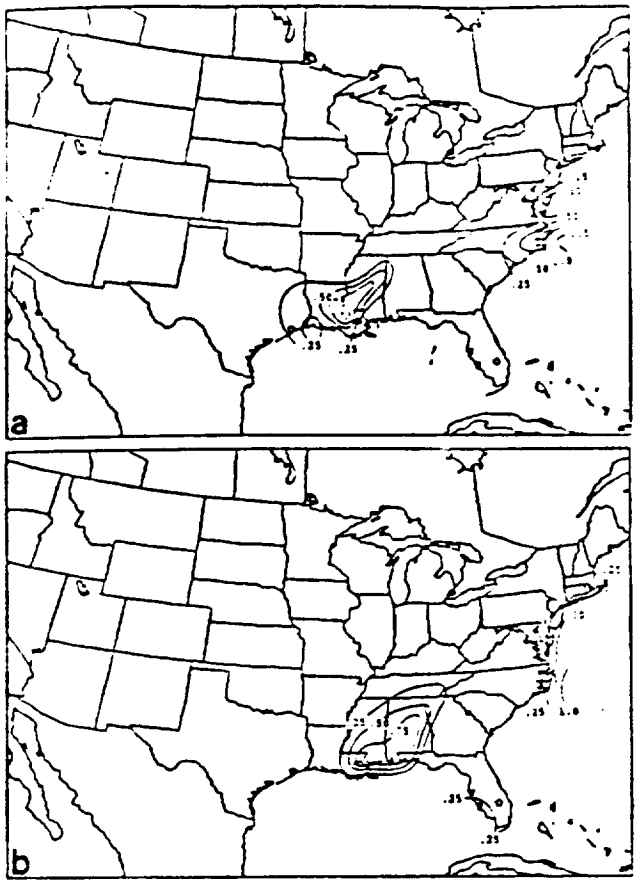

Fig. 5. Six-hour observed precipitation accumulations (in.) ending at (a) 1800 GMT, (b) 0000 GMT.

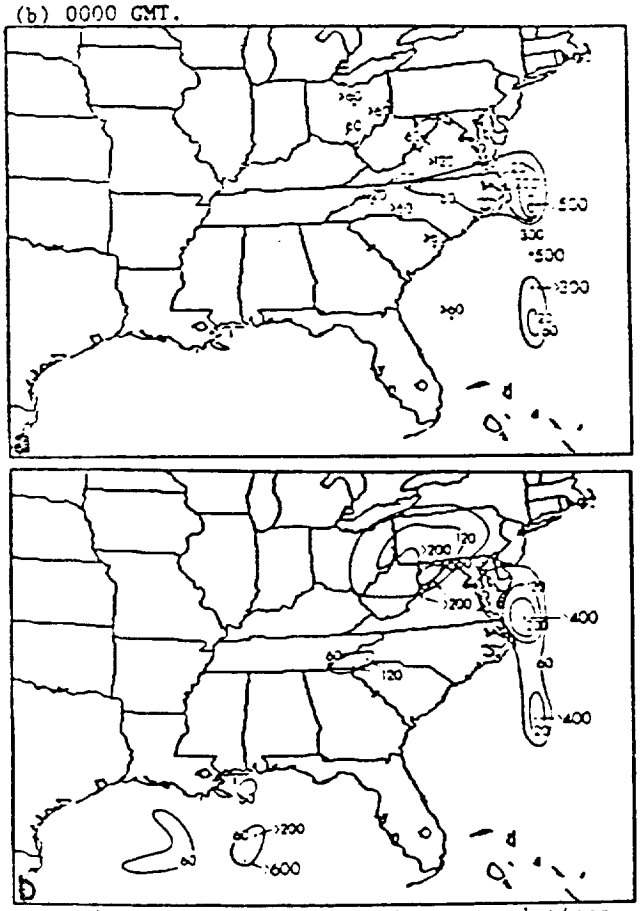

Fig. 6. Six-hour precipitation accumulations (hundredths of cm) from the control forecast ending at (a) 1800, (b) 0000 GMT.

5. EXPERIMENTAL RESULTS AND COMPARISONS

The six-hour precipitation forecasts from 1800 GMT to 0000 GMT of the control and the experiments are compared. To facilitate this comparison, three rectangular domain "boxes" encompassing the major precipitation areas of the control forecast were chosen for analysis (Fig. 7). Area-averaged accumulations, plotted in Fig. 8, were calculated in each box by summing the total accumulations and dividing by the number of grid points.

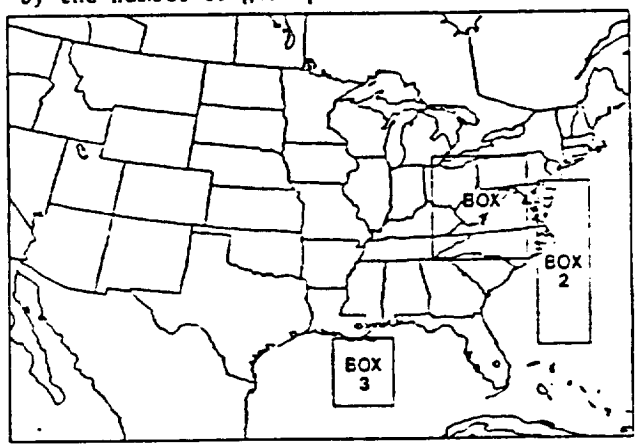

Fig. 7. Areas of precipitation for statistical calculations.

In Experiment 1, accumulations were much lower than those of the control, especially in boxes 2 and 3, where moisture values at 1800 GMT had been reduced by the smoothing process. In these two boxes, accumulations were only 24-30% of the control values. One precipitation maximum was reduced by 50%, and two other maxima found in the control were not forecasted in Experiment 1. Precipitation rates lagged behind the control forecast, and areal coverage was reduced to 68-77% of the control.

The reduced vertical motions of Experiment 2 resulted in lower accumulations that were 40-45% of the control values for the three boxes. Precipitation maxima for this experiment were positioned well when compared to the control, but most maxima were much lower. Area coverage was also reduced, while precipitation rates generally lagged behind the control.

As would be expected, Experiment 3, both lacking initial vertical motion and having lower initial moisture values than the control forecast in the precipitation regions, produced the lowest precipitation accumulations of the three experiments. Fig. 8 reveals that Experiment 3 yielded much lower average accumulations and precipitation rates than the control, with Box 2 having the largest differences. Average accumulations at the end of the forecast were only 4-22% of those from the control forecast, and precipitation covered 6-43% of the control's area of precipitation. This experiment missed completely the precipitation centers over the Atlantic and in the Gulf that were forecasted by the control (Fig. 6b). After beginning with primarily "synoptic scale" conditions, the model was unable to recover in the six-hour period and regenerate the mesoscale fields necessary to

yield detailed precipitation features and higher levels of precipitation accumulation.

An interexperimental precipitation comparison supports the results previously discussed. Comparing the precipitation forecasts between Experiments 2 and 3 shows the effects of smoothing the initial moisture fields, just as done by the comparison between Experiment 1 and the control. Fig. 8 shows that the average accumulations in Experiment 3 were, at most, 50% of the accumulations in Experiment 2. Areas of precipitation were also reduced in Experiment 3. Comparing Experiment 3 with Experiment 1 also showed the effects of suppressing the initial vertical velocities. Again, precipitation accumulations, rates, and areal coverage were reduced significantly. These comparisons are indeed consistent with the comparisons between the control and each experiment.

6. CONCLUSIONS

Four simulations were made with a numerical mesoscale model to determine the effects of suppressing the initial mesoscale information in the moisture and wind fields on the precipitation forecasts. The latter half of a 12-hour control forecast represented an ideal forecast that was "initialized" with fields containing mesoscale as well as synoptic scale structure. The three experiments were degraded versions of this ideal initialization and their forecasts were compared to the control forecast during the period from 1800 GMT 6 March to 0000 GMT 7 March 1982.

The characteristics of the precipitation forecasts of the experiments are not different enough to conclude that either mesoscale moisture or mesoscale vertical velocity at the initial time is more important for producing a forecast closer to that of the control. For example, at the end of the forecast, the average precipitation accumulation over a land area in the smoothed moisture experiment was 67% of the control forecast, while the nondivergent experiment produced accumulations that were 45% of the control. Over the oceans, however, the smoothed moisture experiment produced 24-30% of the control forecast, less than the nondivergent experiment, which produced 40-44% of the control forecast. No general statements can be made about this study, therefore, except to say that degrading one or both of these initial fields produces a drier forecast when compared to the control forecast. First of all, comparisons were made for only a six-hour period, and this may not have been sufficient time for the model to recover from the modifications made. Secondly, these experiments were performed on one case only, with just one model, and as such, generalizations regarding the relative worth of initial moisture and vertical velocities are inappropriate.

This research points out the need for proper initialization of mesoscale moisture and vertical motion information so that more accurate precipitation forecasts may be obtained. Improvement of the data base that is analyzed should be very helpful. More detailed moisture

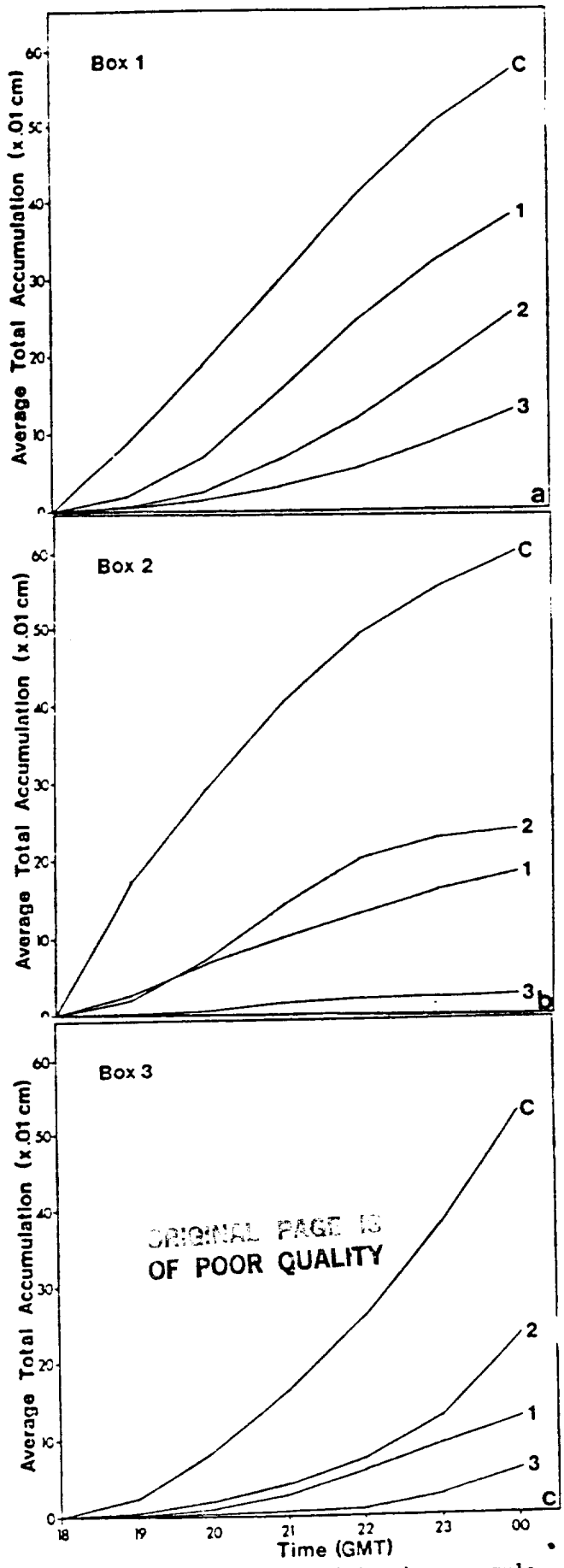

Fig. 8. Area-averaged precipitation accumulations (hundredths of cm) as a function of time for the control forecast (c) and the experiment for (a) Box 1, (b) Box 2, (c) Box 3.

information is available from high-resolution satellite data, satellite cloud and water vapor drift winds would improve the horizontal winds, and thus the vertical motion derived from the convergence/divergence of these winds. Considerable research will be required to determine how to use a satellite mesoscale data to make short-term precipitation forecasts more accurate and timely.

7. ACKNOWLEDGEMENTS

The work of the first author was supported by a National Science Foundation Graduate Fellowship. Computing and data resources were made available through the Cooperative VAS Program with the Marshall Space Flight Center, Control NAS8-34732. The Atmospheric Science Division of NSF provided additional support through Grant ATM-8005369.

8. REFERENCES

Corby, G. A., A. Gilchrist, and R. L. Newson, 1972: A general circulation model of the atmosphere suitable for long period integrations. Quart. J. Roy. Meteor. Soc., 98, 809-832.

Cressman, G. P., 1959: An operational objective analysis system. Mon. Wea. Rev., 87, 367-374.

Kuo, H. L., 1965: On formation and intensification of tropical cyclones through latent heat release by cumulus convection. J. Atmos. Sci., 22, 40-63.

_____, 1974: Further studies of the parameterization of the influence of cumulus convection on large scale flow. J. Atmos. Sci., 31, 1232-1240.

Le Marshall, J. F., W. L. Smith, and G. M. Callan, 1985: Hurricane Debby--an illustration of the complementary nature of VAS soundings and cloud and water vapor motion winds. Bull. Amer. Meteor. Soc., 66, 258-263.

McGregor, J. L., L. M. Leslie, and D. J. Gauntlett, 1978: The ANMRC limited-area model: Consolidated formulation and operational results. Mon. Wea. Rev., 106, 427-438.

Mills, G. A., 1981: An objective limited-area analysis/prognosis experiment using FGGE data in the Australian region. Mon. Wea. Rev., 109, 1898-1913.

Sasaki, Y., 1958: An objective analysis based on the variational method. J. Meteor. Soc. Japan, 36, 875-883.

_____, 1970: Some basic formalisms in numerical variational analysis. Mon. Wea. Rev., 98, 875-883.

Seaman, R. S., R. L. Falconer, and J. Brown, 1977: Applications of variational blending technique to numerical analysis in the Australian region. Aust. Meteor. Mag., 25, 3-23.

High-Order Low-Pass Implicit Tangent Filters for use in Finite Area Calculations

William H. Raymond

Abstract

High-order implicit tangent filters are developed. The implicit tangent filters possess a highly selective amplitude response function and they can be applied relatively close to a boundary. Comparisons are made between the implicit and the traditional or explicit filters. Numerical simulations are performed to test the response in a limited area model. An algorithm to maximize computing efficiency is presented. All tests indicate the desirability and utility of the implicit tangent filter.